Numerical study on retrofitting measures for low-rise URM buildings

Bhattarai, Suman; Messali, Francesco; Esposito, Rita

Publication date
2019

Document Version
Final published version

Citation (APA)
Bhattarai, S., Messali, F., & Esposito, R. (2019). *Numerical study on retrofitting measures for low-rise URM buildings*. Delft University of Technology.

Project number	CM1B06
File reference	CM1B06-WP3-2
Date	26 June 2019
Corresponding author	Rita Esposito (r.esposito@tudelft.nl)

TU Delft Large-scale testing campaign 2019

NUMERICAL STUDY ON RETROFITTING MEASURES FOR LOW-RISE URM BUILDINGS

Authors: Suman Bhattarai, Francesco Messali, Rita Esposito

***Cite as**: Bhattarai, S., Messali, F. and Esposito, R. Numerical study on retrofitting measures for low-rise URM buildings. Report No. CM1B06-WP3-2, 26 June2019. Delft University of Technology.*

This research work was funded by NAM Structural Upgrading stream.

Contents

1 Introduction

This report presents the results of the numerical study on strengthening measures for low-rise unreinforced masonry (URM) buildings. The study aims to assess the efficiency of different strengthening measures applied to URM buildings in terms of seismic capacity (force and displacement) and prevention of the damage, as defined in the plan of approach [1].

First, two configurations of unreinforced masonry (URM) buildings are analysed. Then, different strengthening techniques and materials are applied to the building. The strengthened buildings are analysed to assess the effect of the strengthening measures. The study makes use of nonlinear finite element analyses (NLFEA) with a continuum cracking model. The report presents the results of both static (pushover, NLPO) and incremental dynamic (IDA) nonlinear time history (NLTH) analyses. The results of the two different approaches (NLPO and IDA) are compared with each other to obtain an evaluation of the strengthening measures as accurate as possible.

The two assemblage tests performed at TU Delft [2, 3] are considered as reference for the unreinforced building cases. These tested buildings resemble typical Dutch terraced houses in the Groningen province in the north of The Netherlands. The two full-scale quasi-static cyclic tests were performed at TU Delft on buildings which have same global geometry but different masonry type and pier span [1]. The experimental results are used in this study for the validation of the finite element model that represents the unstrengthened building configuration. The validated finite element model can then be used for simulating the structural performance of the strengthened buildings.

The first configuration of the URM house (Model U1) is based on building TUD_BUILD-1 [2] that was tested at TU Delft in 2015. The typology of the building resembles to the Dutch houses built in the years 1960-1980. The house TUD_BUILD-1 is a two storey building made of calcium silicate (CS) brick masonry. The piers of the house span over two floors and are connected to the transversal walls with a running bond.

The second configuration of the URM house (Model U2) differs from the Model U1 only for the span of the piers. The piers in Model U2 span over one floor only. The configuration of Model U2 resembles the tested house TUD_BUILD-2 [3] but differs for the masonry type: in fact CS bricks were simulated instead of CS elements, to limit the differences to model U1 to the wall-to-floor connectivity only. The nonlinear finite element analyses performed on these two configurations allows to study the effect of this variation on the structural response of the building when subjected to lateral forces.

Three different strengthening techniques are then applied to Model U2: (i) strengthening of URM piers only, (ii) strengthening of URM wall-to-pier connections only, and (iii) strengthening of both URM piers and wall-to-pier connections. Two different strengthening materials, (a) Oriented Strand Board (OSB) Panels and (b) Engineered Cementitious Composites (ECC) are applied over the strengthened components, one at a time, and analysed numerically. The finite element analyses results of the strengthened models are then assessed and compared with the results of the unstrengthened model. The variation of the strengthening techniques and materials is finalized to assess the effect of the adopted measure. A summary of the performed numerical analyses carried out in this study is presented in Table 1.1.

During the study, the performance of the buildings are assessed in terms of pushover capacity curve, dynamic hysteresis and backbone curve, equivalent bilinear curve, displacement profile, crack evolution, and damage levels. Four different damage levels, DL1, DL2, DL3 and DL4 are identified based on the crack evolution. The damage level DL1 represents the first occurrence of a visible crack, the damage level DL2 represents minor damage, the damage level DL3 represents moderate structural damage and the damage level DL4 represents near collapse (NC) state.

The effect of the adopted strengthening technique and material is studied in terms of seismic performance (improvement in both force and displacement capacity) and delay of occurrence of the damage levels. The delay of occurrence of the damage levels (between the strengthened and the unstrengthened model) is assessed on the basis of the difference in the corresponding base shear force and second floor displacement obtained at each damage level. Besides, any significant change in the overall behaviour of the house is also examined on the basis of the comparison of crack evolution, drifts and displacement profile.

Table 1.1 Overview of tests to be performed in the study

No. configuration		Object of the analysis	Purpose
Unstrengthened configurations	U1	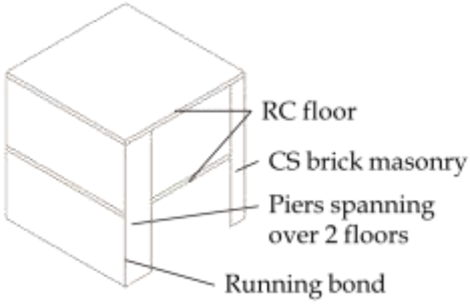	• Model calibration via comparison of NLPO analysis and experimental results. • Comparison NLPO and IDA analyses
	U2	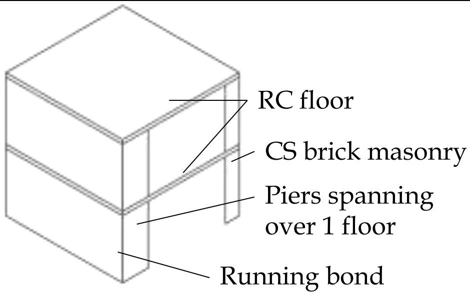	• Study variation of piers geometry via comparison between analyses of configuration U1 and U2.
Strengthened configuration	S1	Configuration U2 with strengthening of URM piers only. 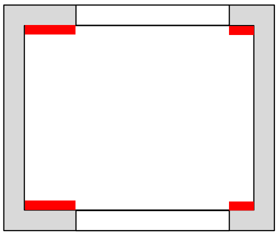 Plan view of the building (in red retrofitting material).	• Study improvement of seismic performances in terms of damage and safety by comparison of analyses U2 and S1. Comparison with analyses S2 and S3 will be also made. • This strengthening measure can improve the global in-plane behaviour of the structure due to larger pier capacity.
	S2	Configuration U2 with strengthening of URM wall-to-pier connection 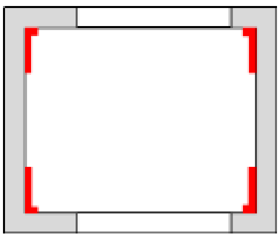 Plan view of the building (in red retrofitting material).	• Study improvement of seismic performances in terms of damage and safety by comparison of analyses U2 and S2. Comparison with analyses S1 and S3 will be also made. • This strengthening measure can improve: ○ out-of-plane behaviour of transversal wall; ○ global in-plane behaviour of the structure due to the flange effect.
	S3	Configuration U2 with strengthening of URM piers and wall-to-pier connection 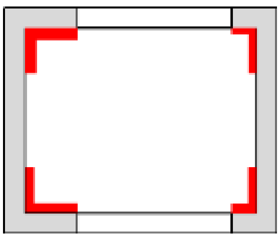 Plan view of the building (in red retrofitting material).	• Study improvement of seismic performances in terms of damage and safety by comparison of analyses U2 and S3. Comparison with analyses S1 and S2 will be also made. • This strengthening measure can improve: ○ out-of-plane behaviour of transversal wall; ○ global in-plane behaviour of the structure due to both large flange effect and in-plane capacity of piers.

The outline of the report is as follows:

- Chapter 2 describes the modelling of the unstrengthening building models, Model U1 and Model U2
- Chapter 3 presents, discusses and compares the results of the nonlinear pushover analyses (NLPO) performed on unstrengthened buildings
- The results of the nonlinear time history analyses performed on Models U1 and U2 are reported in Chapter 4. The results of NLTH and NLPO are also compared in this chapter.
- Chapter 5 provides an overview of different strengthening techniques and materials that are applied to Model U2.
- The results of the NLPO analyses performed on all six strengthened models are presented in Chapter 6. This chapter also includes the evaluation of the effect of the application of the retrofitting measures.
- Chapter 7 reports the results of the dynamic analyses performed on strengthened models. The results of NLTH and NLPO are compared with each other for each strengthened model.
- Chapter 8 summarises the main conclusion of this study.
- Appendix A presents the crack pattern observed from the NLPO and NLTH analyses performed on Model U1 and Model U2
- The drifts and displacement profile at different damage levels of each strengthened model obtained from NLPO analyses are reported in Appendix B.

2 Unstrengthened Buildings

The numerical modelling of two different configurations of two unstrengthened houses is discussed in this chapter. The configuration of the two URM houses that are considered in the study are extensively reported in [2, 3]. The configurations of the URM houses Model U1 and Model U2 are based on the building TUD_BUILD-1 [2] and TUD_BUILD-2 [3] tested at TU Delft. Although Model U1 completely resembles TUD_BUILD-1, Model U2 differs from TUD_BUILD-2 for the masonry type. Both Model U1 and Model U2 are based on CS brick masonry.

The house TUD_BUILD-1 tested at TU Delft consists of CS brick masonry walls (inner leaf) and concrete floor. As mentioned before, the piers are connected to the transversal walls via a running bond. The piers have a limited connection with the concrete floors, meaning that the piers do not support the weight of the concrete floors. The weight of the concrete floors is fully taken by the transversal walls only. All these features are taken into consideration in the finite element models of both Model U1 and Model U2. Both, the tested built specimen (TUD_BUILD-1) and finite element models (Model U1 and Model U2) do not include soil structure interaction, spandrels, roof and the outer leaf of the cavity walls.

Section 2.1 and 2.2 discuss the finite element modelling technique (geometry and finite element discretization) of Model U1 and Model U2, respectively. Section 2.3 discusses the material properties and material model adopted in the analyses.

2.1 Unstrengthened Building Model U1

2.1.1 Geometry of Model U1

The finite element model of the unstrengthened building Model U1 is shown in Figure 2.1. The finite element model adopted in this study is similar to the finite element model proposed by [4] during the MSc Thesis at TU Delft. The load bearing transversal walls span along the global y-direction and support the weight of the concrete floors. It is evident from Figure 2.1 that the piers are of different size. The wider pier (Pier 1) has a width of 1100 mm and the narrow pier (Pier 2) has a width of 600 mm. The total height of the model is 5300 mm, with the inter-storey height of 2700 mm (first floor) and 2600 mm (second floor). The total width of the model (global x-direction) is 5400 mm.

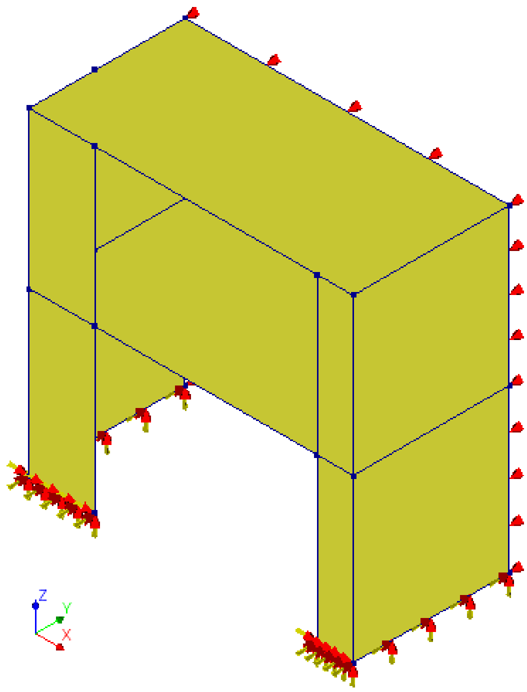

Figure 2.1 Finite element model of house (after the use of symmetry)

As the geometry of the tested building is symmetric along the global y-direction and the study only includes the loading in global x-direction, only half of the structure is modelled, as shown in Figure 2.1. Thus, the length of the model (global y-direction) is equal to 2600 mm. The symmetry of the house model is used to simplify the numerical modelling and reduce the computational cost.

The base of the model is fully restrained to simulate the testing conditions. Similarly, the displacement in the global y-direction of all the edges at the symmetric end (transversal walls and concrete floors) is also restrained. The discussed boundary conditions are clearly shown in the finite element model presented in Figure 2.1.

The use of running bond between the transversal walls and piers allows to model the connection as rigid in the finite element model. Therefore, the transversal walls and the piers share the same nodes. In the tested specimen, the concrete floors on both the levels rest on the transversal walls (that are loadbearing walls). Therefore, to simulate that condition, the edges of the concrete floors and transversal walls in both the floor levels are fully connected.

As the piers in Model U1 span over two floors and have limited connection with the concrete floors, the connection between piers and concrete floor need more detail in the finite element model. In the tested specimen, horizontal anchors are used to connect the concrete floor of the first level to the piers. The anchors are able to transfer the axial force between the connected components in the normal direction (global y-direction) but no significant shear force is transferred in the horizontal direction (global x-direction) and vertical direction (global z-direction). Therefore, interface element with stiffness defined only in the y-direction is used between the concrete floor at the first floor level and piers to imitate this feature in the numerical model.

The concrete floor at the second floor level laid is directly on top of the transversal walls and it is subsequently connected to piers through mortar joints. This means the connection between the concrete floor and piers at second floor level can be assumed to be relatively stiff after the self-weight phase. In the finite element analyses, the self-weight of the concrete floor at each floor is applied as an equivalent line load on the top of the transversal walls. Therefore, considering all the situations, it would be sufficient to model full connection between the top of the piers and the concrete floor at the second floor level to allow the load redistribution during the analysis.

2.1.2 Finite Element Discretization

The masonry walls and the concrete floors in the finite element model are modelled using 8 noded curved shell elements. The eight-noded curved shell element (CQ40S) is based on quadratic interpolation and reduced 2x2 Gauss Integration scheme. A 7-point Simpson integration scheme is used over the thickness (higher than default 3 point integration scheme) to decently capture the out of plane deformation and cracks.

The mesh size adopted during the analysis is 200 mm x 200 mm. The thickness of concrete floors and masonry walls used in the finite element model is consistent with the tested specimen. Table 2.1 summarizes the element type and properties used in the model.

Table 2.1 Summary of finite elements used in the house model

	Masonry Wall	**Concrete Floor**
Element Type	Regular Curved Shell Elements (CQ40S)	Regular Curved Shell Elements (CQ40S)
Integration Points	2 x 2 x 7	2 x 2 x 7
Mesh Size	200 mm	200 mm
Element Thickness	102 mm	165 mm

The interface connection between the piers and the concrete floor at the first floor level is modelled using 3D line interface elements. The interface element adopted in the finite element model (CL24I) is a 6-noded line interface element with quadratic interpolation scheme. The thickness of the interface is equal to the concrete floor thickness. The element properties of the interface is summarized in Table 2.2.

Table 2.2 Summary of interface connection

	Pier – Floor Connection (Interface)
Element Type	6 Node 3D Line Interface (CL24I)
Interpolation Scheme	Quadratic
Integration Points	3 + 3
Mesh Size	200 mm
Element Thickness	165 mm
Element Shape	Flat

2.2 Unstrengthened Building Model U2

As mentioned earlier, the only difference between Model U1 and Model U2 is the vertical span of the piers. Therefore, the finite element model of U2 is similar to the finite element model of U1 except the connection between the piers and the concrete floor at the first floor level. As the self-weight of the concrete floor at each floor is applied as an equivalent line load on the top of the transversal walls, and the connection between the concrete floor and pier at each floor level can be assumed to be relatively stiff after the self-weight phase, it would not be necessary to model the connection between piers and concrete floors in Model U2. Therefore, full connection is assumed between the piers and the concrete floors in the finite element model of Model U2.

2.3 Material Properties and Constitutive Laws

The masonry walls in the finite element models are modelled using Engineering Masonry Model (EMM). EMM is an orthotropic constitutive model that considers tensile, shear and compression failure modes. The values of the material properties used to define EMM are presented in Table 2.3. The values of the elastic moduli, compressive strength and shear properties of the CS brick masonry are obtained from the companion tests. The remaining material properties are obtained from the calibration and/or equations available in the literature [4].

Table 2.3 Material properties used to define masonry walls

Property	Parameter			Unit	Value
Elasticity	Young's Modulus	Perpendicular to head joint	E_x	MPa	2212
		Perpendicular to bed joint	E_y	MPa	3264
	Shear Modulus		G_{xy}	MPa	1306
	Mass Density		ρ	Kg/m^3	1805
Cracking	Tensile Strength	Normal to bed joint	f_{ty}	MPa	0.19
	Tensile Fracture Energy		G_{ft}	N/mm	0.0127
	Angle between stepped diagonal crack and bed joint		θ	rad	0.792
Crushing	Compressive Strength		f_c	MPa	5.84
	Fracture Energy in Compression		G_{fc}	N/mm	17.39
	Factor to Strain at Compressive Strength		n		5
	Unloading Factor		λ		0
Shear Failure	Friction Angle		φ	rad	0.406
	Cohesion		f_{vo}	MPa	0.14

The concrete floors in the finite element model are assumed to behave linear elastic. The material properties of the concrete floor adopted in the model are listed in Table 2.4. As the self-weight of the concrete floor on each floor level is applied as equivalent line load on the top of the transversal wall at respective floor level, the concrete has a mass density equal to zero. The equivalent line load that is applied on the transversal wall is calculated using the density equal to 2400 kgm^{-3}.

Table 2.4 Material properties of concrete

Property	Parameter		Unit	Value
Linear Elastic	Young's Modulus	E_s	MPa	35500
	Poisson's Ratio	ν		0.2
	Mass Density	ρ	Kg/m^3	-

The interface connection used in Model U1 between the piers and the concrete floor at the first floor level is defined using linear elastic properties. The normal stiffness of the interface in y-direction is estimated using the following relation:

$$E_{n,y} = \frac{100\,E}{l_{adj}}$$

Where E is the stiffness of the connected element (masonry in this case as it is weaker than concrete) and the length of the adjacent element, i.e. 200 mm (mesh size). The interface properties are summarized in Table 2.5.

Table 2.5 Material properties of interface connection

Property	Parameter		Unit	Value
Linear Elastic	Normal Stiffness	$E_{n,y}$	N/mm^3	1632
	Shear Stiffness	$E_{t,x}$	N/mm^3	0
		$E_{t,z}$	N/mm^3	0

3 Nonlinear Pushover Analysis of Unstrengthened Buildings

Monotonic nonlinear pushover analyses (NLPO) are carried out on the finite element models, Model U1 and Model U2. The analyses are carried out along both positive and negative x-direction. This chapter discusses the loading method and analysis procedures at the beginning. Later, the results of the numerical model (Model U1) are compared with the experimental results of TUD_BUILD-1. The results of the pushover analyses of both Model U1 and Model U2 are discussed in terms of the capacity curve, damage level identification and drifts.

3.1 Loading Method and Analysis Procedure

A pushover analysis that simulate the mode of application of the load in the experiment is performed for the finite element analyses. A displacement control loading is adopted. At the same time, the same equivalent forces on both the floors is maintained during the analyses.

The loading is applied through vertical rigid steel beam that is connected to the floors through rigid links. This procedure was used in the nonlinear pushover analysis performed on [4]. The vertical rigid steel beam is positioned 1100 mm inward from the façade. A prescribed deformation in x-direction is applied at the midpoint of the rigid steel beam. The boundary condition prescribed in the loading point is such that the rigid steel beam can rotate around the point on the application of the lateral deformation. This generates two equal forces at both ends connected to the floors through rigid links.

The loading point i.e. the middle of the vertical steel beam is restrained in z-direction to prevent vertical motion and in x-direction as a method to apply prescribed deformation in DIANA FEA. In addition, the rotation around z axis is also restrained to prevent the torsion of the beam. The connection of the steel beam and rigid links is restrained in y-direction, thus allowing the beam to rotate only in the xz-plane. The applied boundary condition for this loading method is shown in Figure 3.1.

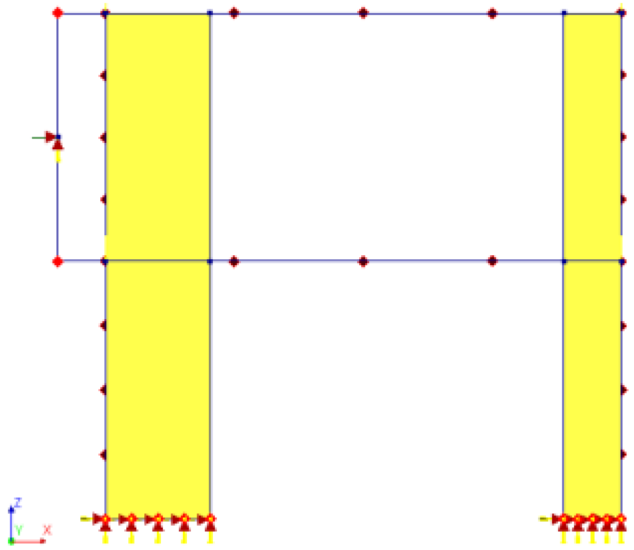

Figure 3.1 Front view of the house model showing boundary conditions and the loading method

The nonlinear pushover analysis is performed for positive and negative displacements in x-direction. First, the equivalent line load which represents the self-weight of the concrete is applied. It is followed by the self-weight of the remaining components (i.e. transversal walls and piers) and then by the monotonic pushover. The equivalent line load and self-weight constitutes the first phase of the analysis and the monotonic pushover constitutes the second phase. The equivalent line load and self-weight are applied in 10 load steps each and the monotonic lateral load is applied in 300 load steps, 0.35 mm per step up to 105 mm for both the directions.

The nonlinear pushover analysis is performed considering both physical and geometrical nonlinearity. The regular Newton Raphson iteration method is adopted with the line search option. The maximum number of iteration is limited to 100 per load step and the satisfaction of either displacement norm or the force norm is considered sufficient for the convergence. The analysis procedure is summarized in Table 3.1. It must be noted that the numerical model is being pushed to 150% of the maximum displacement observed in the test.

Table 3.1 Analysis procedure of the monotonic pushover analysis

Load Steps	Equivalent Line Load	10
	Self – Weight	10
	Monotonic Loading	300 Steps (0.35 mm per Step)
Iteration Method	Maximum Number of Iterations	100
	Iteration Method	Regular Newton – Raphson
	Line Search	Yes
Convergence Criteria	Satisfy either displacement norm (tolerance 0.01) or force norm (tolerance 0.01)	

3.2 Results of Model U1

The results of the monotonic pushover analysis in (both positive and negative) global x-direction are discussed in this section. Section 3.2.1 discusses the behaviour of Model U1 in terms of the capacity curves. Along with the force-displacement curve obtained from NLPO, the bilinear curve produced using the guidelines of NPR [5] is also presented in this section. Then, Section 3.2.2 presents the crack patterns observed in the model. The Damage Levels (DL) are defined in Section 3.2.3 and finally section 3.2.4 discusses the drifts observed in the structure. The numerical results obtained from the finite element analyses are also compared with the experimental results obtained from the house tested in TU Delft, TUD_BUILD-1 [2].

3.2.1 Capacity Curves

The result of the monotonic pushover analyses performed on Model U1 is shown in Figure 3.2. The base shear force plotted in the figure is equal to the double of the reaction force at the loading point of the rigid steel beam. Since the symmetry model was used in the finite element modelling, the reaction force at the loading point was doubled to obtain the base shear force for the full model. The second floor displacement plotted in the graph is extracted from the node shared by the rigid link and the concrete floor at the second floor level. The figure also shows the comparison of the numerical results and the results of the experiment.

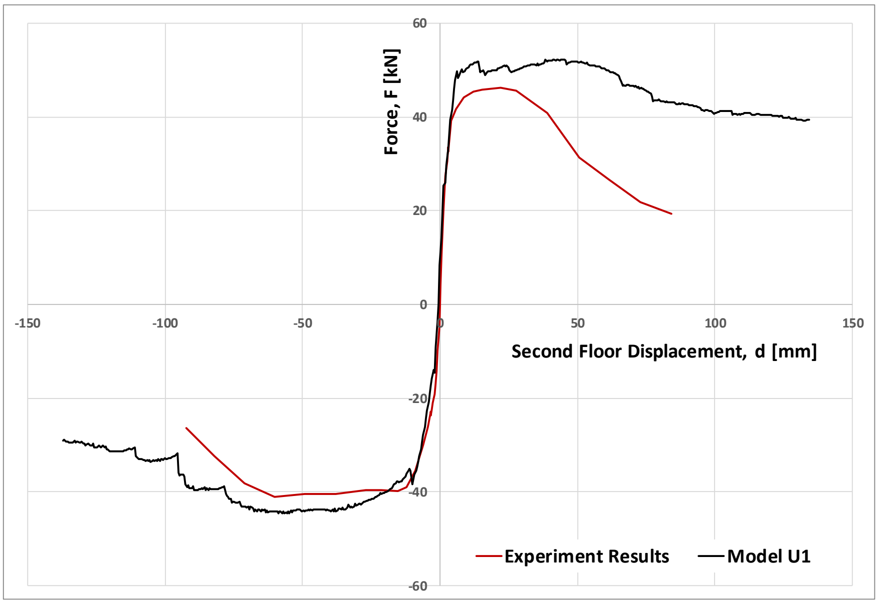

Figure 3.2 Capacity curve of Model U1

It can be observed in the figure that at the initial stage, the stiffness of the numerical model is almost identical to that of the tested model. The finite element model overestimates the maximum shear force of the house compared to the experimental results. Also, it is evident from the figure that the shear force in the numerical model reduces at a slower rate compared to the experimental results. This implies that the numerical model is more ductile than the tested specimen. The peak force obtained from the numerical model is equal to 52.3 kN which is 12 % higher than the one obtained from the tested model.

The nonlinear pushover capacity curve is transformed into equivalent SDOF bilinear curve according to the procedure described in [5]. The first point is obtained by using the condition that the bilinear curve passes through the point of the curve characterized by 60% of the maximum base shear force. Then the horizontal branch of the curve is estimated according to the equal energy rule i.e. the area under the NLPO capacity curve and bilinear curve are equal to each other. The ultimate displacement in the curve is determined as the point where interstorey drift reaches 1.5%. As the base shear force doesn't reduce to 80% of the maximum base shear force until the ultimate displacement capacity, the area under the curve is calculated up to the ultimate displacement capacity itself during the bilinearisation process. Figure 3.3 presents the pushover capacity curve and corresponding bilinear curve in both positive and negative direction.

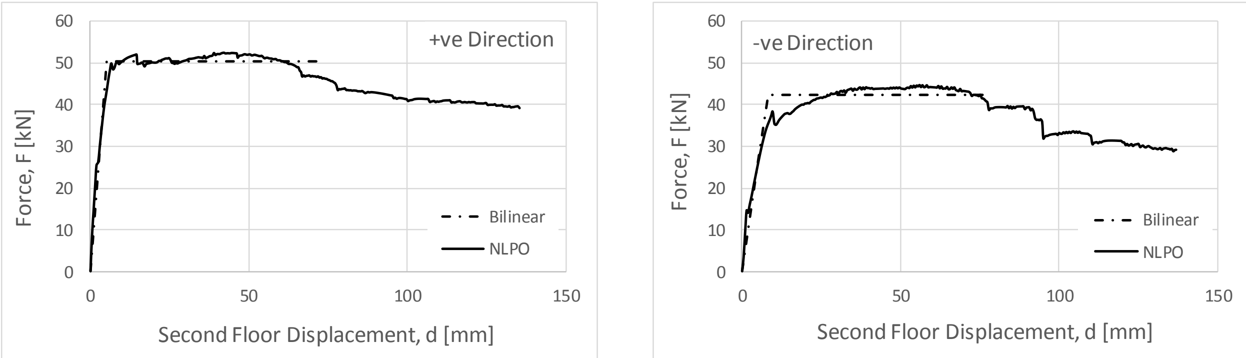

Figure 3.3 Bilinear capacity curve of Model U1

3.2.2 Crack Pattern

The crack pattern observed during the positive monotonic pushover analysis is discussed first. This is followed by the discussion of the crack pattern observed in the negative direction. The crack plots observed in the model are presented in terms of the crack strain. The crack width can be reasonably estimated by multiplying the crack strain with the element size i.e. 200 mm. According to the material properties that have been used for the masonry walls, the cracks with crack strain higher than 0.0007 are considered fully open.

The first cracks that are observed in the house model are located at the top and the bottom of the piers. These cracks continue to expand and the rocking mechanism is observed on both wide and narrow piers when the base shear force and the second floor displacement are equal to 43.62 kN and 5.19 mm, respectively. The crack pattern observed at this stage is shown in Figure 3.4. It can be noted in the figure that in addition to the cracks in piers, the crack openings are also found in the transversal walls along the bottom and the first floor level.

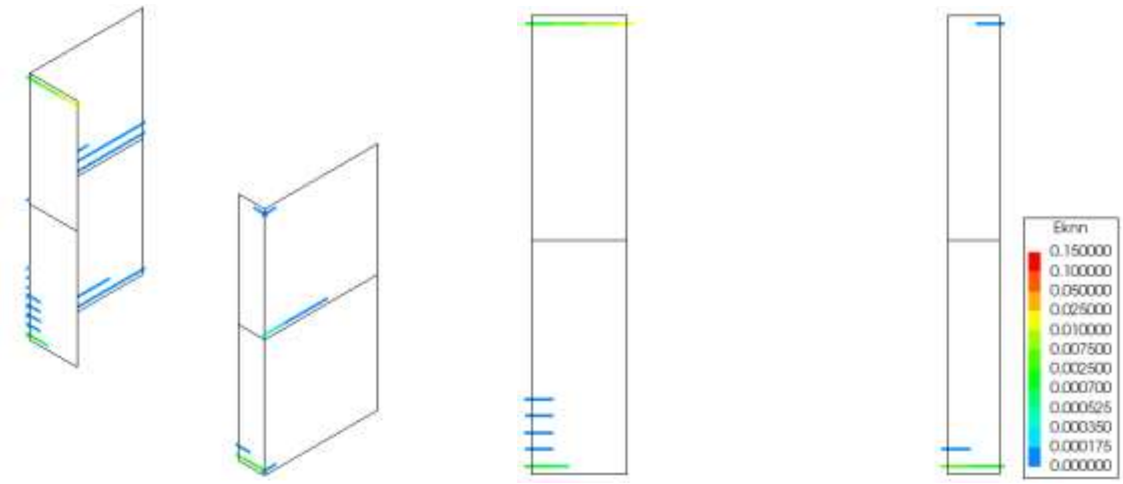

Figure 3.4 Crack pattern showing the beginning of rocking mechanism in piers when loaded in positive direction

Although the position of the main crack remain constant at the top and bottom of the pier, they continue to expand to other areas of the piers and transversal walls. The crack openings are observed in the middle of the wide pier at ground floor when the base shear force and the lateral displacement of second floor are equal to 49.66 kN and 14.77 mm, respectively. The normal crack strain of the cracks observed at this stage are shown in Figure 3.5. The shear cracks in wide pier continue to increase with the increase in the lateral displacement. Figure 3.6 shows the normal crack strain observed in the model when the base shear force and second floor displacement are equal to 50.26 kN and 60.70 mm, respectively. It should be noted that this point lies in the post peak region in the pushover capacity curve.

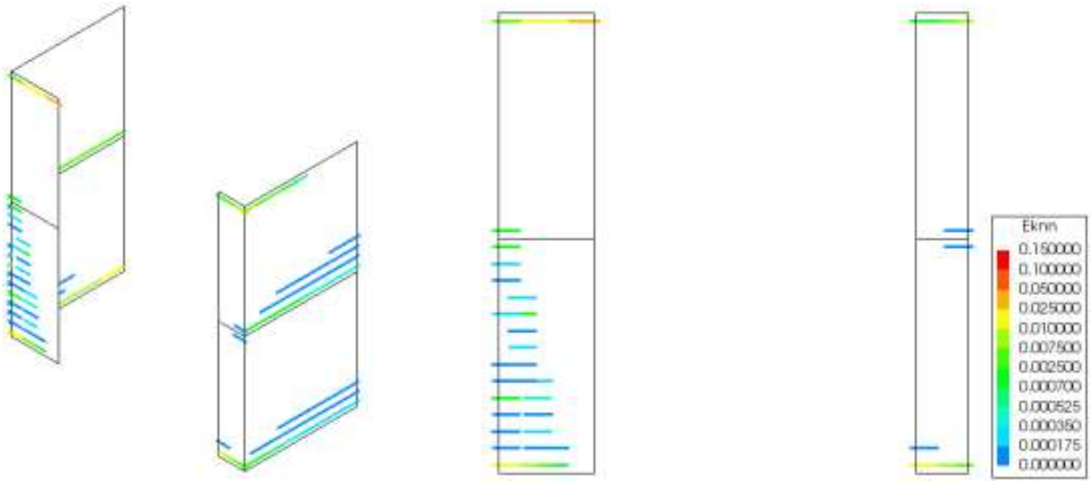

Figure 3.5 Normal crack strain observed when cracks spread along the height of wide pier in ground floor

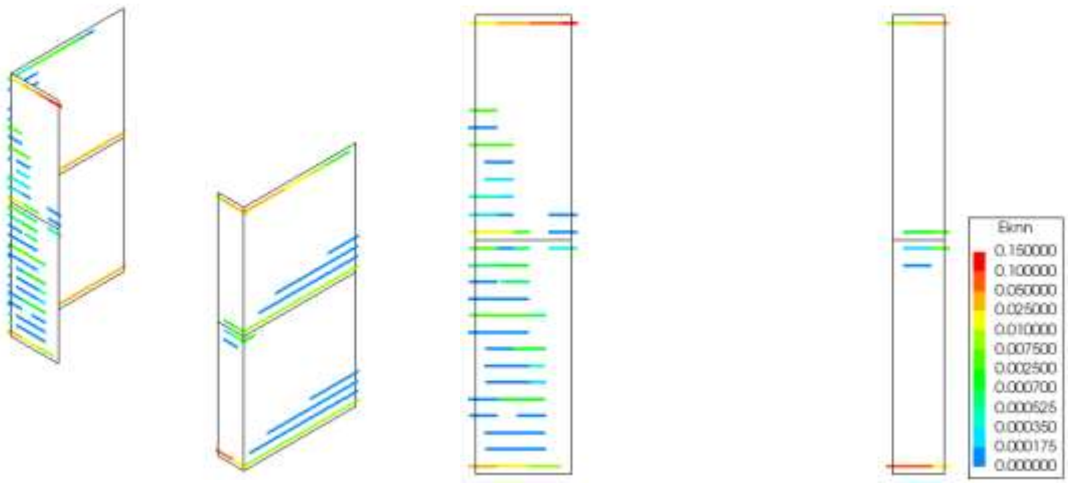

Figure 3.6 Normal crack strain when the wide pier in ground floor is severely damaged

In addition to the three different stages discussed above, it is also important from the perspective of damage evolution to observe the stages where the global drift and the interstorey drift reach (GDL) 0.8% and (IDL) 1.5%, respectively. The global drift and interstorey drift are defined as the ratio of second floor displacement to the total height of the building, and the ratio of the relative floor displacement to the height of the respective floor. Figure 3.7 shows the normal crack strain observed when GDL is reached. Similarly, Figure 3.8 shows the normal crack observed when IDL (first floor level) is reached.

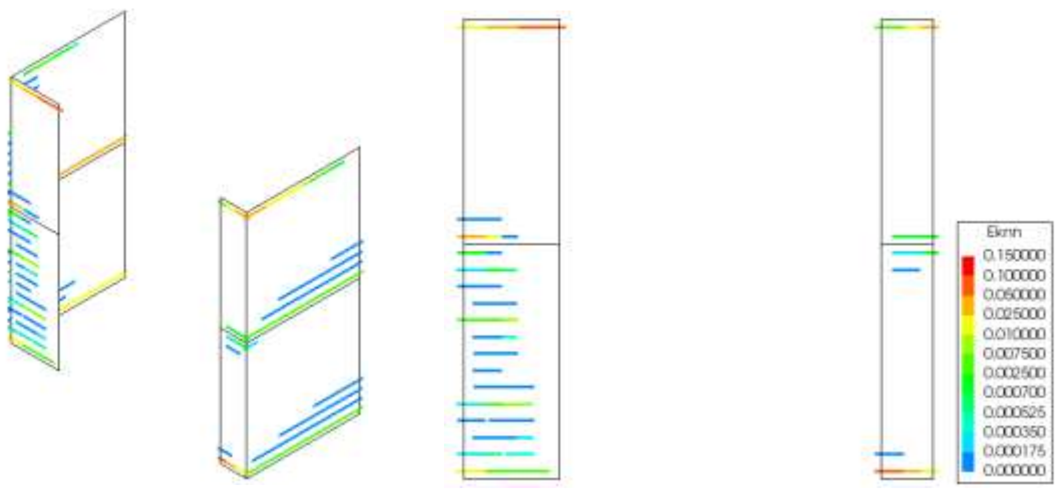

Figure 3.7 Normal crack strain when global drift reaches 0.8%

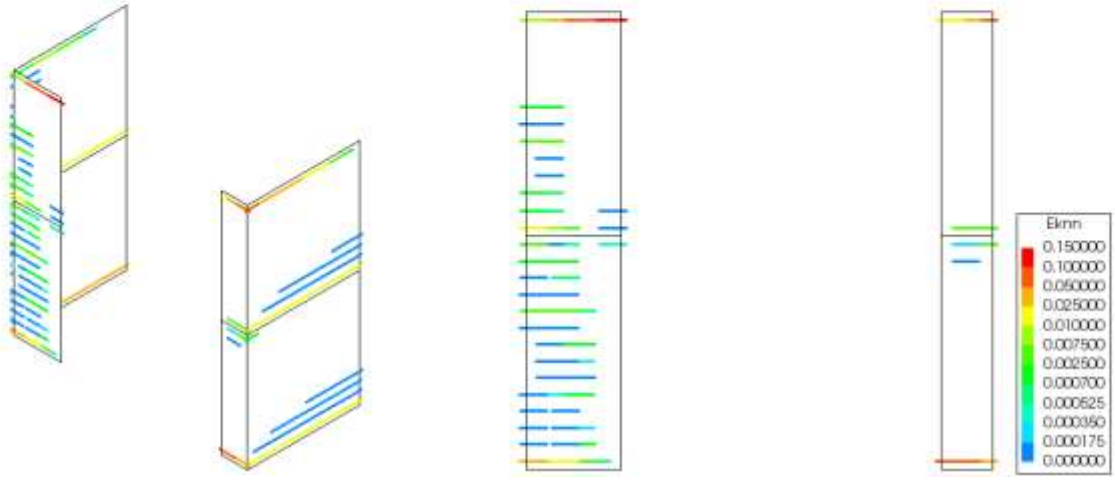

Figure 3.8 Normal crack strain when interstorey drift of ground floor reaches 1.5%

Now, Figure 3.9 – Figure 3.12 represent the crack pattern observed in the house model when pushed in the negative direction. As observed in the positive direction, the position of the main cracks are at the top and the bottom corner of the piers. Figure 3.9 shows the stage just before the rocking mechanism starts in the piers. The base shear force and the second floor displacement at this stage are 27.78 kN and 5.56 mm (in negative direction), respectively. Similarly, Figure 3.10 shows the normal crack strain when the cracks start to open in the narrow pier around the first floor level. Then, Figure 3.11 shows the normal crack strain when the connection of the narrow piers and the first floor is fully cracked. Finally, Figure 3.12 shows the normal crack strain when the interstorey drift reaches (IDL) 1.5% at the first floor level. The shear crack strains in all previously discussed stages are shown in Appendix A.

The rocking mechanism, localisation of flexural cracks at the corners of the piers, and the cracks of the transversal walls observed at bottom and first floor level simulate accurately the observed experimental behaviour. Additionally, the numerical model also reproduced the asymmetric crack pattern and behaviour of the house when loaded in different direction, as observed in the tested specimen TUD_BUILD-1. Similarly, toe crushing is also observed at the bottom right end of the wide pier when loaded in positive direction, and at the bottom left end of the narrow pier when loaded in the negative direction. However, the absence of the evident diagonal crack pattern in the transversal wall and the wide piers in the numerical model highlight the major difference between the finite element model and the tested house.

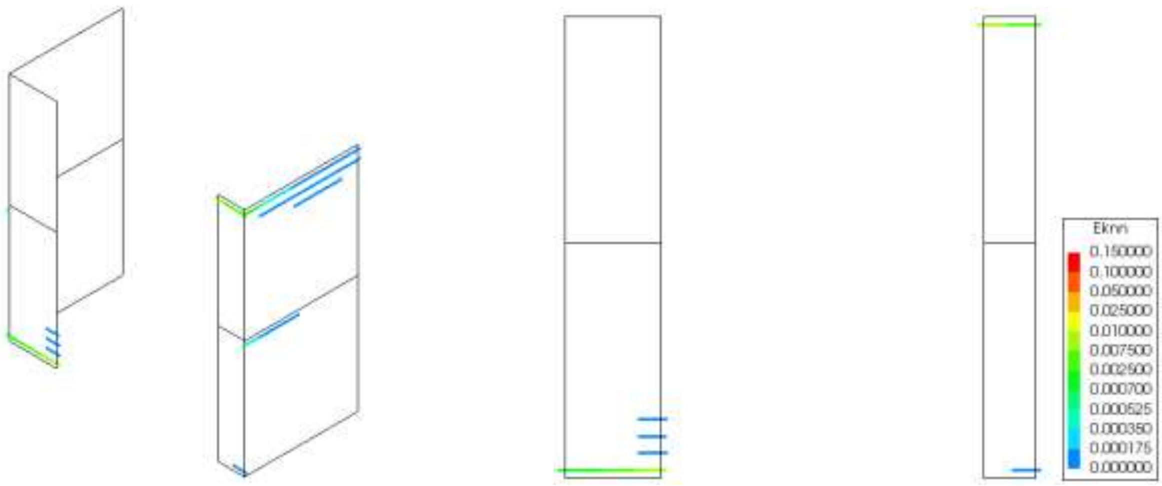

Figure 3.9 Normal crack strain when rocking mechanism is observed in piers when loaded in negative direction

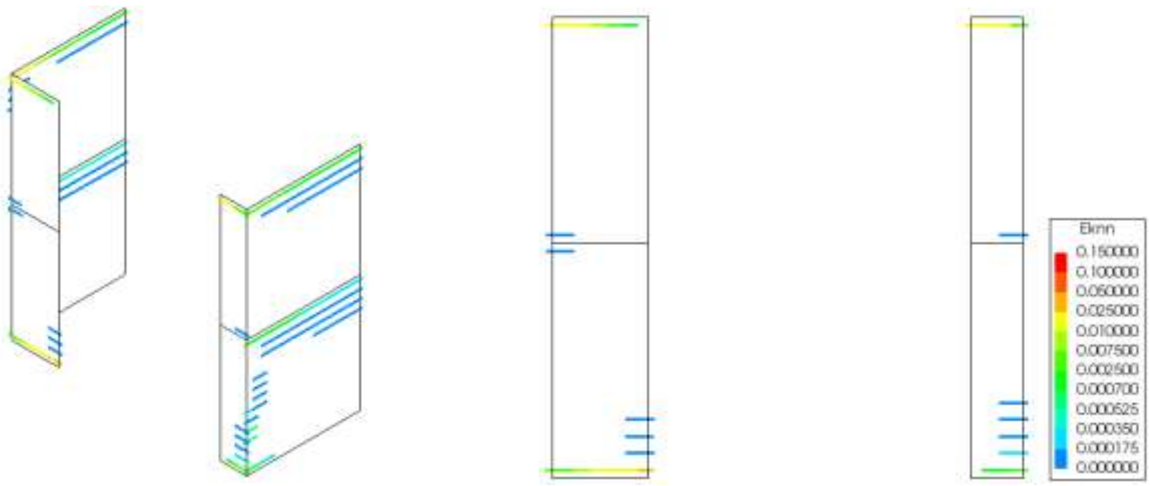

Figure 3.10 Normal crack strain when cracks appear between connection of narrow pier and floor

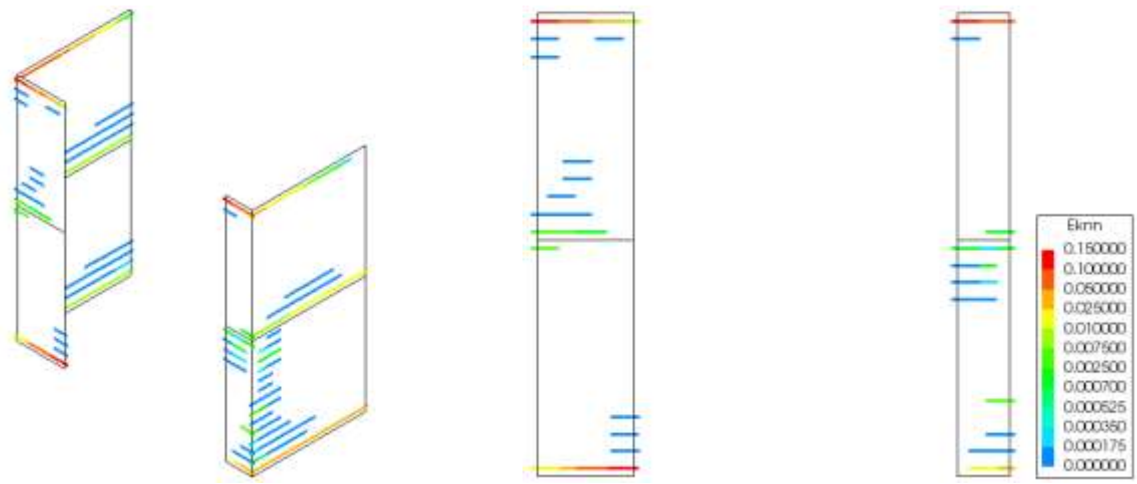

Figure 3.11 Normal crack strain when the connection between the narrow pier and first floor is fully cracked

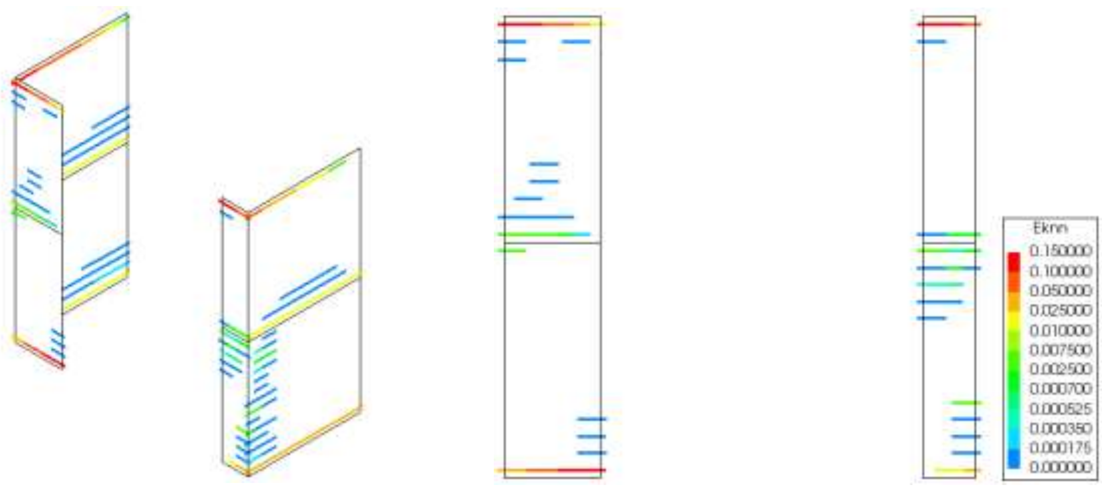

Figure 3.12 Normal crack strain when IDL is reached (loaded in negative direction)

3.2.3 Damage Level Identification

This research aims to study the effect of retrofitting methods and materials in terms of the improvement in the seismic capacity (increase of resistance and deformability) and the delay of the damage. Therefore, as a part of the study, the damage levels are identified first in the unstrengthened case. The four damage levels, (DL1, DL2, DL3 and DL4) are identified on the basis of the damage evolution in the house model.

The damage level DL1 which represents first occurrence of a visible crack corresponds to the point when the rocking mechanism forms in the piers. The DL1 in positive and negative direction are represented by the crack patterns shown in Figure 3.4 and Figure 3.9, respectively. The damage level DL2 represents minor damage. For positive loading it corresponds to the point when cracks appear in the middle of the wide pier. This is the stage when shear cracks appear in the middle of the wide pier at ground floor. The crack pattern shown in Figure 3.5 represents DL2 in positive direction. In the negative direction, DL2 corresponds to the point when shear cracks appear at the connection of the narrow pier and the first floor. The crack pattern shown in Figure 3.10 represents DL2 in negative direction. The damage level, DL3 which represents moderate structural damage is identified as the point when significant damage is observed in the wide pier when loaded in positive direction. This is represented by the crack pattern shown in Figure 3.6. In the negative direction, DL3 is identified as the point when the connection between narrow pier and the first floor is fully cracked. Thus, the crack pattern shown in Figure 3.11 represents DL3 in negative direction. The damage level DL4 which represents near collapse (NC) state is identified as the point when there is either 50% drop in the maximum base shear force or the interstorey drift reaches 1.5%. As the 50% drop in the shear force is not observed in the numerical model, the point where IDL is reached is identified as DL4. The crack pattern shown in Figure 3.6 and Figure 3.12 represent DL4 in positive and negative direction, respectively. The identified damage levels are marked in the capacity curve and is shown in Figure 3.13. The points when GDL is reached in either direction are also marked in the pushover capacity curve.

In addition, Table 3.2 summarizes the damage level identification, the shear force, second floor displacement, normalised base shear force (kG = V/V_{max}), the interstorey drift of the ground floor (i.e. at first floor level d_{r1}) and the global drift d_{r*} at each damage level.

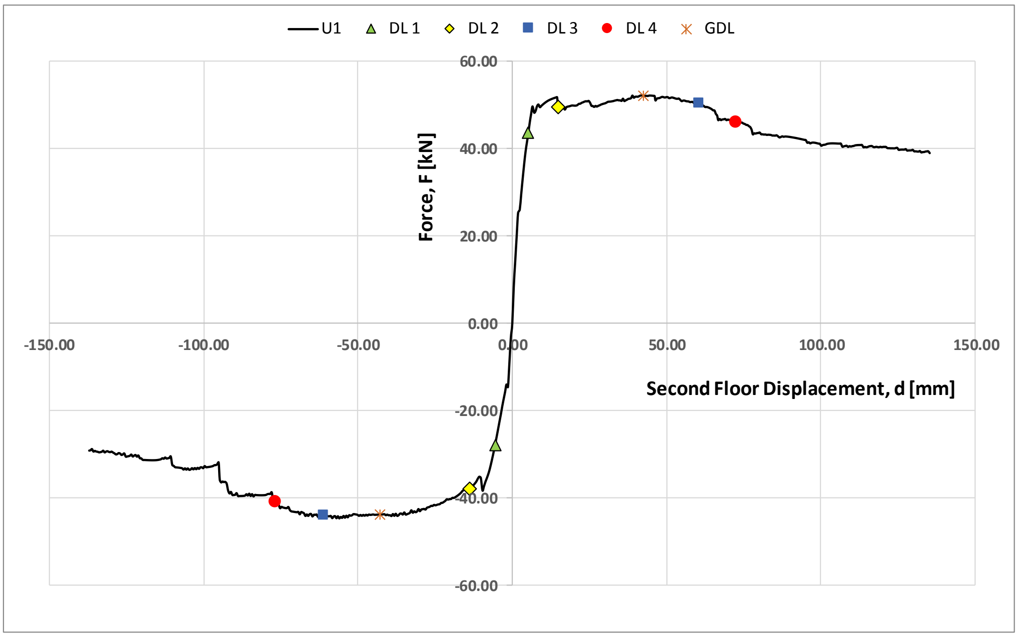

Figure 3.13 Damage levels in Model U1

Table 3.2 Summary of damage levels in Model U1

Damage Levels	Loading Direction	Observed Damage	Force	Second floor displacement	Normalised shear force	Interstorey drift	Global drift
			F	d2	k_G	d_{r1}	d_{r*}
			kN	mm		%	%
DL1	Positive	Initiation of rocking mechanism in piers	43.6	5.19	0.83	0.09	0.09
	Negative	Initiation of rocking mechanism in piers	-27.8	-5.56	0.62	-0.10	-0.10

DL2	Positive	Shear crack appears in the middle of wide pier in ground floor	49.7	14.77	0.95	0.28	0.28
	Negative	Crack appear in connection of narrow pier and first floor	-37.9	-13.92	0.84	-0.24	-0.24
DL3	Positive	Severely damaged wide pier at ground floor	50.3	60.70	0.96	1.25	1.15
	Negative	Connection between narrow pier and first floor fully cracked	-44.1	-61.12	-0.98	-1.18	-1.15
DL4	Positive	IDL is reached	46.4	72.24	0.89	1.50	1.36
	Negative	IDL is reached	-40.8	-77.09	0.91	-1.50	-1.45

3.2.4 Drifts

The interstorey drift observed in the numerical model is presented in Figure 3.14. As mentioned above, the interstorey drift is calculated as the ratio of the relative floor displacement and the interstorey height (2700 mm for the ground floor and 2600 mm for the second floor). The damage levels identified above in Section 3.2.3 are also plotted in the figure. It can be seen that the interstorey drift of two floors are same at the initial stage and then tend to deviate later especially in the positive direction after the damage level DL2 is reached. It is observed that after the growth of shear cracks in the middle of wide pier at ground floor, damage tends to localize in the wide pier at ground floor. This could be the reason for the higher drift of ground floor compared to the first floor in the positive direction. Similarly, observing the crack patterns presented in Figure 3.9 - Figure 3.12 it can be noted that, also when loaded in negative direction, the cracks are more in ground floor than the first floor. However, the difference is not as much as in the positive direction thus justifying the lesser difference between the interstorey drifts in the negative direction. The displacement profile of the house at different damage levels, the points when GDL and IDL is reached is shown in Figure 3.15.

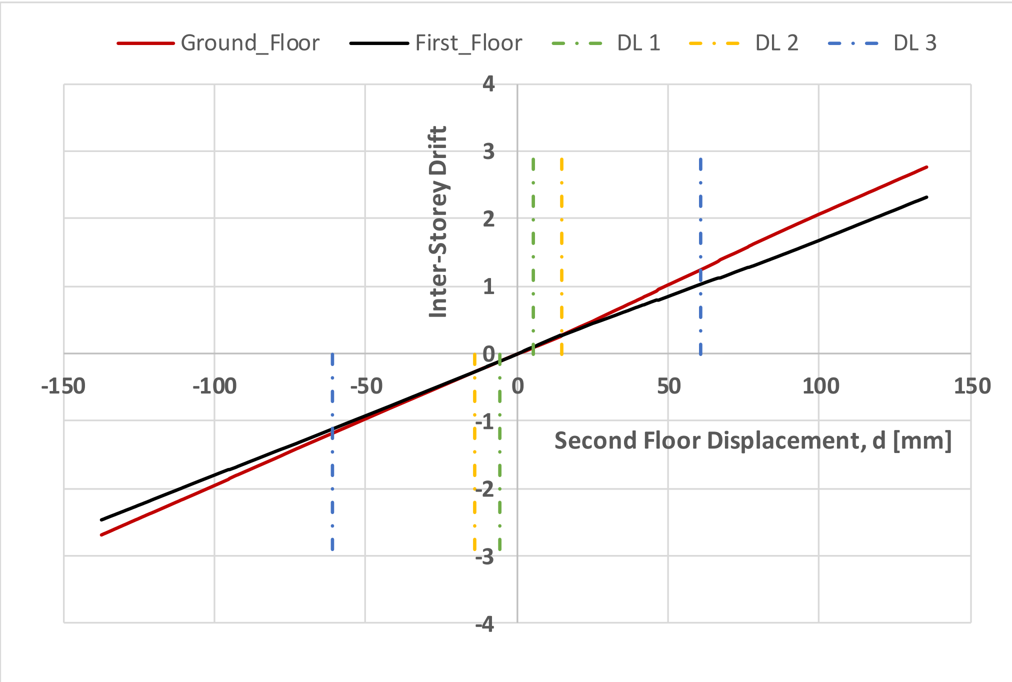

Figure 3.14 Interstorey drift (%) of ground floor and first floor of Model U1

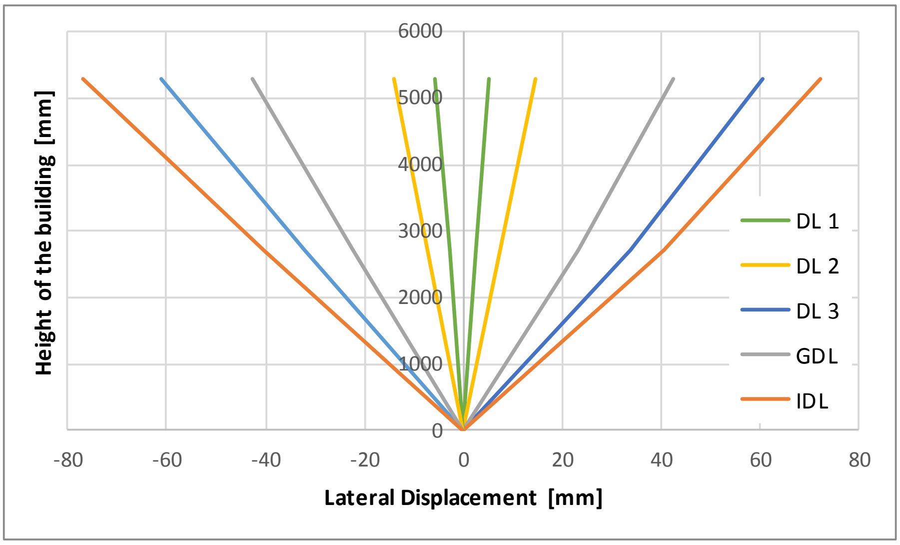

Figure 3.15 Displacement profile of Model U1 at different damage levels

3.3 Results of Model U2

This section discusses the results of the nonlinear pushover analyses performed on the numerical model, Model U2. Like in previous section, first the capacity curves are discussed. It is followed by the damage level identification and discussion of the drifts observed in the house model.

3.3.1 Capacity Curve

The pushover capacity curve of Model U2 is shown in Figure 3.23. The pushover capacity of Model U1 is plotted in the same figure to make a comparison of two different models. The only difference between two models is the span of the piers. It can be observed in the figure that the span of the pier play a crucial role in the capacity and thus the overall behaviour of the house when subjected to lateral force. The maximum base shear force is found to be 79.8 kN which is 53% higher than the one obtained from Model U1. Although the loading point in both the house models were subjected to the same lateral displacement in the analyses, it can be observed from the results presented in Figure 3.16 that Model U2 is stiffer compared to Model U1. The asymmetric behaviour of the house in different loading direction is clearly evident in Model U2 as well. The finite element results suggest that the model reaches a smaller peak load but is more ductile when laterally pushed in the negative direction.

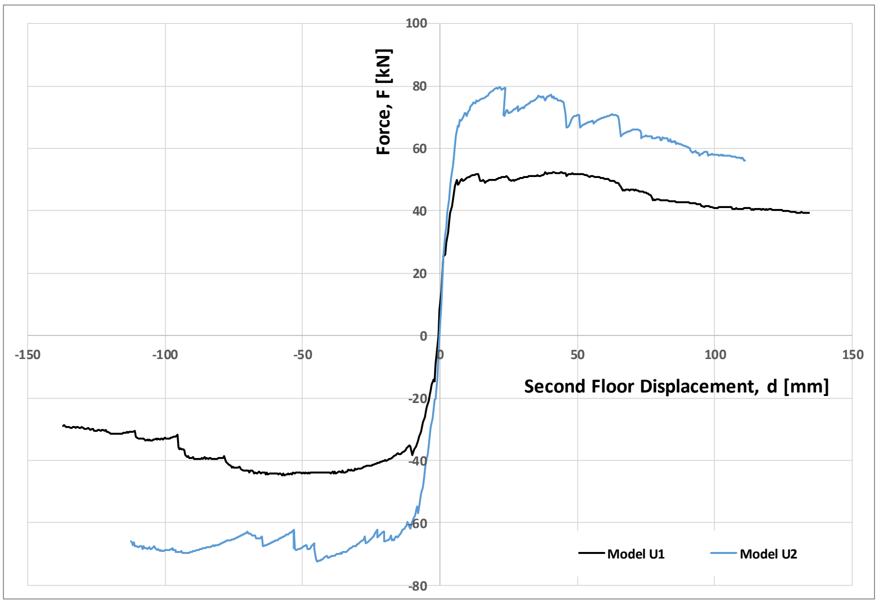

Figure 3.16 Capacity curve of Model U1 and Model U2

The pushover capacity curve obtained from finite element analyses is then converted to the bilinear capacity curve. The procedure described above in section 3.2.1 is used to produce the bilinear capacity curve for Model U2 as well. The bilinear capacity curve in each loading direction is plotted along with the respective pushover capacity curve in Figure 3.24.

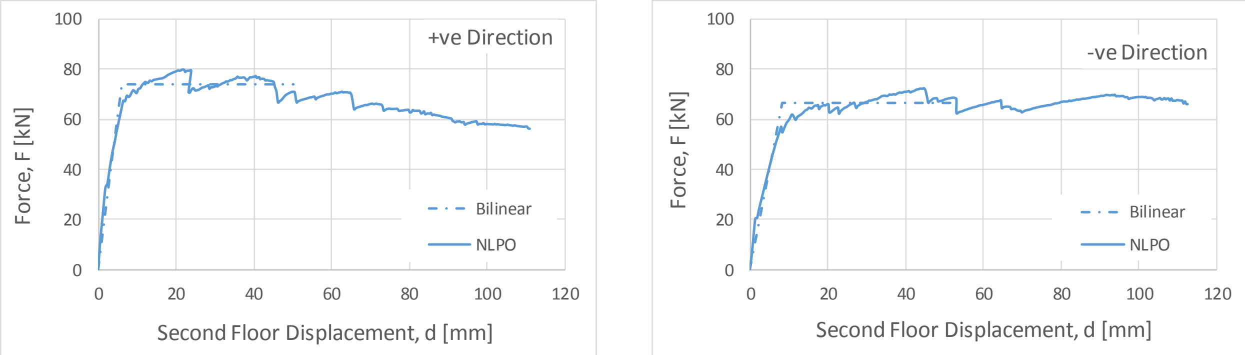

Figure 3.17 Bilinear capacity curve of Model U2

3.3.2 Damage Level Identification

The damage levels in Model U2 are identified in this section. As the damage evolution and crack pattern are different for different loading direction, the damage levels are defined separately for the two loading directions.

The damage level DL1 which represents no visible cracks is identified as the stage just before the piers have rocking mechanism. As the house is loaded in positive direction (right direction) and piers now span only over one floor, the first two piers that exhibit rocking mechanism are the wide pier in the ground floor and the narrow pier in the first floor. The base shear force and the second floor displacement obtained at DL1 are 39.2 kN and 2.85 mm, respectively. The crack pattern at DL1 when loaded in positive direction is shown in Figure 3.18. The damage level DL2 is identified as the point when cracks appear in the middle of the wide pier in the first floor. Further analysis showed that the new cracks are shear cracks. The base shear force and second floor displacement at DL2 are 70.3 kN and 9.86 mm, respectively. The normal crack strain of the cracks observed in the house at DL2 is shown in Figure 3.19.

The damage level DL3 which represents moderate structural damage is identified as the point when cracks spread almost the entire wide pier in ground floor. The shear cracks in wide pier at ground floor are fully open at this stage. The base shear force and second floor displacement at DL2 are 76.8 kN and 39.81 mm, respectively. The normal crack strain of cracks in the model at DL3 is shown in Figure 3.20. The damage level DL4 is identified as the point when interstorey drift of the ground floor reaches 1.5%. The base shear force and second floor displacement at this point are 70.8 kN and 50.22 mm, respectively. The crack pattern of DL3 and DL4 are not too different. The rocking cracks (flexural crack at corners of pier) have opened more in DL4 than DL3. The normal crack strain of the cracks visible in DL4 is shown in Figure 3.21. The shear crack strain of the cracks observed in Model U2 at DL2, DL3 and DL4 when pushed in the positive direction are shown in Appendix A.

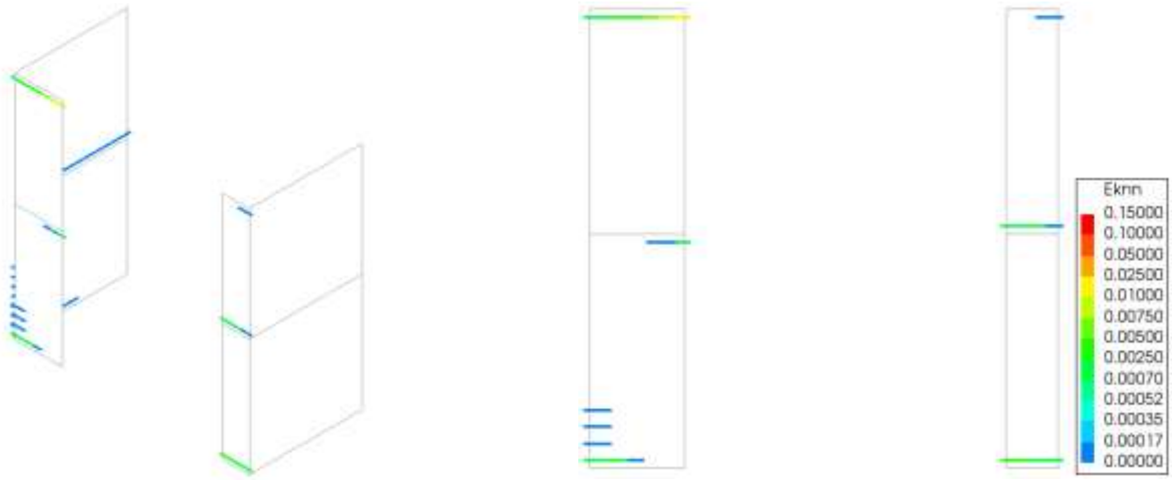

Figure 3.18 Normal crack strain at DL1 when loaded in positive direction

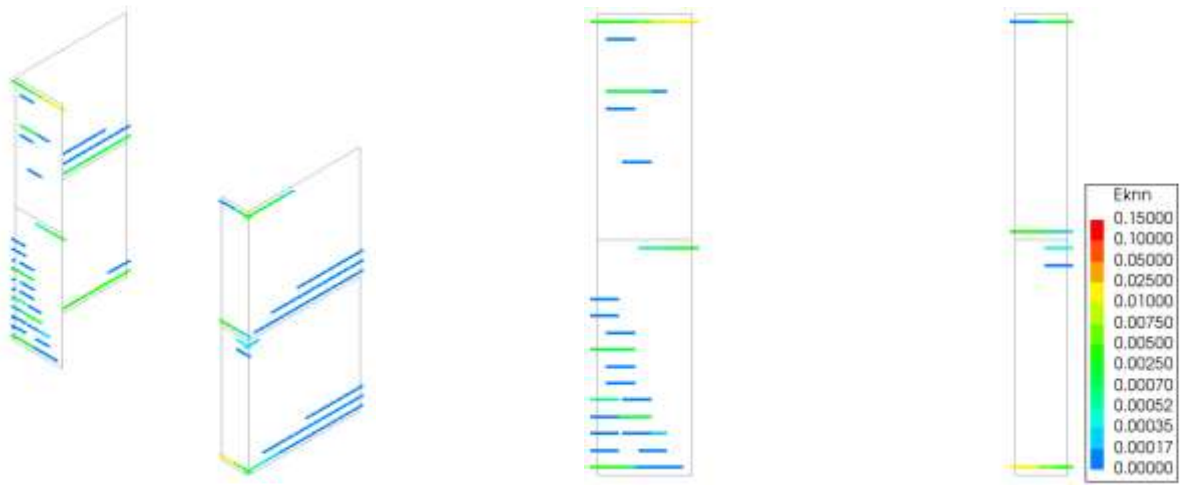

Figure 3.19 Normal crack strain at DL2 when loaded in positive direction

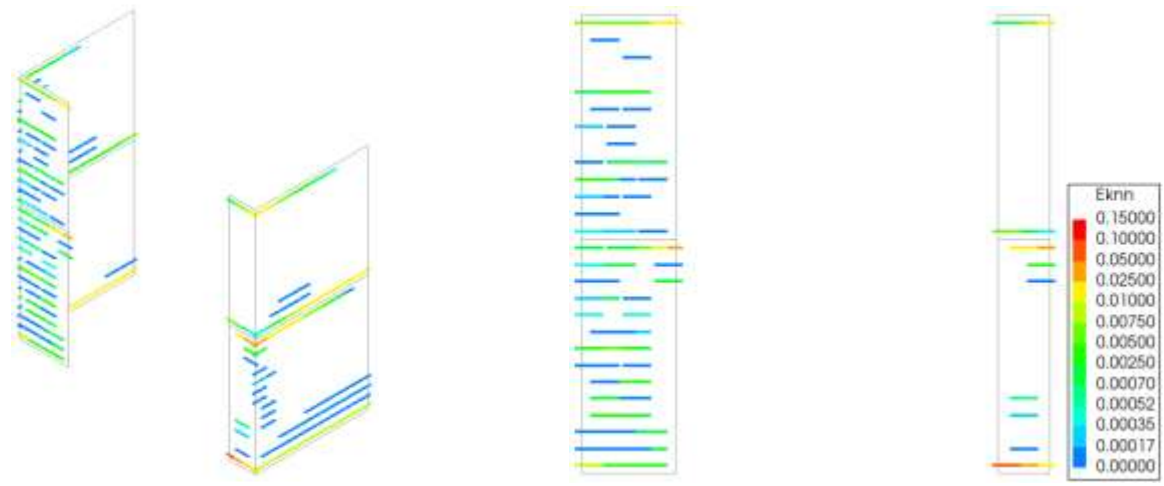

Figure 3.20 Normal crack strain at DL3 when loaded in positive direction

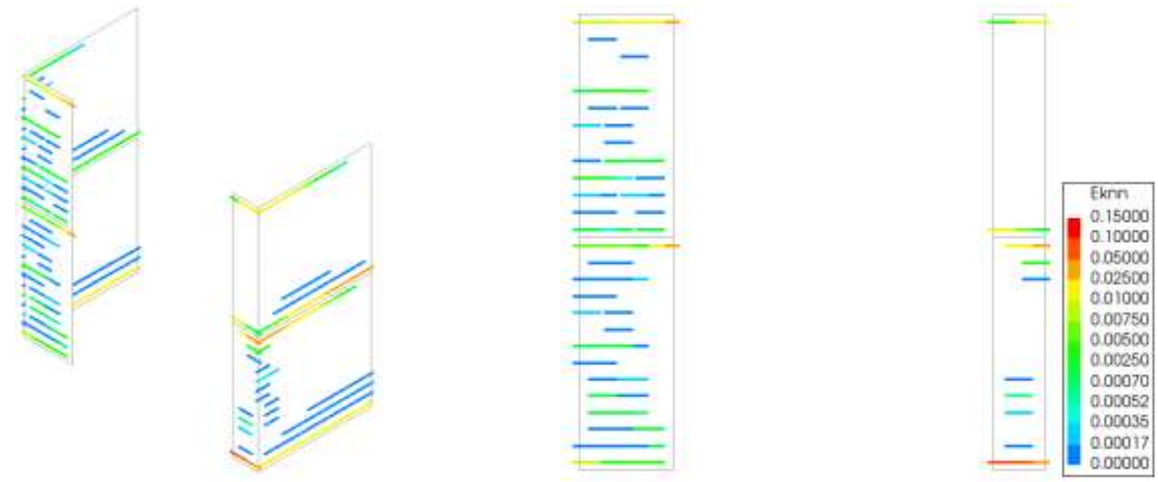

Figure 3.21 Normal crack strain at DL4 when loaded in positive direction

The damage levels in the negative loading direction are also identified with the similar procedure like discussed above. The damage level DL1 is identified as the point just before rocking mechanism is visible in the piers. As the house model is pushed in negative direction, the narrow pier at ground floor and wide pier at first floor exhibit rocking mechanism first. The cracks visible at DL1 in the negative loading direction is shown in Figure 3.22. The absolute value of base shear force and second floor displacement at this level are 40.6 kN and 4.98 mm, respectively.

The damage level DL2 is identified as the point when cracks in the wide pier at ground floor spans over almost the entire ground floor height. In addition, the cracks appear in the narrow pier at the first floor as well. Further analysis of the cracks showed that the cracks are not due to shear. The absolute value of base shear force and second floor displacement at this level are 62.2 kN and 13.44 mm, respectively. The normal crack strain of the cracks visible in DL2 level is shown in Figure 3.23. The shear crack strain is shown in Appendix A.

The damage level DL3 is identified at similar situations in both positive and negative direction. The level DL3 is identified when cracks spread almost the entire wide pier in the ground floor. The difference between the two loading direction is that the cracks appeared when loaded in negative direction is not due to shear. The absolute value of base shear force and second floor displacement at this level are 71.0 kN and 41.64 mm, respectively. The normal crack strain of the observed cracks is shown in Figure 3.24.

As in positive loading direction, the damage level DL4 is identified as the point when the interstorey drift of the ground floor reaches 1.5%. The absolute value of the base shear force and the second floor displacement at this level are 68.6 kN and 52.44 mm, respectively. The crack pattern at DL4 when loaded in the negative direction is shown in Figure 3.25.

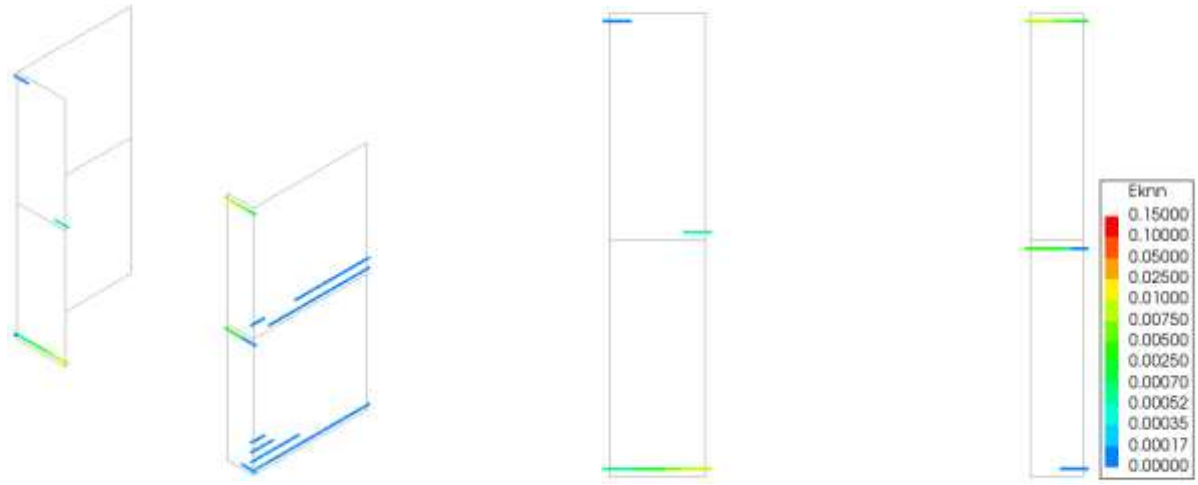

Figure 3.22 Normal crack strain at DL1 when loaded in negative direction

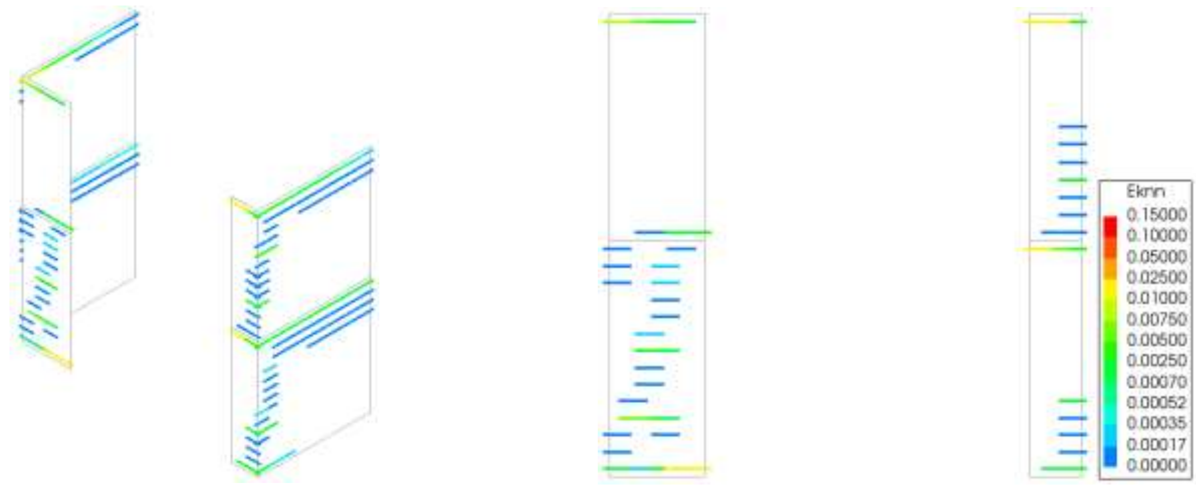

Figure 3.23 Normal crack strain at DL2 when loaded in negative direction

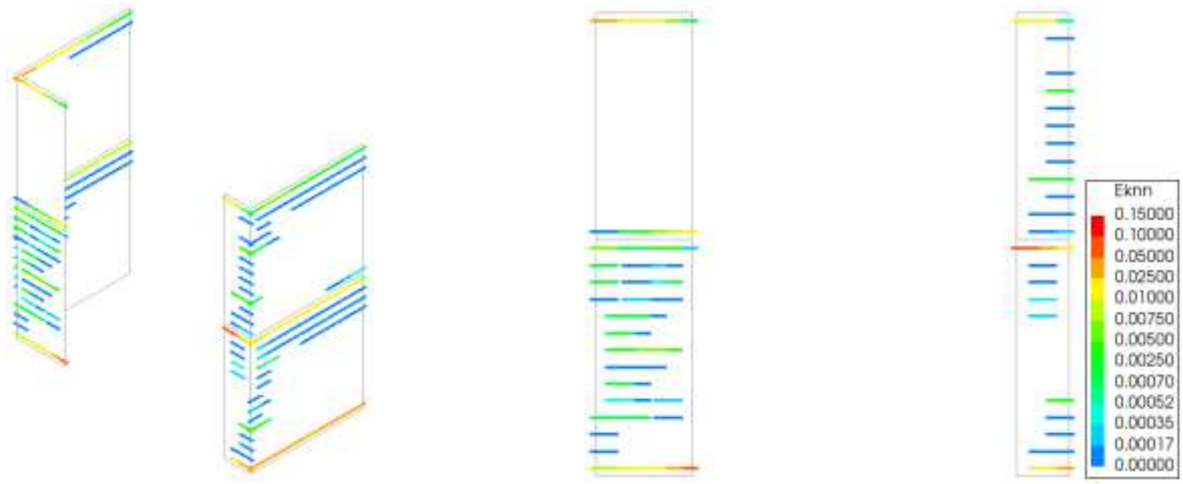

Figure 3.24 Normal crack strain at DL3 when loaded in negative direction

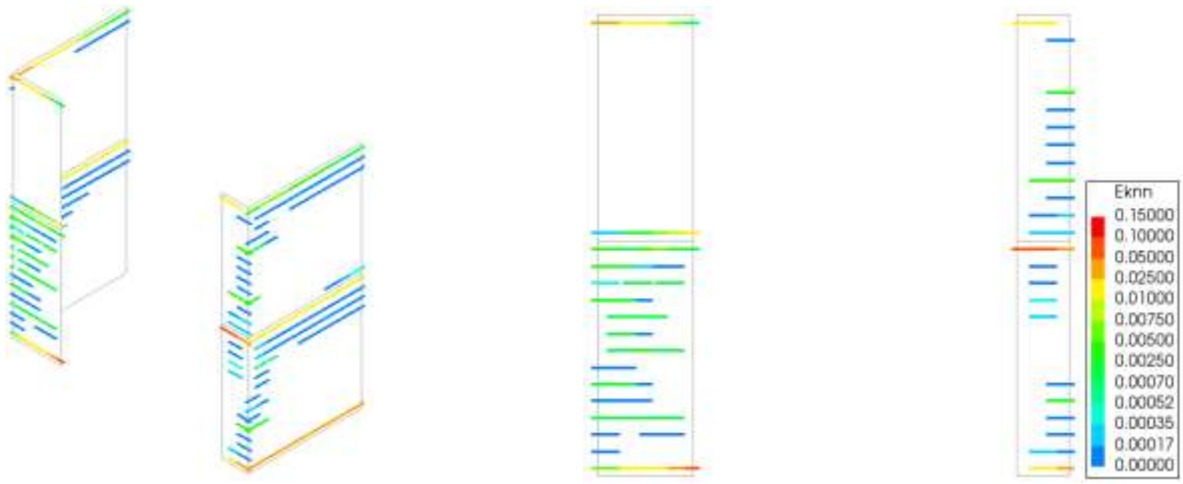

Figure 3.25 Normal crack strain at DL4 when loaded in negative direction

The damage levels discussed before are marked in the pushover capacity curve presented in Figure 3.26. In addition to the damage levels, the point where the global drift (d_{r*}) reaches 0.8% is also marked as GDL (global drift limit). It can be seen in the figure that DL1 is soon after the stiffness of the curve starts to decrease, DL2 is before the peak load reaches and DL3 is in the post peak region.

The criteria used for the identification of the damage levels are summarized in Table 3.3. The table also lists the base shear force, second floor displacement, normalized shear force, global drift limit and the interstorey drift limit of the ground floor level. It should be noted that the criteria used to identify the damage levels in Model U2 are kept consistent to identify the damage levels of the strengthened models analysed later in the study. This helps to make a fair comparison of the effect of different strengthening techniques and materials.

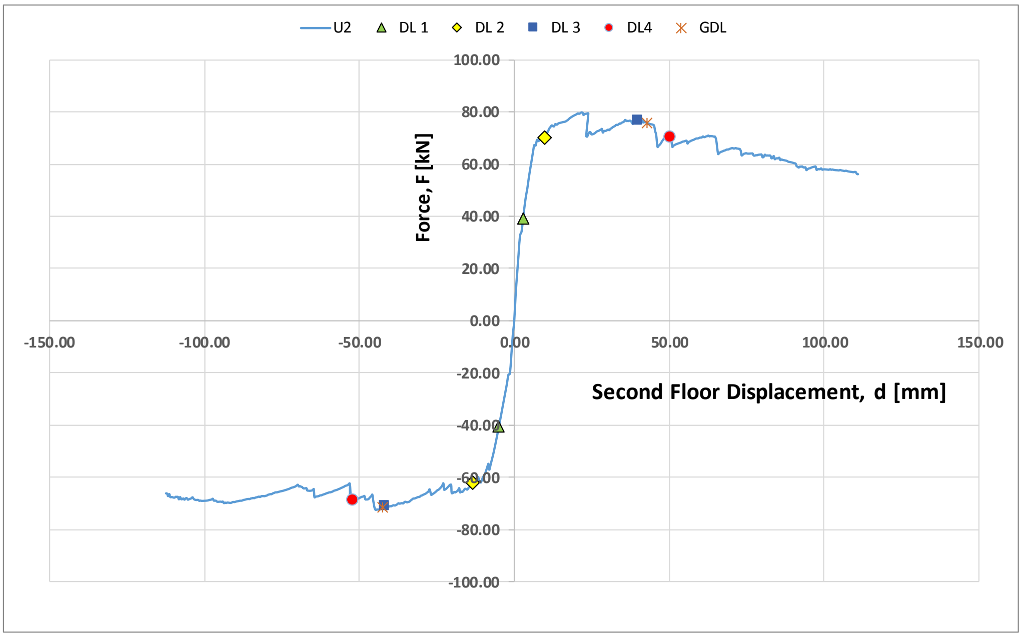

Figure 3.26 Damage levels in Model U2

Table 3.3 Summary of damage levels in Model U2

Damage Levels	Loading Direction	Observed Damage	Force	Second floor displacement	Normalised shear force	Interstorey drift	Global drift
			F	d2	k_G	d_{r1}	d_{r*}
			kN	mm		%	%
DL1	Positive	Initiation of rocking mechanism in piers	39.2	2.85	0.49	0.05	0.05
	Negative	Initiation of rocking mechanism in piers	-40.6	-4.98	0.56	-0.10	-0.09
DL2	Positive	Shear cracks appear in the middle of wide pier in first floor	70.3	9.86	0.88	0.20	0.19
	Negative	Cracks spread across the height of ground floor in wide piers	-62.2	-13.44	0.85	-0.29	-0.25
DL3	Positive	Severely damaged wide pier at ground floor	76.8	39.81	0.97	1.17	0.76
	Negative	Severely damaged wide pier at ground floor	-71.0	-41.64	0.98	-1.13	-0.79
DL4	Positive	IDL is reached	70.8	50.22	0.89	1.50	0.95
	Negative	IDL is reached	-68.6	-52.44	0.94	-1.50	-0.99

3.3.3 Drifts

The interstorey drifts of ground floor and first floor are plotted in Figure 3.27. It can be seen in the figure that the interstorey drift of ground floor is higher than the first floor. The difference in the interstorey drift starts to increase between damage levels DL2 and DL3. The results presented in Figure 3.27 suggest that there is strong localisation of deformation at ground floor, thus indicating the possibility of soft storey mechanism. This is supported by the displacement profile presented in Figure 3.28. The displacement profile at different damage levels, and the points when GDL and IDL are reached is shown in the figure. It is evident from the figure that the ground floor is the soft storey. This result is in agreement with the crack patterns presented above which showed that the damage indeed accumulates in the ground floor.

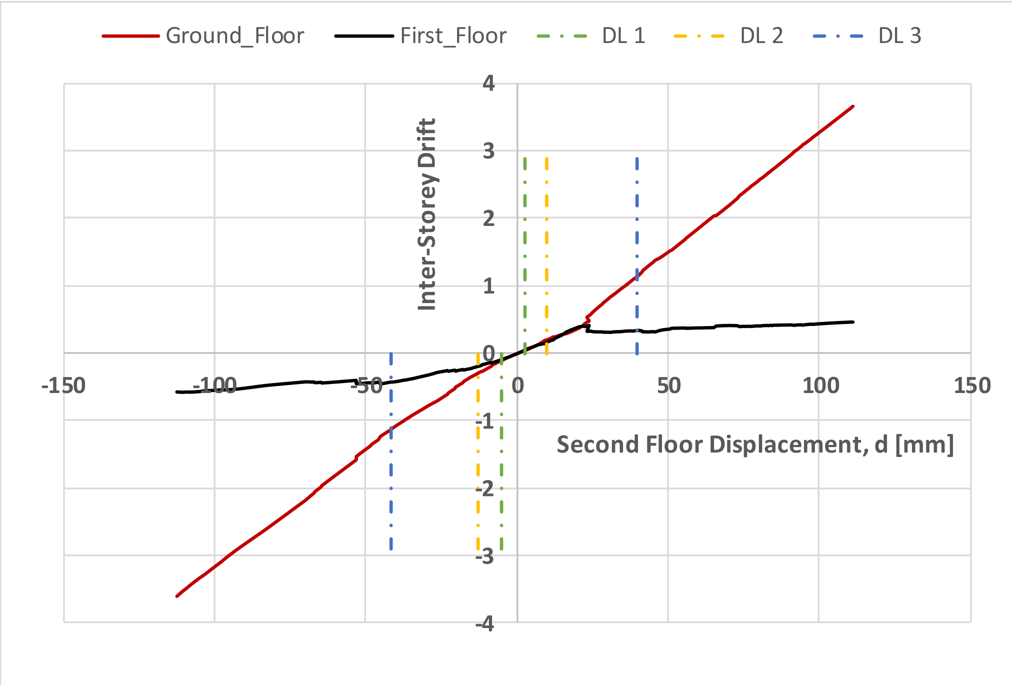

Figure 3.27 Interstorey drift (%) in ground floor and first floor of Model U2

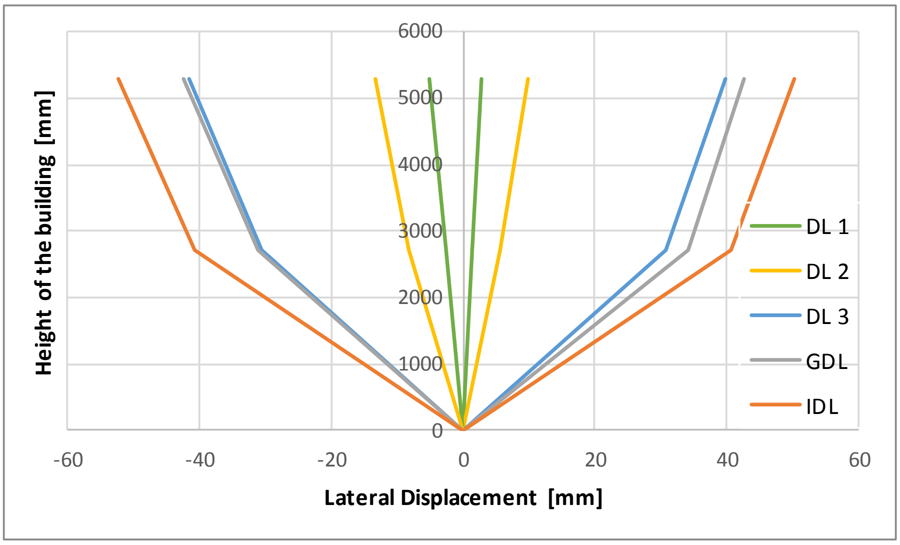

Figure 3.28 Displacement profile of Model U2 at different damage levels

3.4 Summary

This chapter discusses the results of the nonlinear pushover analyses performed on Model U1 and Model U2. The two models differed with each other on the basis of the vertical span of the piers. The piers span over two floors in Model U1 and over each single floor in Model U2. The comparison of numerical results of Model U1 with the experimental results of TUD_BUILD-1 showed that the numerical result captured the asymmetric behaviour of the house in terms of capacity and crack pattern as observed in the experiment. Although the numerical model simulated the rocking behaviour exhibited by the piers, horizontal cracks in masonry and flexural behaviour of the building, some discrepancies are observed between the tested specimen and the finite element model. The absence of the diagonal cracks in piers in the results of the numerical model is considered to be the major difference between the two models. However, as the overall behaviour and many other important characteristics observed in the experiment are closely reproduced by the numerical model, the finite element model used in the study can be considered to be validated. At the end, the crack pattern observed during the damage evolution study are used to define the four different damage levels in the model.

The numerical results of the finite element model, Model U2 showed that the capacity of the building increases when piers span over one floor only compared to the building where piers span over two floors. The further analyses of the drifts and damage evolution indicated the accumulation of deformation and thus the damage at the ground floor level. The damage levels are identified and the criteria used in the identification are justified. The criteria are kept consistent to study the effect of strengthening techniques and strengthening materials that are applied later to Model U2.

4 Nonlinear Time History Analysis of Unstrengthened Buildings

This chapter discusses the results of the nonlinear time history analyses performed on Model U1 and Model U2. The results of NLTH analyses provide information about the structural behaviour under a real seismic event. The incremental dynamic analysis (IDA) method is adopted during the analyses. The loading sequence i.e. the input signal used in the analyses is described in Section 4.1. It is followed by the description of the analysis procedure in Section 4.2. Finally, the results of NLTH analyses performed on Model U1 and U2 are presented and discussed in Section 4.3 and 4.4, respectively.

4.1 Input Signal

As the earthquake signal (applied ground acceleration $a_g(t)$) itself is the loading in NLTH analyses, the rigid beams and links that are used for the loading in NLPO analyses are removed from both the models. Instead, tying is used at the base of the finite element models. All degrees of freedoms at the base are tied to the master node. So, when the input signal is applied to the master node of the base, the whole base is subjected to the same input acceleration. The house model with the master node is shown in Figure 4.1.

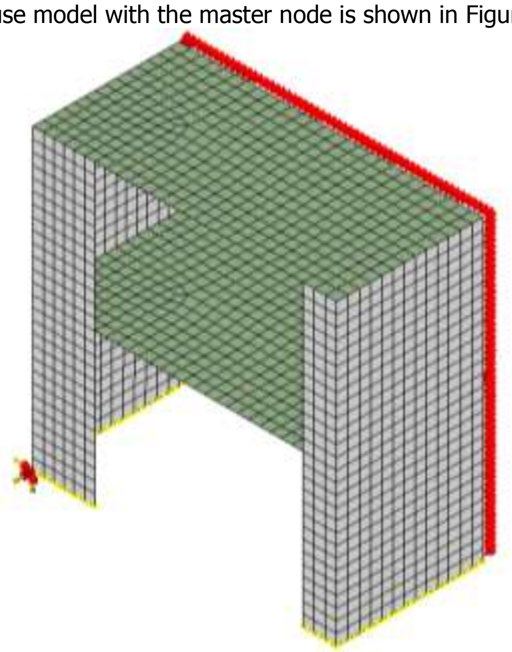

Figure 4.1 Finite element model of the house showing tying, boundary conditions and master node

The loading sequence adopted in the incremental dynamic analyses are defined on the basis of the seismic input signal adopted in shaking table tests on similar building performed at EUCENTRE [6]. The signal that is used in the analyses is shown in Figure 4.2. The earthquake signal is applied along the global x-axis (i.e. parallel to façade piers) because it is the vulnerable loading direction which has been supported by the results of NLPO analyses and the experiment. Also, this helps to make a direct comparison between the results of NLPO and NLTH analyses.

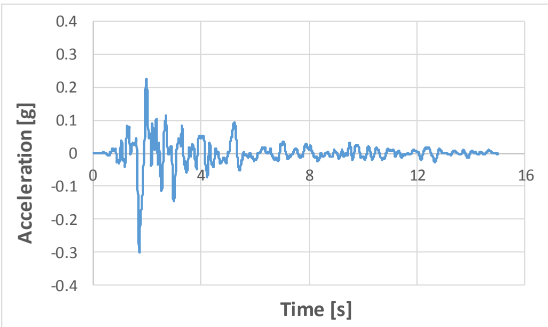

Figure 4.2 Input earthquake signal [6]

The input signal presented above is then scaled to 12 different levels to perform incremental dynamic analysis. Thus, the total signal comprises of 12 scaled signals and each signal is defined as a run of the loading history. The complete applied loading sequence is presented in Table 4.1 and Figure 4.3.

Table 4.1 PGA value for each run

Run	PGA Value [g]
1	0.03
2	0.06
3	0.10
4	0.15
5	0.20
6	0.25
7	0.30
8	0.35
9	0.40
10	0.50
11	0.62
12	0.75

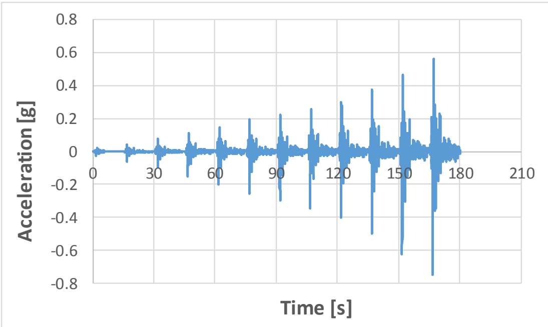

Figure 4.3 Scheme of applied earthquake accelerogram

4.2 Analysis Procedure

During the nonlinear time history analysis, first, the equivalent line load which represents the self-weight of the concrete is applied. It is followed by the self-weight of the remaining components (i.e. transversal walls and piers) and then by the earthquake accelerogram. The application of the equivalent line load and self-weight constitutes the first phase of the analysis and the input of the earthquake accelerogram constitutes the second phase. The equivalent line load and self-weight are applied in 10 load steps each and the earthquake loading is applied in 180000 steps with 0.001 s time step up to 180 s. The NLTH analysis is also performed by including both physical and geometrical nonlinearity. The secant iteration method is adopted with the line search option. The maximum number of iteration is limited to 50 per time step and satisfaction of both displacement norm and the force norm is necessary for the convergence. The analysis procedure is summarized in Table 4.2.

Table 4.2 Analysis procedure

Load Steps	Equivalent Line Load	10
	Self – Weight	10
	Base Acceleration	150060 time steps (12 runs)
Iteration Method	Maximum Number of Iterations	50
	Iteration Method	Secant (BGFS)
	Line Search	Yes
Convergence Criteria	Satisfy both displacement norm (tolerance 0.01) and force norm (tolerance 0.01)	

It should be noted that the concrete floors in the model are assigned with 0 mass density as the self-weight of the concrete is applied in terms of equivalent line load on the top of transversal walls. This is sufficient for the nonlinear pushover analyses i.e. static analysis as mass has effect only during the self-weight phase. However, in dynamic analyses the mass has effect throughout the analysis. Therefore, the model needs some modification to consider the mass of concrete floor during the analysis: surface distributed mass elements (CQ24TM) are used to model the distributed mass of the concrete floors. The distributed mass that is used in the model is calculated using the density of the concrete equal to 2400 kgm^{-3}.

4.3 Results of Model U1

The results of the nonlinear time history analysis performed on Model U1 are presented and discussed in this section. First, the response of the building in terms of base shear force and relative second floor displacement are discussed. Then, the damage levels are identified. The criteria used to define the damage levels in NLPO analysis of Model U1 are used to identify the damage levels in NLTH analyses as well. Finally, the results of NLTH and NLPO are compared with each other.

4.3.1 Hysteresis Curve

The hysteresis curve that shows the relation between the base shear force and the second floor net displacement is shown in Figure 4.4. The house is severely damaged after 10 runs and therefore the results are presented only for the 10 runs only. It can be observed that the maximum relative second floor displacement continues to increase in each run. However, the maximum base shear force stays almost constant after the sixth run. This indicates that the response of the building is more ductile in the later stage of the analysis. The behaviour is actually in agreement with the NLPO results of Model U1 presented in Figure 3.2. The pushover analyses results were found to be ductile as well.

The maximum base shear force and maximum relative second floor displacement get decoupled after five runs. The energy dissipation and residual displacement in positive direction increase with the runs. The maximum base shear force and second floor net displacement are 80.5 kN and 127 mm during the ninth run and tenth run, respectively. It is evident in the figure that the results of the NLTH analysis show large deformation only in the positive direction. Although the applied accelerogram has acceleration signals in both the directions, the positive deformation is more noticeable than the deformation in negative direction. Therefore, the discussion of the results, comparison with NLPO and damage level identification are presented only for the positive direction. The applied signal can be mirrored and applied to the model to have a detailed response in the negative direction.

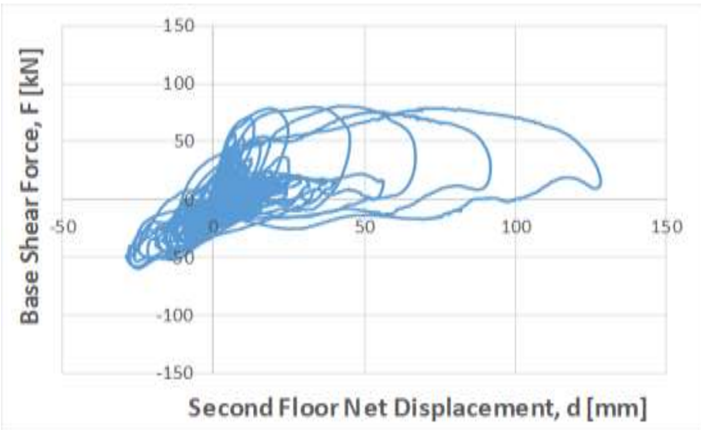

Figure 4.4 Hysteresis curve of Model U1

4.3.2 Damage Levels Identification

The results of NLTH analysis are used to identify the damage levels similar to the NLPO analysis of Model U1. The state of the house model at four damage levels are summarized in Table 4.3.

Table 4.3 Summary of damage levels of Model U1 according to NLTH results

Damage Levels	Loading Direction	Observed Damage	Force	Second floor displacement	Normalised shear force	Interstorey drift	Global drift
			F	d2	k_G	d_{r1}	d_{r*}
			kN	mm		%	%
DL1	Positive	Initiation of rocking mechanism in piers	35.2	3.18	0.44	0.06	0.06
DL2	Positive	Crack appears in the middle of wide pier in ground floor	57.2	6.95	0.71	0.13	0.13

DL3	Positive	Severely damaged wide pier in ground floor	78.5	18.66	0.98	0.34	0.35
DL4	Positive	IDL is reached	76.1	54.56	0.95	1.50	1.03

The crack pattern observed in the house model at damage levels DL1, DL2, DL3 and DL4 are presented in Appendix A. The figures also show the deformed state of the piers and transversal walls at those stages.

4.3.3 Comparison with NLPO

The pushover capacity curve obtained from NLPO analysis of Model U1 is plotted along with the results of NLTH analysis in Figure 4.5. In addition, the dynamic capacity curve is also presented for the positive direction. The dynamic capacity curve is obtained by taking the points corresponding to maximum base shear force in all ten runs. In addition, the point corresponding to maximum second floor displacement in the tenth run is also considered for the dynamic capacity curve.

The initial stiffness of the building shown by the results of NLPO and NLTH analyses are in good agreement with each other. Although, the overall behaviour of the curve is comparable, (i.e. the initial stiffness, ductile behaviour after peak load is reached, damage evolution) there are some remarkable differences between the results of two analyses. The peak shear force obtained in NLTH analysis is 60% higher than the one obtained from NLPO analysis. Also, the displacement capacity of the house is found to be slightly lower based on the results of NLTH as compared to the results of NLPO. The possible explanation of this might be the accumulation of damage in IDA compared to the monotonic pushover.

The damage levels are marked in the pushover capacity curve and dynamic capacity curve presented in Figure 4.6. It can be noted in the figure that the damage level DL1 occurs almost at the same point according to the results of NLTH and NLPO analyses. The difference between DL2 according to NLPO and NLTH is about 10% in terms of both second floor displacement and the base shear force. However, DL3 according to NLTH occurs at about 60% higher base shear force and 60% lower second floor displacement than the NLPO results. This shows that with the increase in the nonlinearity, the difference in the displacement capacity of the house obtained from two analyses continue to increase. The value of DL4 computed for the NLTH analysis is smaller due to the more localisation of damage in the ground floor compared to the NLPO analysis.

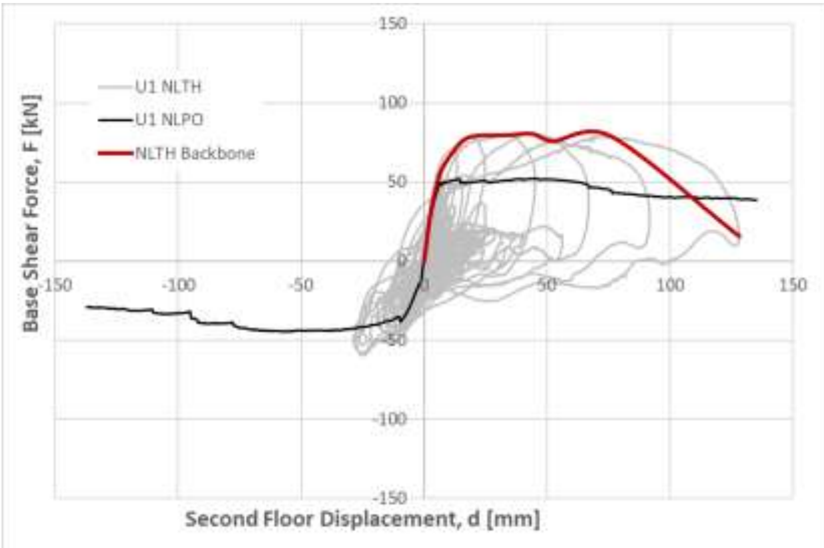

Figure 4.5 Hysteresis curve, Pushover capacity curve and Dynamic capacity curve of Model U1

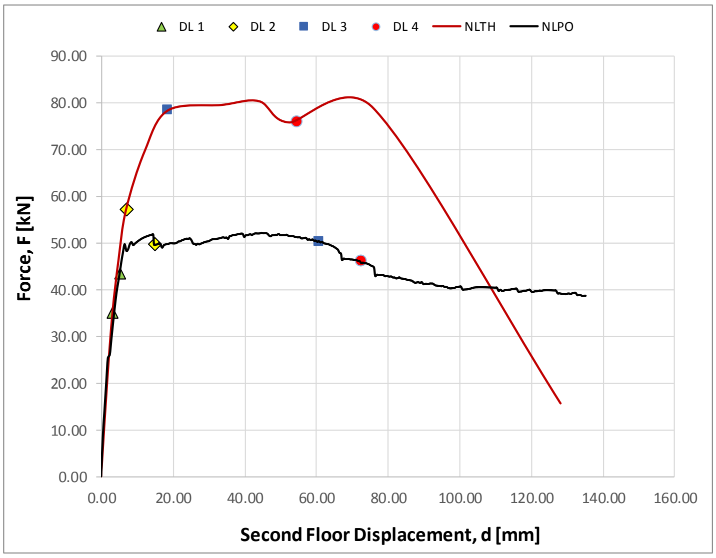

Figure 4.6 Damage levels of Model U1

4.4 Results of Model U2

The results of NLTH analysis performed on Model U2 are presented in the following. Similar to Model U1, first the response of the building is discussed in terms of the base shear force and second floor displacement. It is followed by the damage levels identification, and finally a comparison between the results of the NLPO analysis and NLTH analysis of Model U2 is presented.

4.4.1 Hysteresis Curve

The results of the base shear force and second floor relative displacement are plotted against each other in Figure 4.7. As the model is severely damaged after the tenth run and the damage level DL4 is already reached in the tenth run, the results are presented only up to 10 runs. It can be observed in the figure that the peak base shear force stays approximately between 90 to 120 kN after 6 runs. It was expected that with the evolution of the damage, the base shear force would decrease too. However, such characteristic is not observed. But the effect of the damage evolution can be noticed in the second floor relative displacement after the eighth run. During the ninth and the tenth runs the second floor displacement increases by significant amount and the inelastic deformation is also observed. Like in NLTH results of Model U1, the large deformation is observed only in the positive direction. Therefore, the damage levels and dynamic capacity curve are only presented for the positive direction.

It can be observed in Figure 4.7 that the energy dissipation increases along with the inelastic deformation at higher runs. The maximum base shear force and the second floor displacement are found to be 109 kN and 57.6 mm, respectively. The maximum base shear force and maximum second floor displacement do not occur at the same time already from the seventh run.

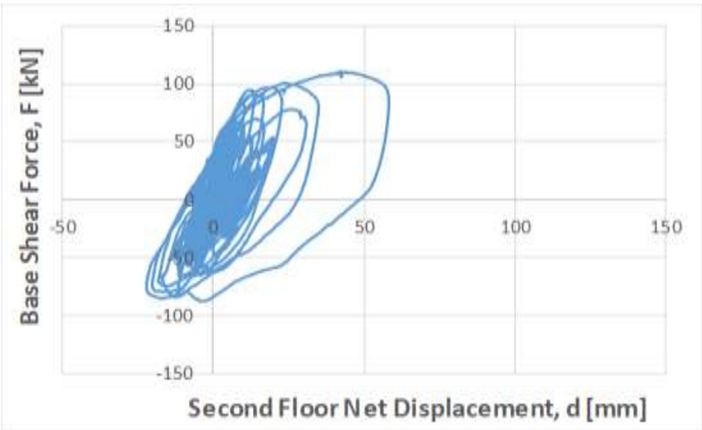

Figure 4.7 Hysteresis curve of Model U2

4.4.2 Damage Levels Identification

The damage levels are identified next. The criteria defined above in section 3.3.2 to identify damage levels based on NLPO results of Model U2 are kept consistent. The base shear force, second floor displacement, interstorey of ground floor and global drift at four damage levels in the positive direction are presented in Table 4.4.

Table 4.4 Summary of damage levels of Model U2

Damage Levels	Loading Direction	Observed Damage	Force	Second floor displacement	Normalised shear force	Interstorey drift	Global drift
			F	d2	k_G	d_{r1}	d_{r*}
			kN	mm		%	%
DL1	Positive	Initiation of rocking mechanism in piers	36.1	2.18	0.33	0.04	0.04
DL2	Positive	Shear crack appears in the middle of wide pier in first floor	76.8	7.24	0.70	0.14	0.14
DL3	Positive	Severely damaged wide pier at ground floor	96.6	19.64	0.87	0.51	0.37
DL4	Positive	IDL is reached	90.0	50.56	0.83	1.50	0.95

The crack pattern observed in the house model at above mentioned four damage levels is similar to the one presented for NLPO analysis of Model U2.

4.4.3 Comparison with NLPO

The pushover capacity curve obtained from NLPO of Model U2, hysteresis curve obtained from Model U2 and proposed dynamic capacity curve are presented in Figure 4.8. The dynamic capacity curve of Model U2 is obtained by considering the points corresponding to maximum base shear force for the first nine runs and the point corresponding to maximum displacement for the last run.

The initial stiffness of the building obtained from the results of NLPO and NLTH are in good agreement with each other. However, as observed above in Model U1, the results of NLTH have higher capacity in terms of the base shear force and lower in terms of the displacement capacity. The maximum base shear force obtained from NLTH is approximately 36% higher than the maximum base shear force obtained from NLPO. The reduced displacement capacity according to results of NLTH is reasonable as NLTH takes into account the accumulation of damage unlike the monotonic pushover analyses. Amidst all the differences, it must be noted that the overall behaviour of the building, initial stiffness, cracking pattern and damage level evolution are very similar to each other.

The damage levels identified in NLPO capacity curve and dynamic capacity curve is presented in Figure 4.9. The damage levels DL1 and DL2 occur almost at similar state according to both NLPO and NLTH analyses. Similarly, DL4 i.e. when interstorey drift of ground floor reaches 1.5% also occurs at almost similar second floor displacement (a soft storey mechanism occurs for both the models). However, the corresponding base shear force is about 20 kN higher in NLTH than NLPO. DL3 on another hand occur at lower displacement capacity according to NLTH.

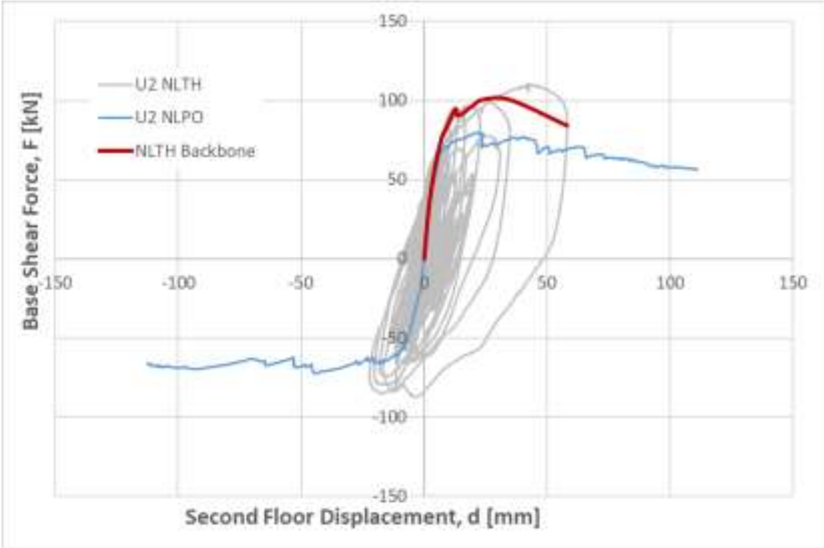

Figure 4.8 Hysteresis curve, pushover capacity curve and dynamic capacity curve of Model U2

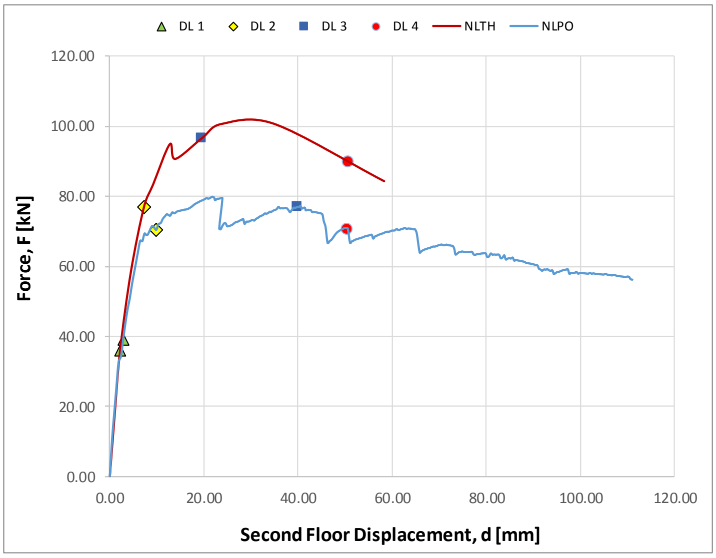

Figure 4.9 Damage levels of Model U2

4.5 Summary

The nonlinear time history analyses performed on Model U1 and Model U2 provided information about the seismic behaviour of buildings. The results of NLTH were compared with the results of NLPO and comparisons are made in terms of the base shear capacity, displacement capacity, damage levels, initial stiffness, overall behaviour and crack evolution. The results indicated that the NLTH analyses of Model U1 and Model U2 give higher base shear capacity and lower displacement capacity compared to the NLPO analyses. This resulted in the difference in corresponding base shear force and second floor displacement at which damage levels are identified. However, good agreement is observed between NLTH and NLPO in terms of the initial stiffness exhibited by the building, overall behaviour of the house and crack evolution. The house Model U1 shows more flexural behaviour according to both NLPO and NLTH which is common for the piers spanning over two floor. And, the house Model U2 had localization of displacement and damage at ground floor according to both NLPO and NLTH. Amidst the differences in the corresponding base shear force and second floor displacement, it can be justifiably argued that both NLPO and NLTH have good agreement with each other when it comes to the seismic behaviour of the house, the crack evolution, and the definition of the damage levels.

5 Strengthening Techniques and Materials

The main goal of this research is to study the effect of different strengthening techniques and materials on the seismic capacity of the URM houses. Therefore, different strengthening techniques and materials are applied to the house configuration Model U2. Section 5.1 discusses three different strengthening techniques that are applied and section 5.2 discusses two different materials that are used for strengthening.

5.1 Strengthening Techniques

Three different strengthening techniques are chosen, based on the configuration of the unstrengthened building Model U2. The numerical results of nonlinear pushover analyses and nonlinear time history analyses performed on Model U2 showed that the global behaviour of the house is governed by the failure of the piers. Therefore, it is very important to assess the effect of strengthening the piers on the seismic behaviour and capacity of Model U2.

It is already mentioned in chapter 2 that the transversal walls are connected to piers via a running bond. As the overall response is governed by the piers, it could be interesting to assess the importance of strengthening the connection between piers and transversal walls as well. Experiments performed on similar houses have shown that a part of the transversal wall moves together along with piers when connected with a running bond [2, 7]. This process is called "flange effect". Therefore, a part of transversal wall, "flange" is strengthened along with a part of the pier in second strengthening technique. Finally, both "flanges" and piers are strengthened as the third strengthening technique. The three techniques are summarized and presented below:

5.1.1 Technique S1

The strengthening technique S1 constitutes of strengthening the piers only. The piers of Model U2 are modelled with layered shell elements (CQ40L in finite element software DIANA FEA) with two layers of materials, masonry and strengthening material. The two materials (layers) are fully bonded when modelled using the layered shell elements. The finite element model of Model S1 is shown in Figure 5.1. The strengthened components are highlighted with green colour.

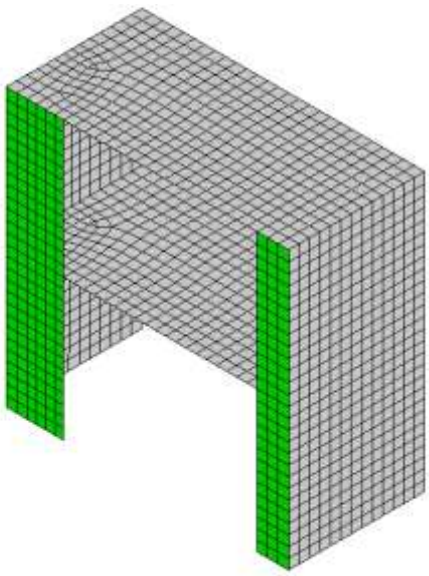

Figure 5.1 Finite element model of S1 (Strengthening of piers)

5.1.2 Technique S2

The strengthening technique S2 constitutes of strengthening the "flanges" and a part of piers. This technique mainly strengthens the connection and improves the interaction of transversal walls and piers. The flange width is determined using the relation proposed in [7]. It is suggested that the effective width of rectangular flange for a transversal wall whose width is less than two times the height can be calculated using:

$$L_f = \frac{(4h - L_i)L_i}{8h}$$

where L_{fi}, L_i and h represent width of flange, width of transversal wall and height of the transversal wall, respectively. In addition to the flange, one-third of the piers are also strengthened to improve the connection of the transversal walls and the piers. The finite element model of Model S2 is shown in Figure 5.2. The strengthened components are highlighted with green colour.

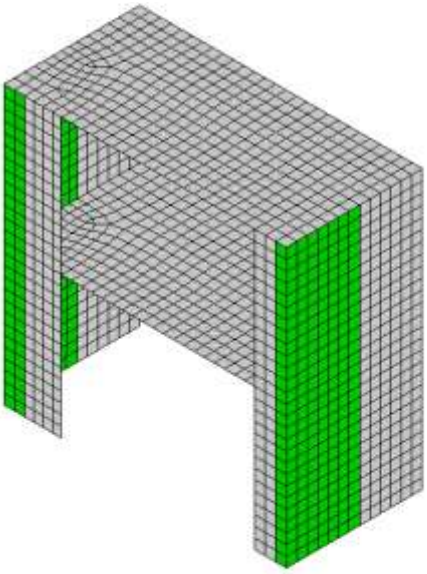

Figure 5.2 Finite element model of S2 (Strengthening of flanges and part of piers)

5.1.3 Technique S3

The strengthening technique S3 constitutes strengthening both the "flanges" and the piers. The width of the flange is same as the one used in Model S2. The finite element model of Model S3 is shown in Figure 5.3. The strengthened components are highlighted with green colour.

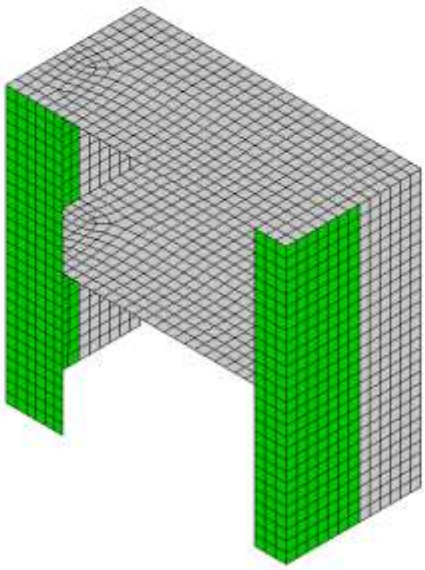

Figure 5.3 Finite element model of S3 (Strengthening of flanges and piers)

5.2 Strengthening Materials

The proposed strengthening techniques require the application of an additional material over the existing structure. This material is applied over the components that are described above in Section 5.1. As mentioned above, the strengthened material is assumed to be fully bonded to the masonry. Two different materials are chosen based on the observed failure mechanism, strengthening techniques and materials used in practice in similar houses [8, 9, 10, 11, 12, 13].

The two strengthening materials mentioned above are applied one at a time to each strengthened models (Model S1, Model S2 and Model S3). Then, both nonlinear pushover analysis and nonlinear time history analysis are performed on each model to investigate the effect of strengthening techniques and strengthening materials. The results of the analyses are presented in Chapters 6 and 7.

5.2.1 Material A – Oriented Strand Board (OSB)

First, Oriented Strand Board (OSB) panels are selected to strengthen the URM house. OSB belongs to the family of engineered wood and is increasingly used in constructions due to its light weight and favourable mechanical properties. The application of OSB panels to strengthened a masonry house was tested at the EUCENTRE laboratory and the results showed that the capacity of the house improved by more than 250% [12]. The material properties used for the panels are based on the material properties used in the blind prediction of the same building that provided a fair estimate of the actual structural behaviour [11]. The material properties of OSB obtained from literatures were calibrated during the blind prediction to match the experimental and numerical results of a masonry wall strengthened using OSB panel. The calibration exercise [11] also allowed to assess the accuracy of the assumption of perfect bond between OSB panels and masonry walls. A Rankine-Hill Anisotropic model is adopted to model the anisotropic behaviour of the OSB panels. The thickness of the panels is adopted to be 18 mm. The material properties used for OSB panels are summarized in Table 5.1.

Table 5.1 Material properties of OSB Panels (Material A)

Symbol	Description	Adopted Value
ρ	Mass Density [kgm^{-3}]	590
E	Elastic Modulus [MPa]	1820
v	Poisson's Ratio	0.3
f_{t0}	Tensile strength parallel to grain [MPa]	2.5
f_{t90}	Tensile strength perpendicular to grain [MPa]	0.9
f_{c0}	Compressive strength parallel to grain [MPa]	35
f_{c90}	Compressive strength perpendicular to grain [MPa]	5
G_{f0}^{I}	Mode I fracture energy parallel to grain [Nmm^{-1}]	70
G_{f90}^{I}	Mode I fracture energy perpendicular to grain [Nmm^{-1}]	50
G_{c0}	Compressive fracture energy parallel to grain [Nmm^{-1}]	130
G_{c90}	Compressive fracture energy perpendicular to grain [Nmm^{-1}]	70
k_p	Equivalent plastic strain corresponding to peak compressive stress	0.001

5.2.2 Material B – Engineered Cementitious Composites (ECC)

Second, Engineered Cementitious Composites (ECC) is applied to strengthen the URM house. The engineered cementitious composites (ECC) is a thin layer of ductile fibre reinforced mortar material. It is considered as a family of materials rather than a single material which belongs to the broad class of fibre reinforced concrete (FRC) [8]. The ECC exhibits a tensile strain capacity of 3-5% and fine, multiple cracking when subjected to direct tension. Previous studies (both numerical and experimental) have shown that the use of ECC can lead to the improvement of the seismic performance of the building in terms of capacity, ductility, stiffness and energy dissipation [8, 9, 10]. The material properties used for the ECC are based on the material properties of ECC adopted in [8, 9, 10]. The total strain based crack model with rotating cracks is used to model the ECC. A thickness of 13 mm for the ECC is adopted. The material properties used for ECC are summarized in Table 5.2.

Table 5.2 Material properties of ECC (Material B)

Symbol	Description	Adopted Value
ρ	Mass Density [kgm^{-3}]	2000
E	Elastic Modulus [MPa]	20000
v	Poisson's Ratio	0.3
	Tensile curve	Multilinear
$f_{t,1}$	First crack stress [MPa]	2.8
$\varepsilon_{t,1}$	First crack strain	0.00014
$f_{t,max}$	Maximum stress [MPa]	3.75
$\varepsilon_{t,max}$	Strain corresponding to maximum strain	0.035
$f_{f,red}^{I}$	Residual stress [MPa]	0.0375
	Compression curve	Thorenfeldt
f_c	Compressive strength [MPa]	30

6 Nonlinear Pushover Analysis of Strengthened Buildings

This chapter discusses the results of monotonic nonlinear pushover analyses performed on finite element models of strengthened houses. First, Material A (OSB Panels) is used in models S1, S2 and S3. Then, the models are analysed using Material B (ECC). The results of the pushover analyses are presented in terms of capacity curve and damage levels. The comparison is made between the results of Model U2 and each strengthened case. It should be noted that the definitions of damage levels are kept consistent with Model U2 to make a meaningful comparison between the considered cases. The loading method and analyses procedures are kept the same as in Model U2 in all analyses, as described in Section 3.1. The drifts and displacement profile observed in each strengthened model are presented in Appendix B.

6.1 Results of Model S1 – A

The results of the monotonic pushover analyses along global x-direction performed on Model S1 strengthened using OSB panels are discussed in this section. Section 6.1.1 presents the pushover capacity curve and bilinear capacity curve. The damage levels are identified in Section 6.1.2. Finally, comparisons are made between Model U2 and Model S1-A.

6.1.1 Capacity Curve

The pushover capacity curve obtained from the finite element analysis of Model S1-A is plotted along with the pushover capacity curve of Model U2 in Figure 6.1. The maximum base shear force (positive direction) in Model S1-A is found to be 104 kN which is approximately 30% higher than the unstrengthened case. Also it can be observed in the figure that the stiffness of the strengthened model slightly improves compared to Model U2. Both the models have almost similar deformation in the second floor at the end of the analysis.

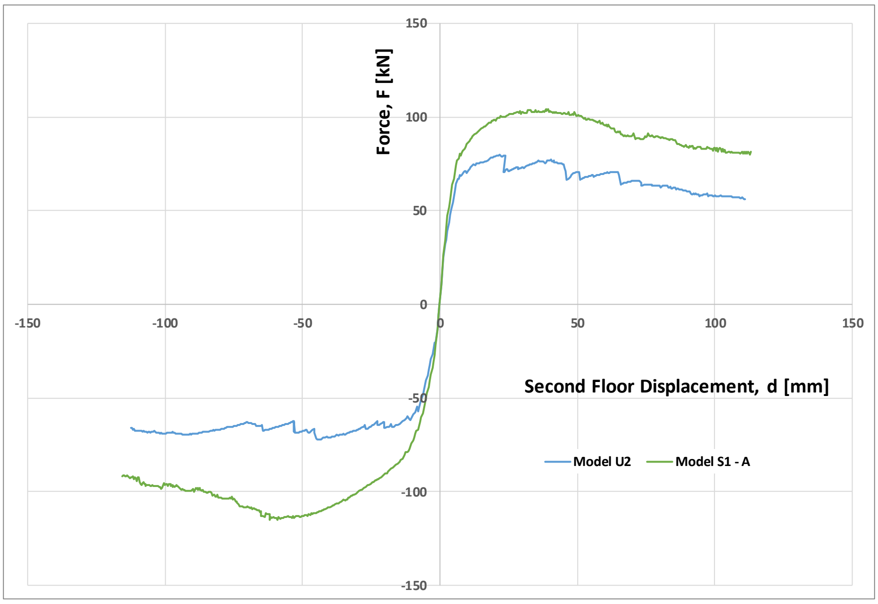

Figure 6.1 Capacity curve of Model S1-A

The pushover capacity curve is then converted to the bilinear capacity curve. The procedure used to produce the bilinear capacity curve is similar to the one used for Model U1 and Model U2. As there is no 20% drop in the base shear force until the end of the analysis, the ultimate displacement capacity is taken to be the point when interstorey drift of ground level reaches 1.5%. The bilinear capacity curve of Model S1-A is presented in Figure 6.2. It can be observed in the figure that the bilinear capacity and the pushover capacity are almost similar to each other.

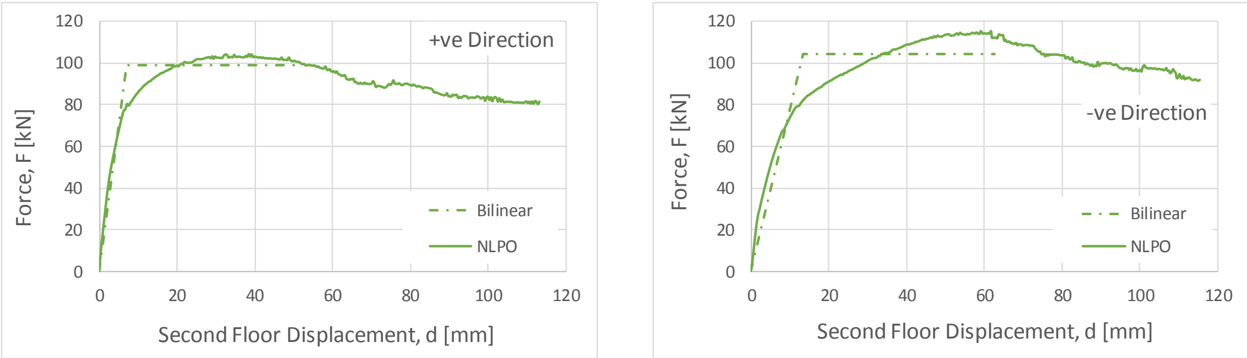

Figure 6.2 Bilinear capacity curve of Model S1-A

6.1.2 Damage Levels

The damage levels are identified next in Model S1-A. The same criteria used for identifying damage levels in Model U2 is used for Model S1-A as well. The damage levels in Model S1-A is summarised in Table 6.1. Also, the four damage levels and the point when global drift limit is reached are marked in the capacity curve and presented in Figure 6.3. It should be noted that the point when interstorey drift reaches 1.5% is same as DL4. The cracking pattern observed in Model S1-A is similar to the crack pattern observed in Model U2. The cracks develop on the corner of piers at first and then spread all over the wide pier by the end of the analysis.

Table 6.1 Summary of damage levels in Model S1-A

Damage Levels	Loading Direction	Observed Damage	Force	Second floor displacement	Normalised shear force	Interstorey drift	Global drift
			F	d2	k_G	d_{r1}	d_{r*}
			kN	mm		%	%
DL1	Positive	Initiation of rocking mechanism in piers	63.7	4.57	0.61	0.09	0.09
	Negative	Initiation of rocking mechanism in piers	-53.1	-5.45	0.46	-0.11	-0.10
DL2	Positive	Shear cracks appear in the middle of wide pier in first floor	95.7	16.82	0.92	0.39	0.32
	Negative	Cracks spread across the height of ground floor in wide piers	-87.4	-17.21	0.76	-0.37	-0.32
DL3	Positive	Severely damaged wide pier at ground floor	100.6	50.63	0.97	1.44	0.95
	Negative	Severely damaged wide pier at ground floor	-112.9	-51.42	0.98	-1.15	-0.97
DL4	Positive	IDL is reached	99.4	52.43	0.95	1.50	0.99
	Negative	IDL is reached	-111.8	-62.79	0.97	-1.50	-1.18

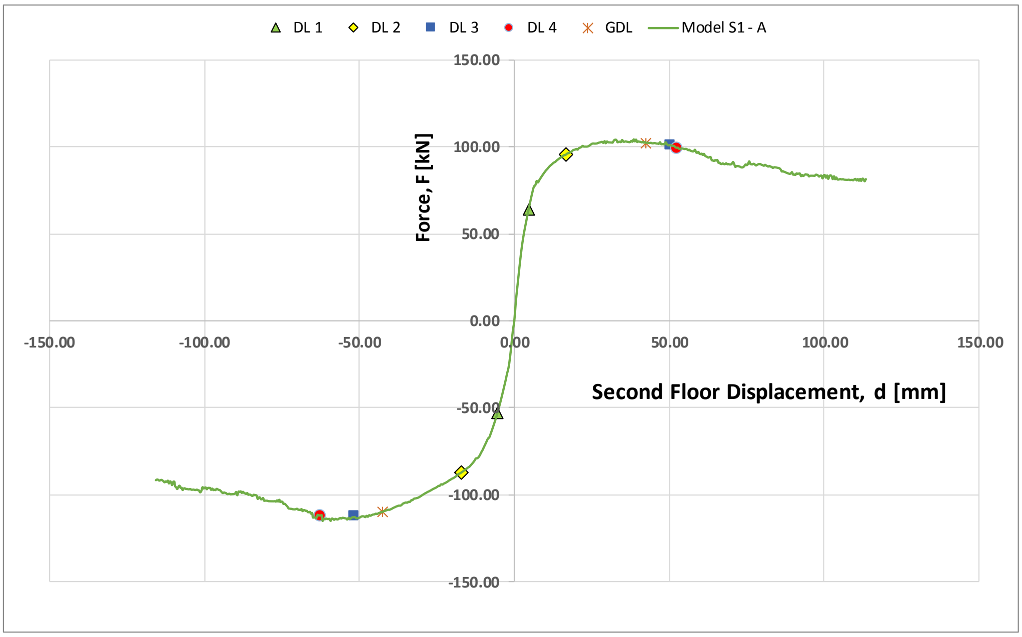

Figure 6.3 Damage Levels in Model S1-A

6.1.3 Comparison with Model U2

The effect of applying an overlay of OSB panels over piers in URM could be observed in terms of the improvement in initial stiffness, increase in capacity and delay in the damage levels.

Loaded in Positive direction:
The peak base shear force increased by about 30% due to the adopted strengthening technique. The damage level DL1 is identified at the second floor displacement and base shear force equal to 4.57 mm and 63.66 kN in Model S1-A as compared to 2.85 mm and 39.20 kN in Model U2. Similarly, the base shear force at DL2, DL3 and DL4 increased by 36%, 31%, and 40%, respectively in Model S1-A compared to Model U2. The second floor displacement at DL2, DL3 and DL4 increased by 70.5%, 27.2% and 4.4%, respectively in Model S1-A than Model U2. These results show that the damage is delayed in Model S1-A as a result of the strengthening.

Loaded in Negative direction:
The peak base shear force increased by about 55% in Model S1-A. The base shear force at DL1, DL2, DL3 and DL4 increased by 30%, 41%, 59% and 63%, respectively in Model S1-A compared to Model U2. Similarly, the second floor displacement at DL1, DL2, DL3 and DL4 increased by 9.3%, 32.1%, 23.5% and 19.7%, respectively in Model S1-A.

Although the capacity curve and damage levels are significantly affected by the strengthening of piers, the overall behaviour of the house, crack pattern and failure mechanism do not change significantly. The crack pattern is similar to the ones presented in Section 3.2. Also, a soft storey mechanism is observed at the first floor level in Model S1-A, similar to Model U2.

6.2 Results of Model S2 – A

The results of nonlinear pushover analyses performed on Model S2 with material A (OSB Panels) are presented in this section.

6.2.1 Capacity Curve

The capacity curve of Model S2-A is presented along with the capacity curve of Model U2 in Figure 6.4. The maximum base shear force (positive direction) in Model S2-A is found to be 106 kN, 32.8% higher compared to Model U2. The initial stiffness of the building is almost similar to Model U2 meaning that the strengthening technique doesn't have influence on the stiffness of the house. The capacity curve of Model S2-A has softening branch in the post peak region unlike the results of Model U2 and Model S1-A. Like in previous analyses, the pushover capacity curve is converted to the bilinear capacity curve and presented in Figure 6.5. The bilinear capacity of Model S2-A is slightly smaller than the pushover capacity.

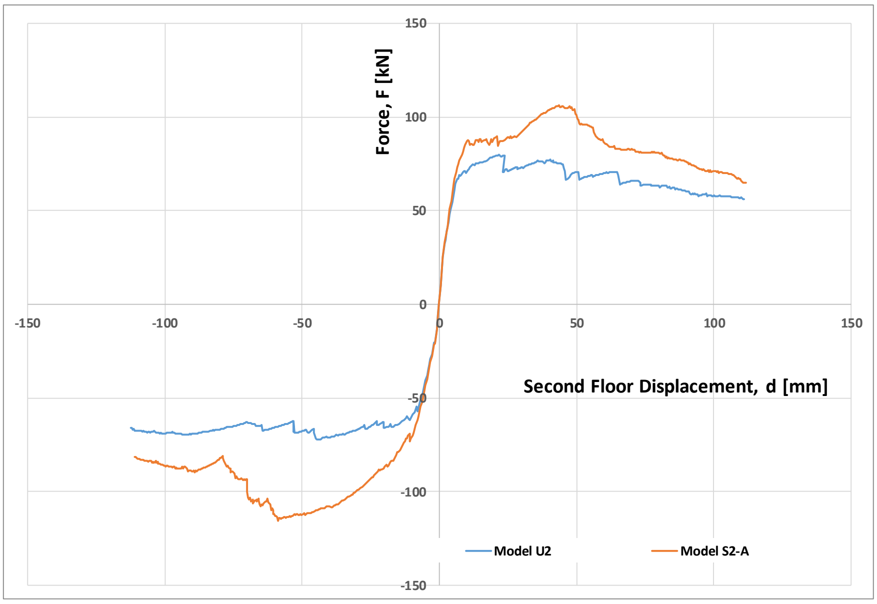

Figure 6.4 Capacity curve of Model S2-A

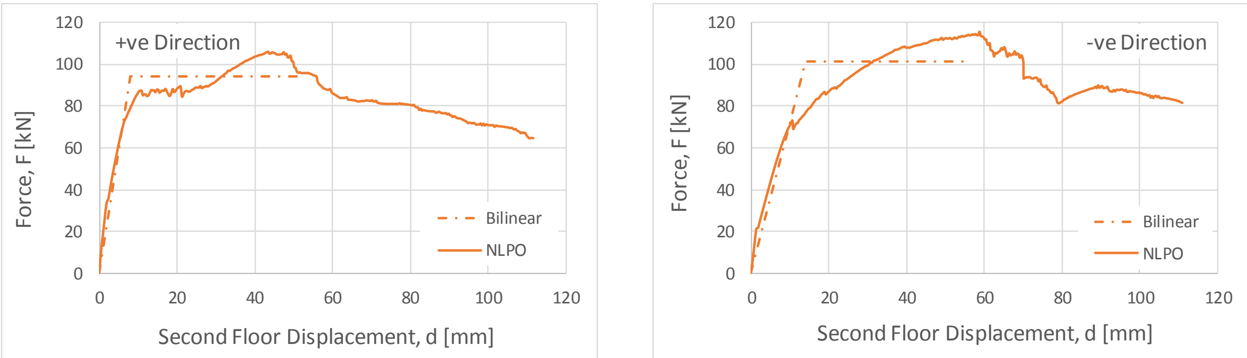

Figure 6.5 Bilinear capacity curve of Model S2-A

6.2.2 Damage Levels

The damage levels are identified next. The crack evolution is analysed to identify the damage levels. The findings are summarised in Table 6.2. The four damage levels and the point when global drift limit is reached (GDL) are marked in the pushover capacity curve in Figure 6.6. The crack pattern and evolution in Model S2-A is found to be similar to Model U2 and Model S1-A.

Table 6.2 Summary of damage levels in Model S2-A

Damage Levels	Loading Direction	Observed Damage	Force	Second floor displacement	Normalised shear force	Interstorey drift	Global drift
			F	d2	k_G	d_{r1}	d_{r*}
			kN	Mm		%	%
DL1	Positive	Initiation of rocking mechanism in piers	59.4	4.74	0.56	0.08	0.09
	Negative	Initiation of rocking mechanism in piers	-46.1	-5.42	0.40	-0.11	-0.10
DL2	Positive	Shear cracks appear in the middle of wide pier in first floor	87.8	13.37	0.83	0.33	0.25
	Negative	Cracks spread across the height of ground floor in wide piers	-85.5	-19.25	0.74	-0.48	-0.36

DL3	Positive	Severely damaged wide pier at ground floor	105.5	45.28	1.00	1.28	0.85
	Negative	Severely damaged wide pier at ground floor	-111.7	-49.35	0.97	-1.28	-0.93
DL4	Positive	IDL is reached	96.3	51.63	0.91	1.50	0.97
	Negative	IDL is reached	-113.8	-56.54	0.99	-1.50	-1.07

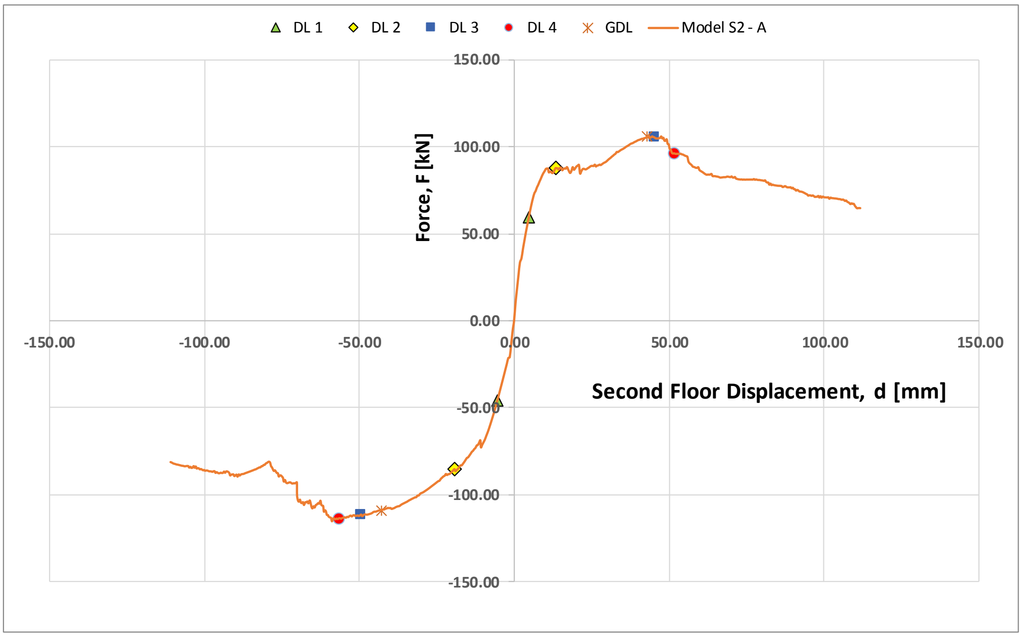

Figure 6.6 Damage levels in Model S2-A

6.2.3 Comparison with Model U2

The effect of applying an overlay of OSB panels over flanges in transversal walls and a part of piers in URM could be observed in terms of the increase in capacity and delay in the damage levels.

Loaded in Positive direction:
The peak base shear force increased by 32.8% due to the adopted strengthening technique. The base shear force at DL1, DL2, DL3 and DL4 increased by 51%, 25%, 37% and 36%, respectively in Model S2-A compared to Model U2. Similarly, the second floor displacement at DL1, DL2, DL3 and DL4 increased by 66.2%, 35.6%, 13.7% and 2.8%, respectively in Model S2-A. These results show that the damage is delayed in Model S2-A as a result of the strengthening.

Loaded in Negative direction:
The peak base shear force increased by about 55% in Model S2-A. This shows that the effect of strengthening is more in the negative direction. The base shear force at DL1, DL2, DL3 and DL4 increased by 13%, 38%, 57% and 65%, respectively in Model S2-A compared to Model U2. Similarly, the second floor displacement at DL1, DL2, DL3 and DL4 increased by 8.7%, 47.8%, 18.5% and 7.8%, respectively in Model S2-A.

Although the capacity curve and damage levels are significantly affected due to the strengthening of flanges and part of piers, the overall behaviour of the house, crack pattern and failure mechanism are not affected. The crack pattern similar to the ones presented in Section 3.2 is found in Model S2-A. Also, the soft storey mechanism is observed at the first floor level in Model S2-A, similar to Model U2 and Model S1-A.

6.3 Results of Model S3 – A

This section presents the results of nonlinear pushover analyses performed on Model S3 with OSB panels (Material A).

6.3.1 Capacity Curve

The pushover capacity curve of Model S3-A obtained from the monotonic pushover analyses is presented in Figure 6.7. The capacity curve of Model U2 is also shown in the figure. The maximum shear force in the positive direction is 127 kN, 59% higher than the unstrengthened case. It can be observed in the figure that the initial stiffness of the strengthened building is higher than the unstrengthened building. The capacity curve of Model S3-A has a softening branch in the post peak region which is followed by the ductile behaviour. As the strengthening technique S3 is the combination of S1 and S2, the response is also the combination of two responses. The pushover capacity curve is then converted to bilinear curve and presented in Figure 6.8. The bilinear capacity of Model S3-A is almost similar to the pushover capacity in the positive direction and slightly smaller in the negative direction.

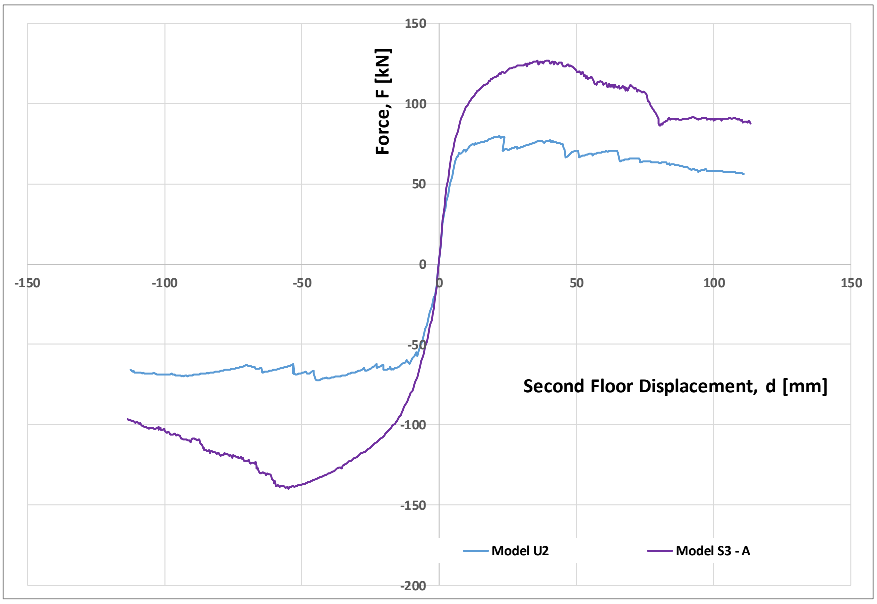

Figure 6.7 Capacity curve of Model S3-A

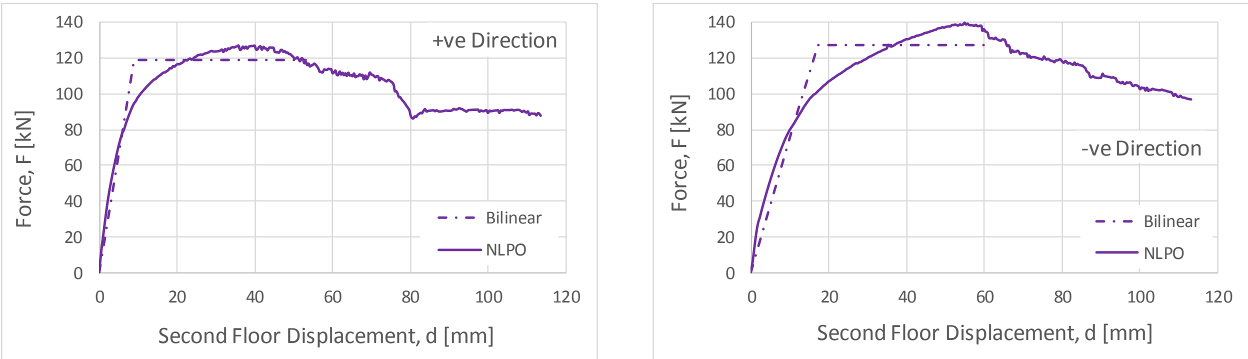

Figure 6.8 Bilinear capacity curve of Model S3-A

6.3.2 Damage Levels

As in previous models, the damage levels are identified next. The Table 6.3 summarises the four damage levels identified in Model S3-A. The crack evolution is analysed and same criteria used in Model U2, S1-A and S2-A are adopted to identify the damage levels. The crack pattern and evolution is similar to the one presented for Model U2 in section 3.2.2. The damage levels and the point when global drift reaches 0.8% are then marked in the pushover capacity curve and presented in figure 6.13. It can be observed in Figure 6.9 that the damage level DL1 occurs when the building starts to lose stiffness, damage level DL2 occurs before the peak load is attained, damage level DL3 occurs around the peak region and damage level DL4 i.e. IDL occurs in the post peak region.

Table 6.3 Summary of damage levels of Model S3-A

Damage Levels	Loading Direction	Observed Damage	Force	Second floor displacement	Normalised shear force	Interstorey drift	Global drift
			F	d2	k_G	d_{r1}	d_{r*}
			kN	mm		%	%
DL1	Positive	Initiation of rocking mechanism in piers	67.3	4.62	0.53	0.09	0.09
	Negative	Initiation of rocking mechanism in piers	-51.6	-5.00	0.37	-0.10	-0.09
DL2	Positive	Shear cracks appear in the middle of wide pier in first floor	109.9	15.32	0.87	0.34	0.29
	Negative	Cracks spread across the height of ground floor in wide piers	-100.8	-17.00	0.72	-0.38	-0.32
DL3	Positive	Severely damaged wide pier at ground floor	123.5	45.16	0.97	1.23	0.85
	Negative	Severely damaged wide pier at ground floor	-137.2	-49.34	0.98	-1.18	-0.93
DL4	Positive	IDL is reached	118.1	53.14	0.93	1.50	1.00
	Negative	IDL is reached	-136.2	-60.03	0.97	-1.50	-1.13

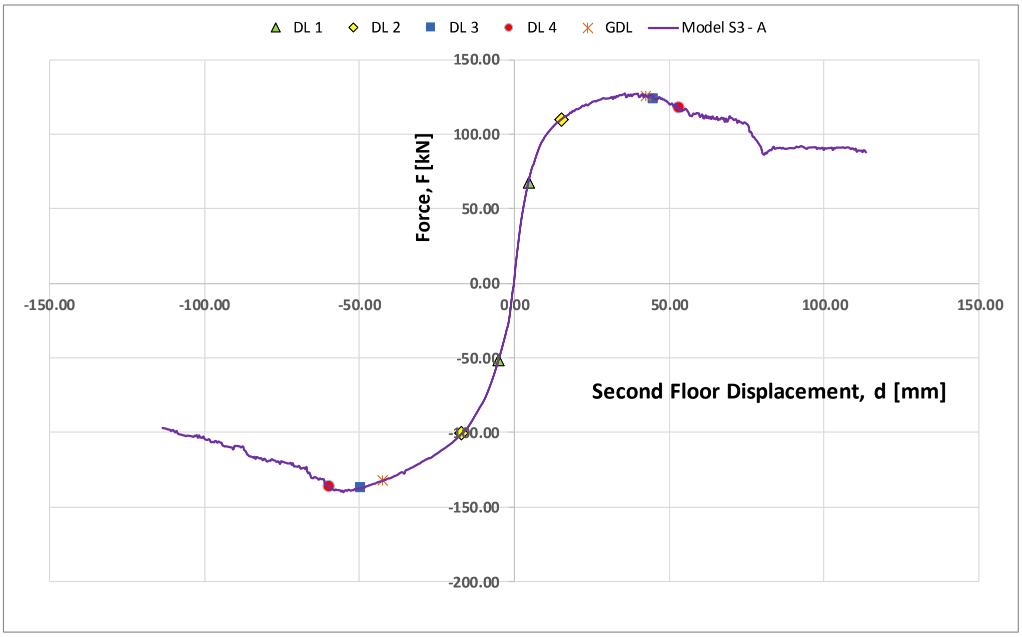

Figure 6.9 Damage levels in Model S3-A

6.3.3 Comparison with Model U2

The effect of applying an overlay of OSB panels over flanges in transversal walls and piers in URM could be observed in terms of the increase in stiffness, capacity and delay in the damage levels.

Loaded in Positive direction:
The peak base shear force increased by 59% due to the adopted strengthening technique. The base shear force at DL1, DL2, DL3 and DL4 increased by 72%, 56%, 61% and 67% respectively in Model S3-A compared to Model U2. Similarly, the second floor displacement at DL1, DL2, DL3 and DL4 increased by 62.0%, 55.3%, 13.4% and 5.8%, respectively in Model S3-A. These results show that the damage is delayed in Model S3-A as a result of the strengthening.

Loaded in Negative direction:
The peak base shear force increased by about 90% in Model S3-A when loaded in negative direction. This shows that the effect of strengthening is more in the negative direction. The base shear force at DL1, DL2, DL3 and DL4 increased by 27%, 63%, 93% and 98%, respectively in Model S3-A compared to Model U2. Similarly, the second floor displacement at DL1, DL2, DL3 and DL4 increased by 0.4%, 30.5%, 18.5% and 14.5%, respectively in Model S3-A.

Although the capacity curve and damage levels are significantly affected due to strengthening of flanges and piers, the overall behaviour of the house, crack pattern and failure mechanism are not affected. The crack pattern similar to the ones presented in Section 3.2 is found in Model S3-A as well. Also, the soft storey mechanism is observed at the first floor level in Model S3-A, similar to Model U2, Model S1-A and Model S2-A.

6.4 Results of Model S1 - B

The results of nonlinear pushover analyses performed on Model S1 using material B i.e. engineered cementitious composites are presented in this section.

6.4.1 Capacity Curve

The pushover capacity curve of Model S1-B obtained from nonlinear finite element analyses is presented along with the capacity curve of Model U2 in Figure 6.10. The maximum shear force in Model S1-B in the positive direction is obtained to be 131 kN, 64.7% higher compared to Model U2. Similarly, the maximum shear force in negative direction is -144 kN, almost double compared to Model U2. This shows that the strengthening is more effective in the negative direction. In addition to the improvement in the base shear capacity, the improvement in the stiffness of the building is also clearly evident from Figure 6.10. The bilinear capacity curve of Model S1-B is presented in Figure 6.11. During the process of obtaining the bilinear curves, the area under the pushover capacity curve is considered only up to the point where the base shear force reduces to 80% of the maximum base shear in post peak region. It can be seen in the figure that the bilinear capacity and pushover capacity are almost similar in negative direction, but slightly different in the positive direction.

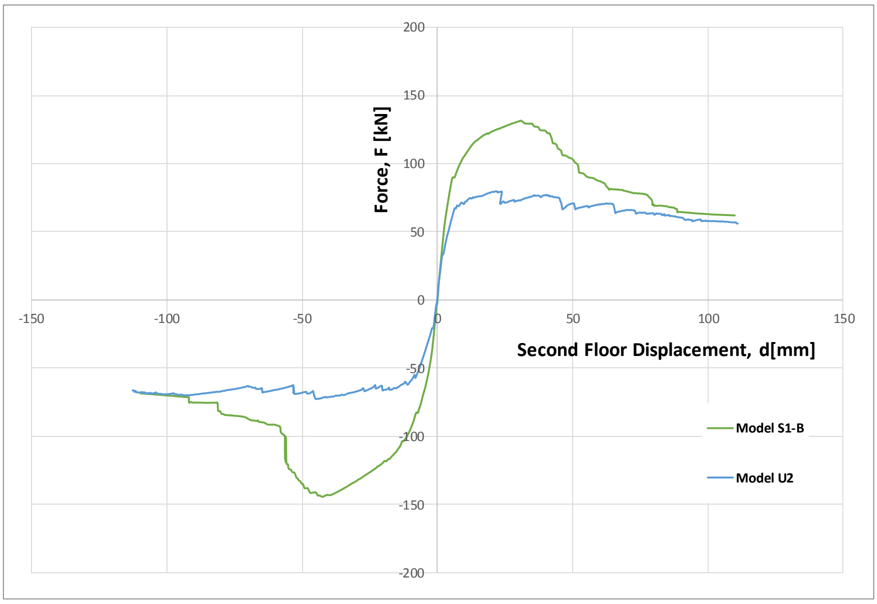

Figure 6.10 Capacity curve of Model S1-B

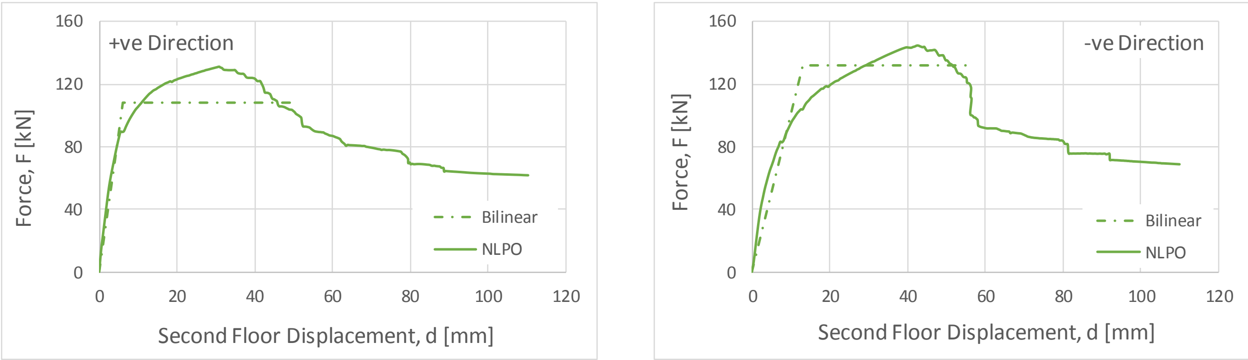

Figure 6.11 Bilinear capacity curve of Model S1-B

6.4.2 Damage Levels

As in previous models, the damage levels are identified next. The summary of the four damage levels identified in Model S1-B is presented in Table 6.4. It should be noted that the capacity curve of Model S1-B consisted of a point where the shear force dropped to half of the maximum base shear force in the post peak region. However, the damage level DL4 is still defined at the point where interstorey drift (IDL) reaches 1.50%. This helps to make a fair and direct comparison with all models analysed during the research. Also the difference is not much between the points where IDL is reached and where there is 50% drop in the base shear force. The damage levels and the point when the global drift reaches 0.8% (GDL) are marked in the capacity curve in Figure 6.12.

Table 6.4 Summary of damage levels in Model S1-B

Damage Levels	Loading Direction	Observed Damage	Force	Second floor displacement	Normalised shear force	Interstorey drift	Global drift
			F	d2	k_G	d_{r1}	d_{r*}
			kN	mm		%	%
DL1	Positive	Initiation of rocking mechanism in piers	85.6	5.04	0.65	0.10	0.09
	Negative	Initiation of rocking mechanism in piers	-70.8	-5.51	0.49	-0.11	-0.10
DL2	Positive	Shear cracks appear in the middle of wide pier in first floor	120.1	16.68	0.92	0.37	0.31
	Negative	Cracks spread across the height of ground floor in wide piers	-118.5	-19.20	0.82	-0.40	-0.36
DL3	Positive	Severely damaged wide pier at ground floor	106.9	45.99	0.82	1.33	0.87
	Negative	Severely damaged wide pier at ground floor	-134.2	-50.50	0.93	-1.19	-0.95
DL4	Positive	IDL is reached	100.6	50.93	0.77	1.50	0.96
	Negative	IDL is reached	-111.8	-56.24	0.77	-1.50	-1.06

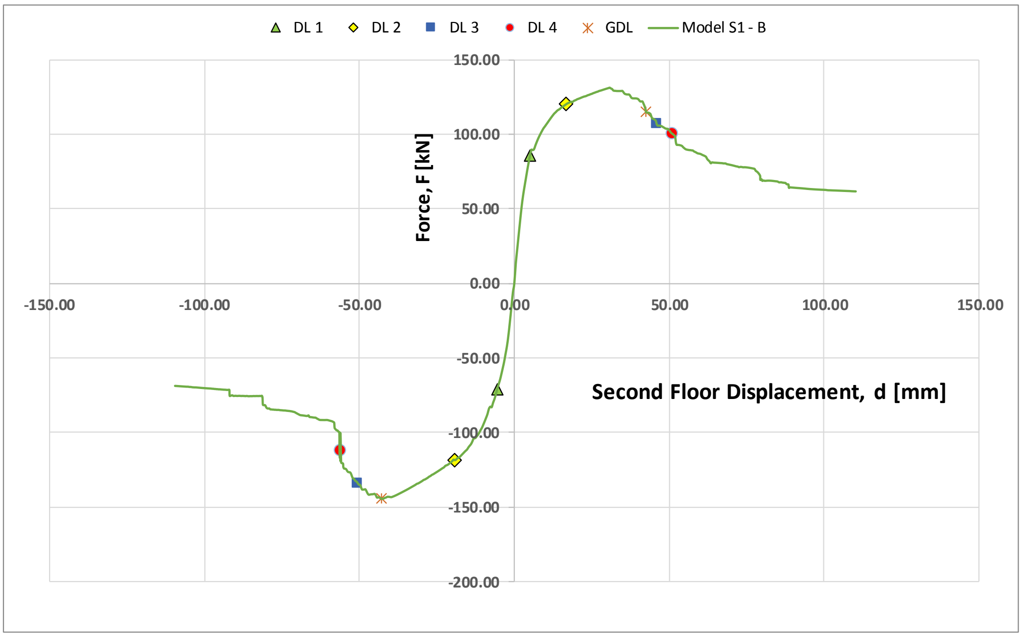

Figure 6.12 Damage levels in Model S1-B

6.4.3 Comparison with Model U2

The effect of applying an overlay of ECC over piers in URM could be observed in terms of the increase in stiffness, capacity and delay in the damage levels. The capacity curve of Model S1-B has a significant drop in the shear force in post peak region compared to Model U2. The response of Model S1-B is less ductile compared to Model U2. This is mainly due to the damage in ECC in the toe of piers due to crushing in the post peak region.

Loaded in Positive direction:
The base shear force at DL1, DL2, DL3 and DL4 increased by 118%, 71%, 39% and 42%, respectively in Model S1-B compared to Model U2. Similarly, the second floor displacement at DL1, DL2, DL3 and DL4 increased by 77.0%, 69.1%, 15.5% and 1.4%, respectively in Model S1-B. These results show that the damage is delayed in Model S1-B as a result of the strengthening.

Loaded in Negative direction:
The base shear force at DL1, DL2, DL3 and DL4 increased by 74%, 92%, 89% and 63%, respectively in Model S1-B compared to Model U2. Similarly, the second floor displacement at DL1, DL2, DL3 and DL4 increased by 10.6%, 47.3%, 21.3% and 7.2%, respectively in Model S1-B.

Although the capacity curve and damage levels are significantly affected due to strengthening of piers, the overall crack pattern is not affected. The crack pattern similar to the ones presented in Section 3.2 is found in Model S1-B as well. The damage is mainly accumulated in the wide piers. Also, the soft storey mechanism is observed at the first floor level in Model S1-B, similar to Model U2 and models strengthened using material A.

6.5 Results of Model S2 - B

The results of monotonic nonlinear pushover analyses performed on Model S2-B is presented in this section. Like in previous models, the pushover capacity curve, bilinear capacity curve, damage levels and drifts are presented and the results are compared with Model U2.

6.5.1 Capacity Curve

The pushover capacity curve of Model S2-B is presented in Figure 6.13. The maximum base shear force in the positive direction in Model S2-B is 140 kN, approximately 80% higher than the unstrengthened building. Similarly, the maximum base shear force in the negative direction in Model S2-B is 139 kN, about 92% higher than Model U2. As observed above in Model S2-A, the initial stiffness of the building is not affected much due to the adopted strengthening technique in Model S2-B as well. The bilinear capacity curves of Model S2-B are presented in Figure 6.14. As the interstorey drift limit is reached above than the 20% drop of the shear force, the bilinear curves are obtained using the area of the pushover capacity curve up to the point where IDL is reached.

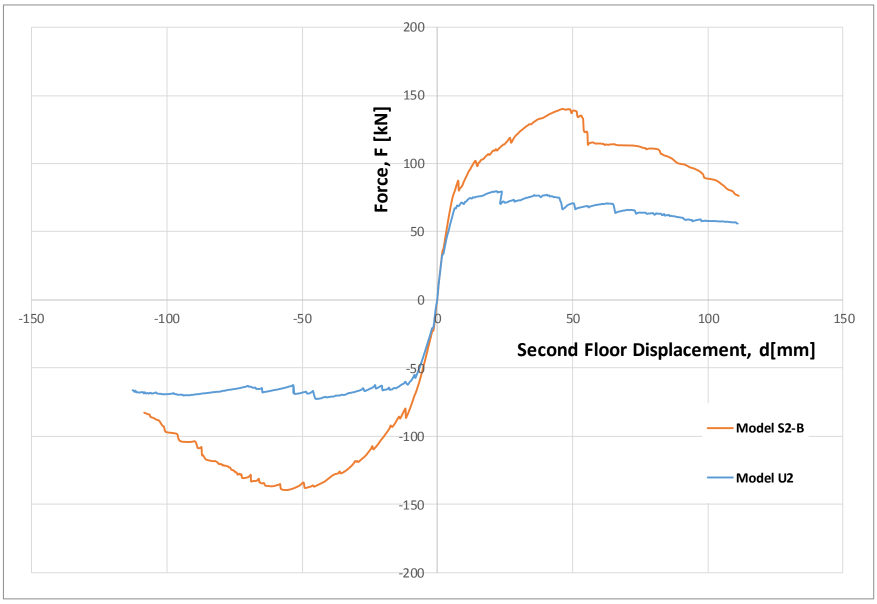

Figure 6.13 Capacity curve of Model S2-B

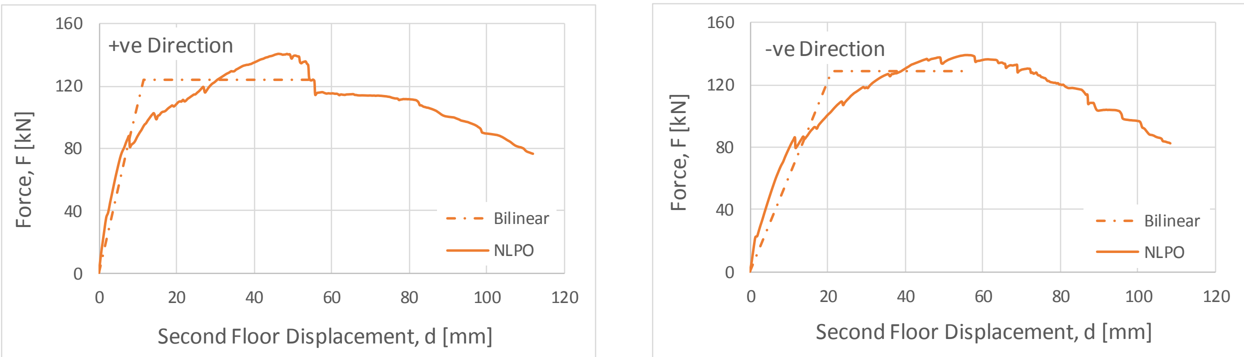

Figure 6.14 Bilinear capacity curve of Model S2-B

6.5.2 Damage Levels

The damage levels are identified in Model S2-B as well using the same criteria defined above for Model U2 and strengthened cases using material A. The summary of the damage levels is presented in Table 6.5. The damage levels and GDL are marked in the capacity curve and shown in Figure 6.15. The crack pattern and crack evolution are found to be similar to other previous models.

Table 6.5 Summary of damage levels in Model S2-B

Damage Levels	Loading Direction	Observed Damage	Force F kN	Second floor displacement d2 Mm	Normalised shear force k_G	Interstorey drift d_{r1} %	Global drift d_{r*} %
DL1	Positive	Initiation of rocking mechanism in piers	78.3	6.10	0.56	0.11	0.12
	Negative	Initiation of rocking mechanism in piers	-54.4	-5.87	0.39	-0.12	-0.11
DL2	Positive	Shear cracks appear in the middle of wide pier in first floor	98.4	14.77	0.70	0.36	0.28
	Negative	Cracks spread across the height of ground floor in wide piers	-91.7	-16.15	0.66	-0.39	-0.30
DL3	Positive	Severely damaged	138.9	44.29	0.99	1.18	0.84

		wide pier at ground floor					
	Negative	Severely damaged wide pier at ground floor	-135.8	-45.99	0.98	-1.22	-0.87
DL4	Positive	IDL is reached	132.9	53.92	0.95	1.50	1.02
	Negative	IDL is reached	-138.9	-54.65	1.00	-1.50	-1.03

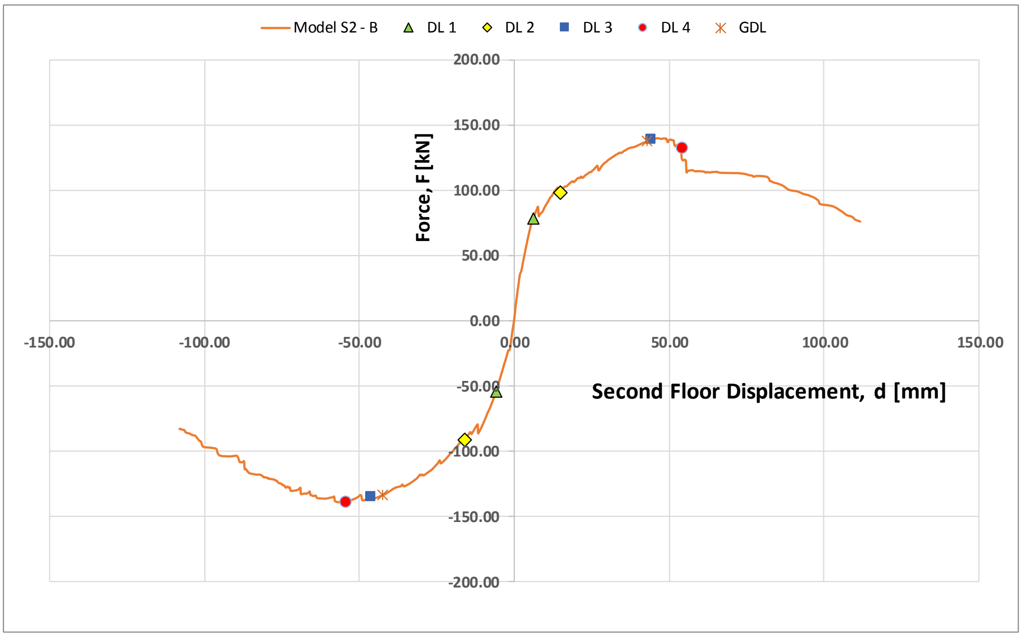

Figure 6.15 Damage levels in Model S2-B

6.5.3 Comparison with Model U2

The effect of applying an overlay of ECC over flanges and part of piers in URM could be observed in terms of the increase in capacity and delay in the damage levels.

Loaded in Positive direction:
The base shear force at DL1, DL2, DL3 and DL4 increased by 100%, 40%, 81% and 88%, respectively in Model S2-B compared to Model U2. Similarly, the second floor displacement at DL1, DL2, DL3 and DL4 increased by 114.2%, 49.7%, 11.2% and 7.4%, respectively in Model S2-B. These results show that the damage is delayed in Model S2-B as a result of the strengthening.

Loaded in Negative direction:
The base shear force at DL1, DL2, DL3 and DL4 increased by 34%, 49%, 91% and 102%, respectively in Model S2-B compared to Model U2. Similarly, the second floor displacement at DL1, DL2, DL3 and DL4 increased by 17.7%, 24.0%, 10.5% and 4.2%, respectively in Model S2-B.

Although the capacity curve and damage levels are significantly affected due to the strengthening of flanges and part of piers, the overall crack pattern is not affected. The crack pattern similar to the ones presented in Section 3.2 is found in Model S2-B as well. The damage is mainly accumulated in the wide piers. Also, the soft storey mechanism is observed at the first floor level in Model S2-B, similar to Model U2.

6.6 Results of Model S3 - B

The results of nonlinear pushover analyses performed on Model S3 strengthened using material B (Engineered Cementitious Composites) are presented in this section.

6.6.1 Capacity Curve

Figure 6.26 shows the capacity curve of Model S3-B and the unstrengthened model, Model U2. Due to the adopted strengthening technique and material, the maximum base shear force increased by 124% and 173% in the positive and negative direction, respectively. Besides the improvement in the base shear force, the increase in the stiffness of the strengthened building is also clearly visible in Figure 6.16. The results presented in Figure 6.10, Figure 6.13 and Figure 6.16 for Model S1-B, Model S2-B and Model S3-B, respectively have shown that Models S1-B and S3-B have more pronounced softening compared to Model S2-B. The reason behind such difference in the behaviour is the adopted strengthening techniques. The piers are fully strengthened in models S1-B and S3-B. The strengthened material i.e. ECC is applied with a compressive strength of 30 MPa and parabolic softening. When toe crushing initiates in piers during the pushover analyses, the ECC undergoes compressive softening as well which is reflected by the significant drop in the shear force in the post peak region of the capacity curves. However, in Model S2-B, ECC is not applied to the toe of piers. The ECC therefore does not undergo crushing and the response is more ductile than Model S1-B and Model S3-B.

The pushover capacity curve of Model S3-B is converted to bilinear curves and presented in Figure 6.17. The area of the pushover capacity curve is considered only up to the point where shear force reduces to 80% of the maximum base shear force during the process of converting pushover curve to the bilinear curve.

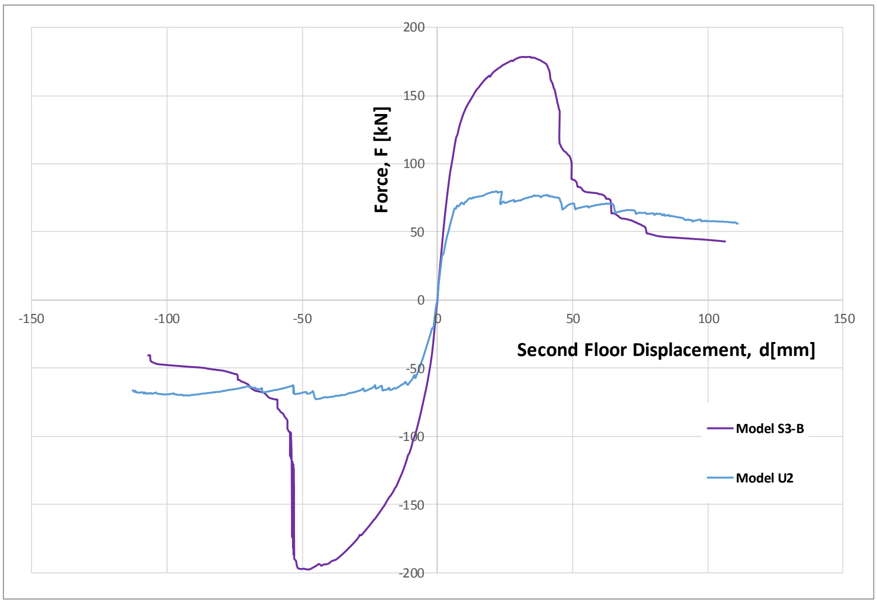

Figure 6.16 Capacity curve of Model S3-B

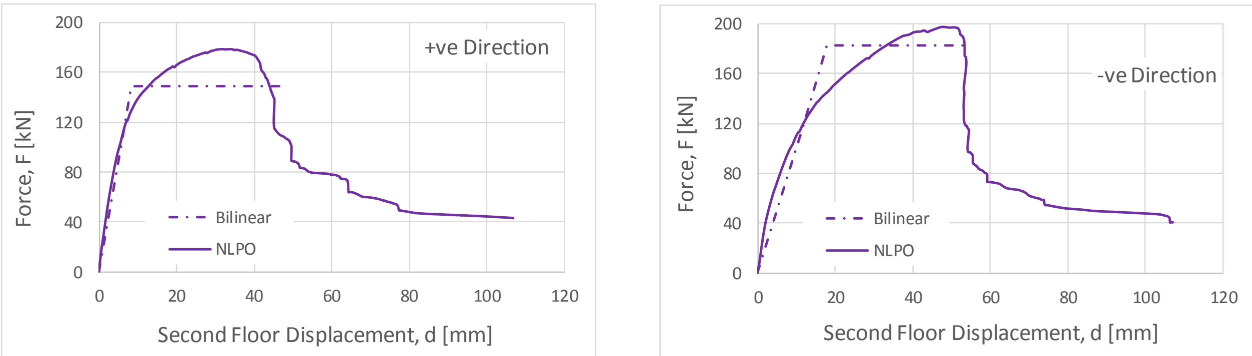

Figure 6.17 Bilinear capacity curve of Model S3-B

6.6.2 Damage Levels

The damage levels identified in Model S3-B using the same criteria described above are summarised in Table 6.6. The damage levels and point where GDL is reached are marked in the capacity curve and shown in Figure 6.18. Like Model S1-B, the capacity curve of S3-B also has the point where shear force reduces to half of the maximum shear force. However, this point is not defined as DL4 and still the point where IDL is reached is considered as DL4 for the direct comparison of results.

Table 6.6 Summary of damage levels in Model S3-B

Damage Levels	Loading Direction	Observed Damage	Force	Second floor displacement	Normalised shear force	Interstorey drift	Global drift
			F	d2	k_G	d_{r1}	d_{r*}
			kN	mm		%	%
DL1	Positive	Initiation of rocking mechanism in piers	103.6	5.58	0.58	0.10	0.10
	Negative	Initiation of rocking mechanism in piers	-84.9	-6.43	0.43	-0.12	-0.12
DL2	Positive	Shear cracks appear in the middle of wide pier in first floor	155.3	14.87	0.87	0.30	0.28
	Negative	Cracks spread across the height of ground floor in wide piers	-147.7	-18.80	0.75	-0.39	-0.35
DL3	Positive	Severely damaged wide pier at ground floor	152.5	43.61	0.85	1.21	0.82
	Negative	Severely damaged wide pier at ground floor	-195.8	-45.62	0.99	-1.03	-0.86
DL4	Positive	IDL is reached	105.8	48.79	0.59	1.50	0.92
	Negative	IDL is reached	-123.5	-53.22	0.62	-1.50	-1.00

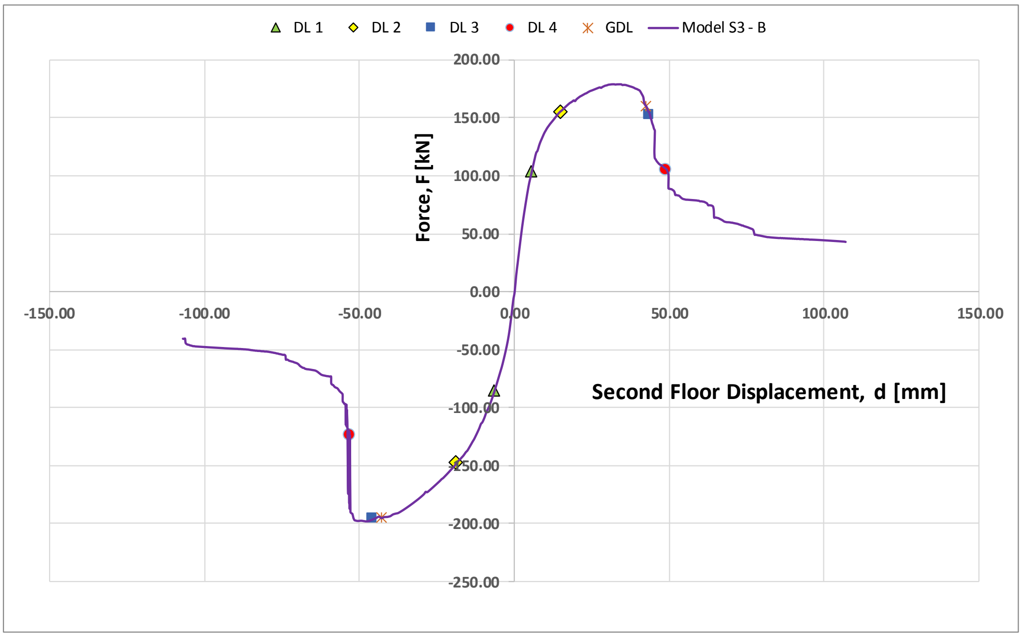

Figure 6.18 Damage levels in Model S3-B

6.6.3 Comparison with Model U2

The effect of applying an overlay of ECC over flanges and piers in URM could be observed in terms of the increase in stiffness, capacity and delay in the damage levels. The capacity curve of Model S3-B has a significant drop in the shear force in post peak region compared to Model U2. This is mainly due to the damage in ECC in the toe of piers due to crushing in the post peak region.

Loaded in Positive direction:
The base shear force at DL1, DL2, DL3 and DL4 increased by 164%, 121%, 99% and 49%, respectively in Model S3-B compared to Model U2. Similarly, the second floor displacement at DL1, DL2, DL3 and DL4 increased by 95.7%, 50.8%, 9.6% and 2.8%, respectively in Model S3-B. These results show that the damage is delayed in Model S3-B as a result of the strengthening.

Loaded in Negative direction:
The base shear force at DL1, DL2, DL3 and DL4 increased by 109%, 139%, 176% and 80%, respectively in Model S1-B compared to Model U2. Similarly, the second floor displacement at DL1, DL2, DL3 and DL4 increased by 29.0%, 44.3%, 9.6% and 1.5%, respectively in Model S3-B.

Although the capacity curve and damage levels are significantly affected due to strengthening of flanges and piers, the overall crack pattern is not affected. The crack pattern similar to the ones presented in Section 3.2 is found in Model S3-B as well. Also, the soft storey mechanism is observed at the first floor level in Model S3-B, similar to Model U2 and other strengthened models.

6.7 Discussion and Summary of Results of Nonlinear Pushover Analyses

The results of nonlinear pushover analyses performed on strengthened models have shown improvement in the base shear capacity and displacement capacity compared to the unstrengthened model. Although the second floor displacement at which damage levels occur have increased due to the use of the strengthening measures, the increase in the ultimate displacement capacity (i.e. DL4) is not much compared to the increase in the base shear capacity. This means the adopted strengthening materials and strengthening techniques improve the strength of the building but not the ductility. However, it should be taken into account that, given the lack of a consolidated literature and/or experimental tests that allows to determine the maximum displacement capacity of strengthened buildings, the same IDL used for the URM model was selected. However, when ECC was used, significant drops of strength were observed for displacements slightly larger than the IDL, and thus a small increase of ductility would be anyhow expected.

In general, it is observed that the improvement in shear force capacity is higher in negative direction compared to the positive direction. The reason for this could be that larger strengthened area (wide piers) is in the compressive side when pushed in the negative direction. The strengthening techniques S1 and S3 did not only improve the shear force capacity and displacement, but also the stiffness of the building. This is mainly due to the strengthening of piers in models S1 and S3 unlike in S2 where only one-third of the pier is strengthened.

The results of the analyses have also highlighted the importance of choosing appropriate strengthening material according to the adopted strengthening technique. The results of Model S1-B and S3-B are found to be less ductile compared to Model S2-B. This is due to the toe crushing of ECC overlaid piers in Models S1-B and S3-B. As the layer of ECC is not applied around the compressive toe of piers in Model S2-B, the response is more ductile. The results have indicated that the increase in the capacity of the building due to the use of ECC is higher compared to the models strengthened using OSB panels. However, it should be noted that the material properties used for ECC are obtained directly from the literature and no calibration exercise is performed to take into account the perfect bond assumed between masonry and ECC layer.

The damage levels are identified based on the crack evolution and damage observed. The damage levels DL1, DL2 and DL3 which represent no visible cracks, light structural damage and moderate structural damage, respectively are identified as points before piers exhibit rocking mechanism, cracks appear in middle of piers and cracks spread all over the pier, respectively. The damage level DL4 on the other hand is defined as the point when interstorey drift limit is reached i.e. 1.5%. Although this definition of DL4 is reasonable for an unstrengthened case, it represents more of a lower bound value for the strengthened case. The difference between DL3 and DL4 is found to be very low when this definition of DL4 is used for the strengthened cases. This shows the need of the new definition of the ultimate displacement capacity especially for the strengthened cases. Therefore, it is recommended to investigate new method of determining the ultimate displacement capacity based on both numerical and experimental studies of the strengthened buildings.

The pushover capacity curves and bilinear capacity curves of Model U2 and models strengthened using material A (OSB panels) are presented in Figure 6.19. Similarly, Figure 6.20 shows the comparison of the pushover capacity curves and bilinear capacity curves of Model U2 and models strengthened using material B.

The increment in the shear force and second floor displacement at different damage levels due to the use of different strengthening measures in positive and negative loading direction are shown in Figure 6.23 and Figure 6.24, respectively.

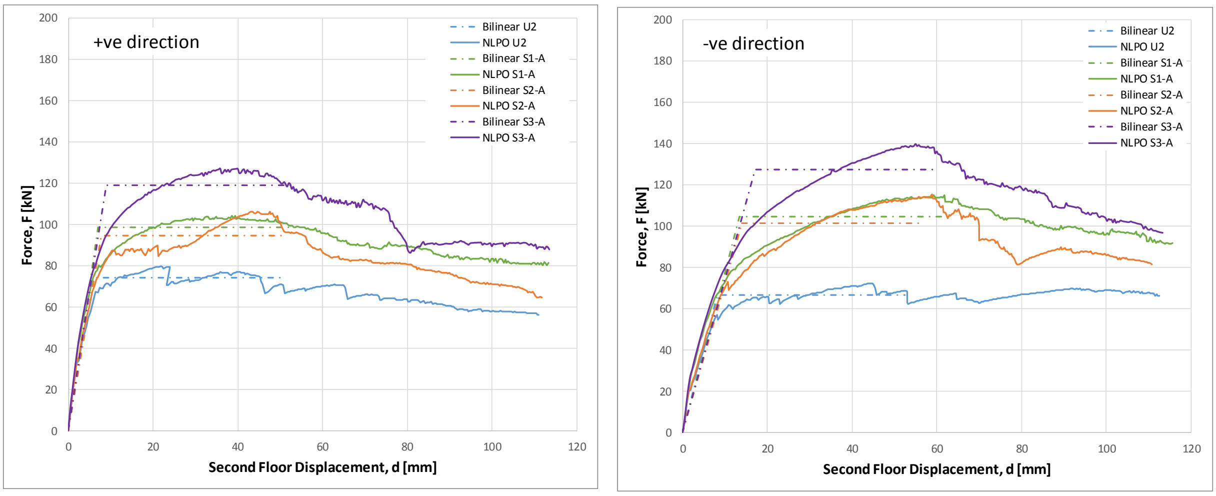

Figure 6.19 Comparison of Model U2 with models strengthened using Material A

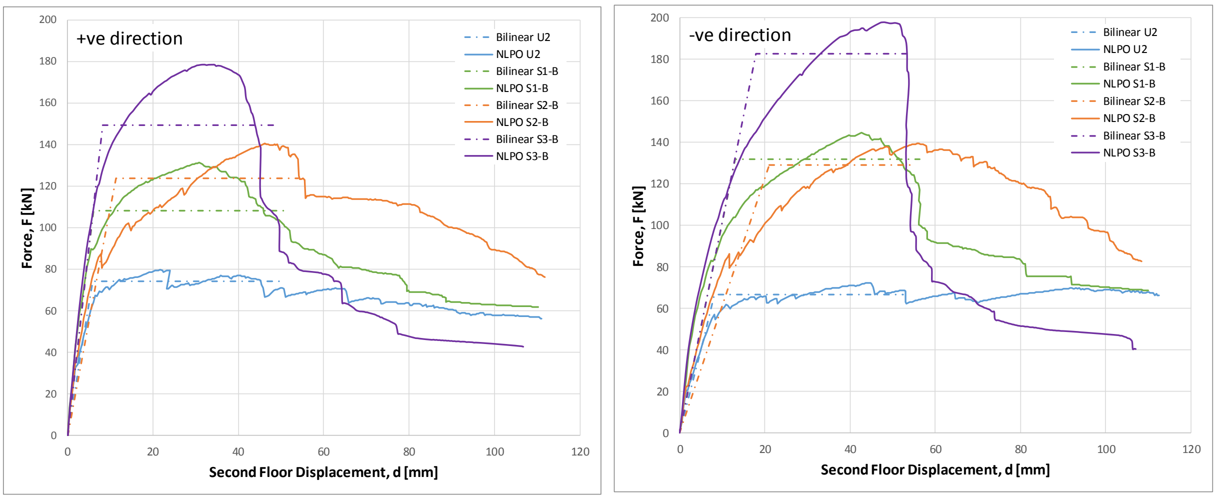

Figure 6.20 Comparison of Model U2 with models strengthened using Material B

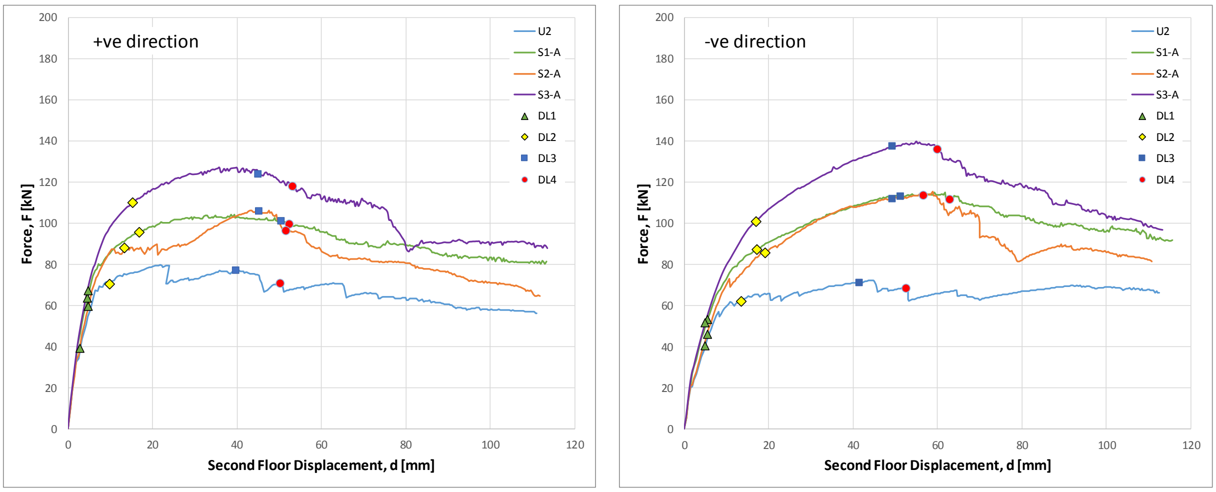

Figure 6.21 Comparison of damage levels between U2 and strengthened models using Material A

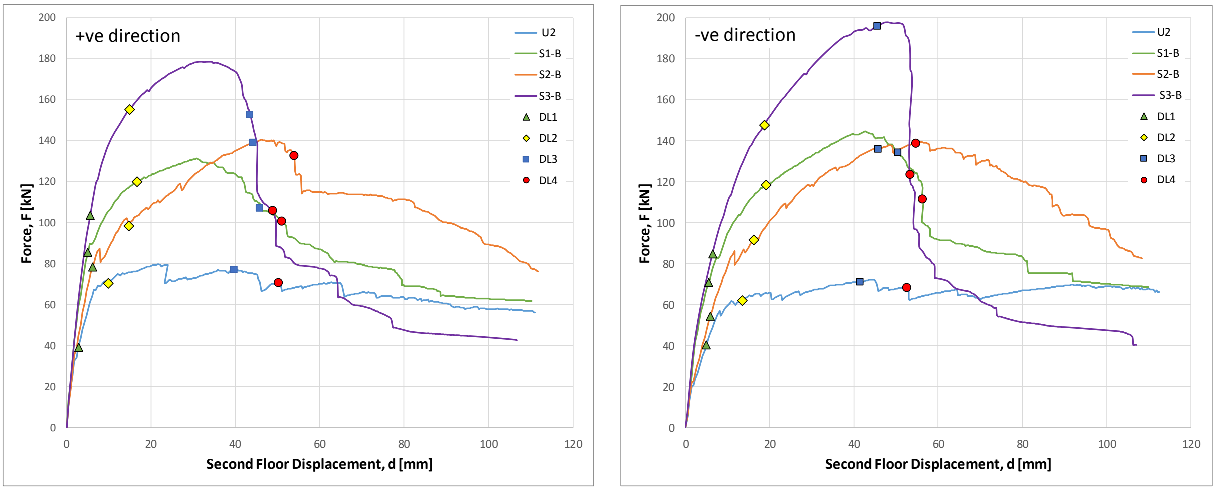

Figure 6.22 Comparison of damage levels between U2 and strengthened models using Material B

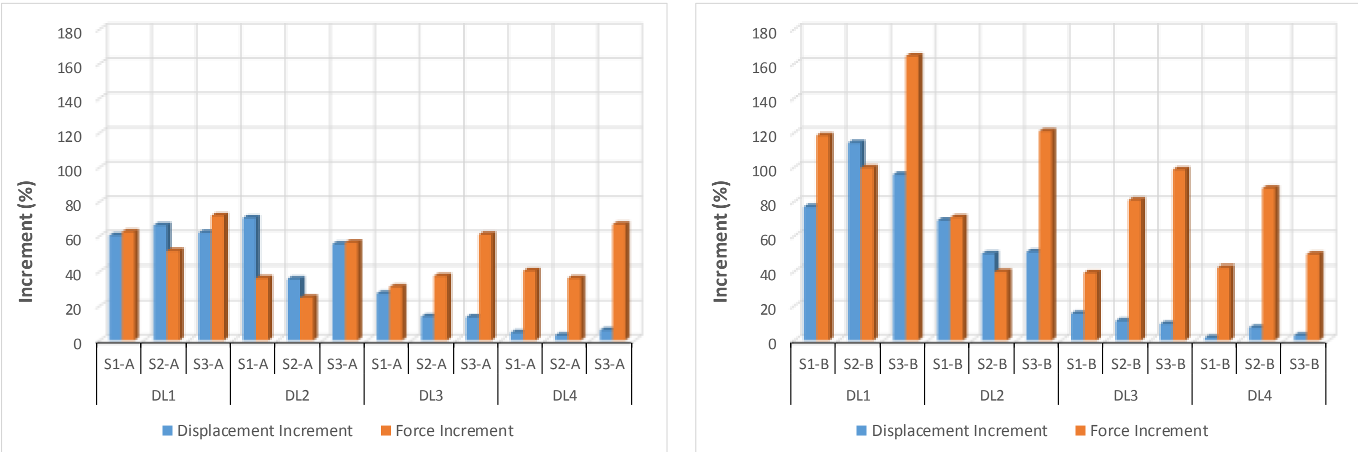

OSB ECC

Figure 6.23 Increment in force and displacement capacity in positive direction at different damage levels using different strengthening techniques and materials

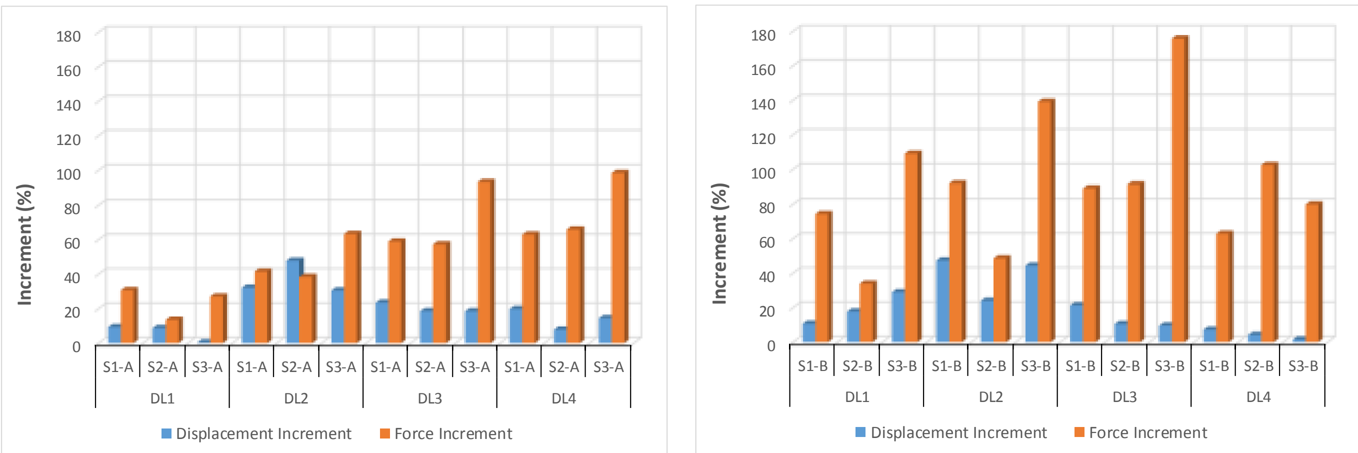

OSB ECC

Figure 6.24 Increment in force and displacement capacity in negative direction at different damage levels using different strengthening techniques and materials

7 Nonlinear Time History Analysis of Strengthened Buildings

The results of nonlinear time history analyses of strengthened buildings are discussed in this chapter. The Model U2 strengthened using strengthening techniques S1, S2 and S3 and materials A and B defined above in chapter 5 are analysed when subjected to an earthquake signal. The modelling technique, analysis procedure and earthquake signal adopted in the analyses are similar to the one used above in NLTH analysis of Model U1 and Model U2. The results of each model are presented in terms of hysteresis curve, damage level identification and comparison with the corresponding NLPO results. The results like damage level identification, dynamic capacity curve and comparison with NLPO are presented only for the positive direction due to two reasons: NLTH analysis is performed by applying the signal only in the positive direction, and to stay consistent with the results presented and discussed above in chapter 4.

7.1 Results of Model S1-A

This section presents the results of NLTH analysis performed on Model S1 strengthened using material A i.e. OSB panels. The results are presented only up to the end of the tenth run because the house is severely damaged after the tenth run and also the damage level DL4 is identified in the tenth run itself.

7.1.1 Hysteresis Curve

The hysteresis curve of Model S1-A is shown in Figure 7.1. The maximum base shear force and second floor net displacement are found to be 129 kN and 53.5 mm, respectively, both in the tenth run. The energy dissipation and residual displacement continue to increase with the increase in runs due to the increase in nonlinearity in the model.

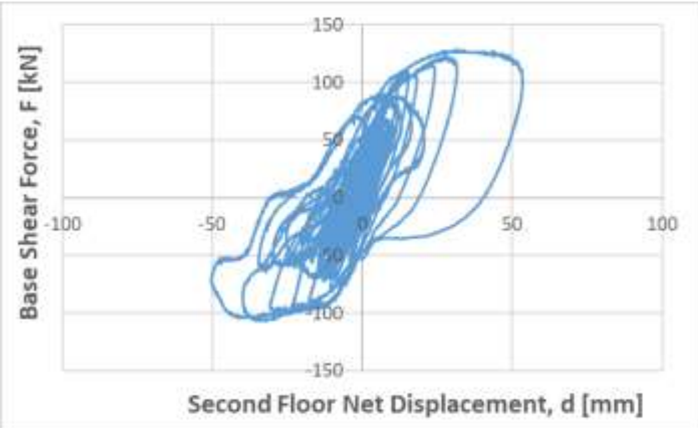

Figure 7.1 Hysteresis curve of Model S1-A

7.1.2 Damage Levels Identification

The damage levels in Model S1-A are identified next. The base shear force, second floor displacement, normalized shear force, interstorey drift and global drift obtained at four damage levels are summarized in table 7.1. The values presented in Table 7.1 are based on the dynamic capacity curve which is the backbone curve of NLTH results and is shown in Figure 7.2. When the base shear force and second floor displacement obtained at four damage levels in Model S1-A (NLTH) is compared with the corresponding components in Model U2 (NLTH), it can be found that both the base shear force and second floor displacement have increased in Model S1-A compared to Model U2. However, it should be noted that the damage levels occurred around the same time in both the models. Though the delay in damage levels could be observed in terms of the base shear force and second floor displacement, the delay could not be observed in terms of the time/signal.

Table 7.1 Summary of damage levels in Model S1-A

Damage Levels	Loading Direction	Observed Damage	Force	Second floor displacement	Normalised shear force	Interstorey drift	Global drift
			F	d2	k_G	d_{r1}	d_{r*}
			kN	mm		%	%
DL1	Positive	Initiation of rocking mechanism in piers	35.0	1.97	0.27	0.04	0.04
DL2	Positive	Crack appears in the middle of wide pier in ground floor	89.4	7.95	0.69	0.16	0.15
DL3	Positive	Severely damaged wide pier in ground floor	115.9	24.21	0.90	0.53	0.46
DL4	Positive	IDL is reached	98.7	53.46	0.77	1.50	1.01

7.1.3 Comparison with NLPO

The pushover capacity curve, hysteresis curve and dynamic capacity curve of Model S1-A are presented together in Figure 7.2. The dynamic capacity curve is obtained by taking points corresponding to maximum base shear force in the first nine runs and the points corresponding to maximum second floor net displacement in the tenth run.

The initial stiffness of the building shown by results of NLPO and NLTH are in very good agreement with each other. Also the peak base shear force occur almost at the same second floor net displacement in both the models. However, the peak base shear force in NLTH is 25% higher than in the NLPO analysis.

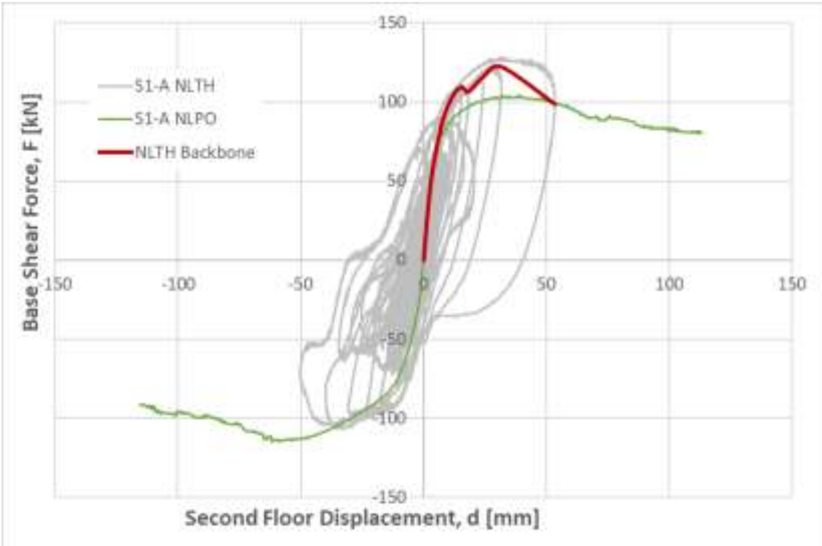

Figure 7.2 Hysteresis curve, Pushover capacity curve and Dynamic capacity curve of Model S1-A

The damage levels are marked in both the pushover capacity curve and dynamic capacity curve, and shown in Figure 7.3. The damage levels DL1, DL2 and DL3 occur above in NLTH analysis compared to NLPO analysis. This observation is similar to the one discussed above for Model U1 and Model U2 as well. The same reasoning holds true for this case as well. As there is accumulation of damage in NLTH analysis, it is reasonable to observe damage at lower second floor net displacement. The interstorey drift limit is reached almost at the same point in both NLPO and NLTH analyses. Besides these similarities, both NLPO and NLTH analyses exhibited similar crack pattern, displacement profile and overall behaviour of the house.

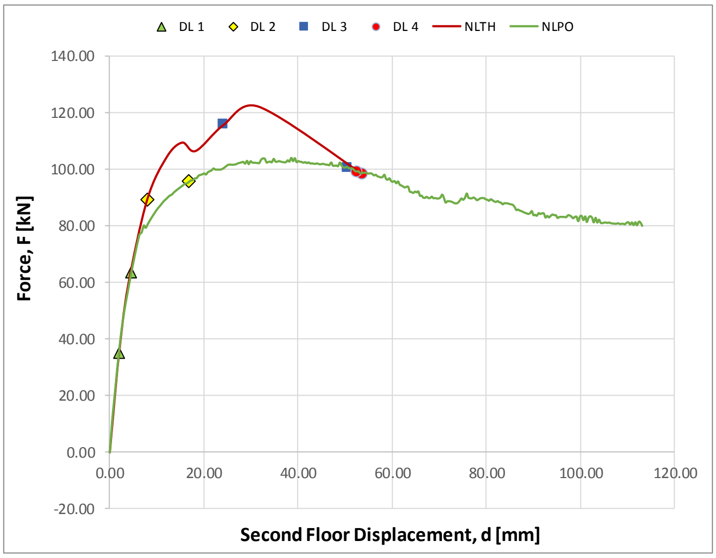

Figure 7.3 Damage levels of Model S1-A

7.2 Results of Model S2-A

The results of dynamic analysis performed on Model S2 strengthened using material A is shown in this section.

7.2.1 Hysteresis Curve

Figure 7.4 shows the hysteresis curve of Model S2-A obtained from the nonlinear time history analysis. The results are presented only for the first ten runs because the damage level DL4 is identified already in the ninth run. The maximum base shear force and second floor net displacement are found to be 136 kN and 63.1 mm, respectively, both in the tenth run. The residual displacement is higher towards the end of the analysis, especially in the positive direction. The result is as expected due to the accumulation of damage towards the end of the analysis and also because the input signal is applied in the positive direction.

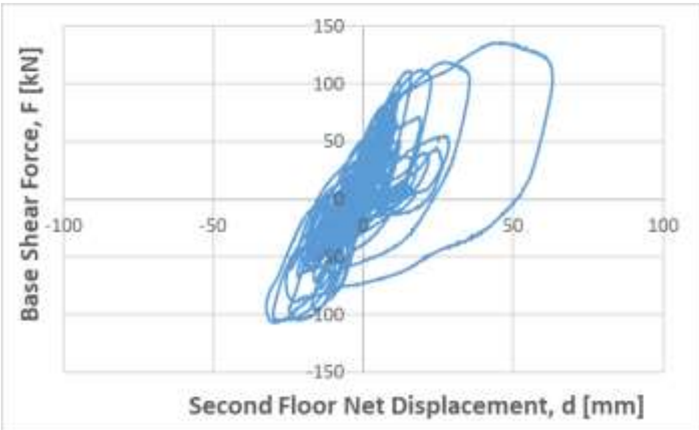

Figure 7.4 Hysteresis curve of Model S2-A

7.2.2 Damage Levels Identification

The damage levels are identified and presented with the corresponding second floor displacement, base shear force, normalised shear force and global drift in Table 7.2. The findings of Model S2-A is similar to the findings presented for Model S1-A. The damage levels, DL2 DL3 and DL4 are delayed in terms of the base shear force and second floor displacement due to the adopted strengthening strategy. However, the damage levels occurred at the same time in both the strengthened and unstrengthened cases.

Table 7.2 Summary of damage levels in Model S2-A

Damage Levels	Loading Direction	Observed Damage	Force	Second floor displacement	Normalised shear force	Interstorey drift	Global drift
			F	d2	k_G	d_{r1}	d_{r*}
			kN	mm		%	%
DL1	Positive	Initiation of rocking mechanism in piers	35.4	2.07	0.26	0.04	0.04
DL2	Positive	Crack appears in the middle of wide pier in ground floor	80.8	7.09	0.59	0.13	0.13
DL3	Positive	Severely damaged wide pier in ground floor	112.3	19.67	0.83	0.41	0.37
DL4	Positive	IDL is reached	118.4	57.10	0.87	1.50	1.08

7.2.3 Comparison with NLPO

The hysteresis curve, pushover capacity curve and dynamic capacity curve of Model S2-A are presented together in Figure 7.5. The dynamic capacity curve is obtained by taking the points corresponding to maximum base shear force in all ten runs. The point corresponding to maximum second floor displacement in the tenth run is also considered to obtain the dynamic capacity curve. It can be seen in the figure that the initial stiffness of the building exhibited by both NLTH and NLPO analyses are in good agreement with each other. When considering the hysteresis curve and pushover capacity curve, it can be observed that the maximum base shear force occur almost at the same second floor net displacement. However, the maximum base shear force from NLTH is about 28% higher than NLPO maximum base shear force.

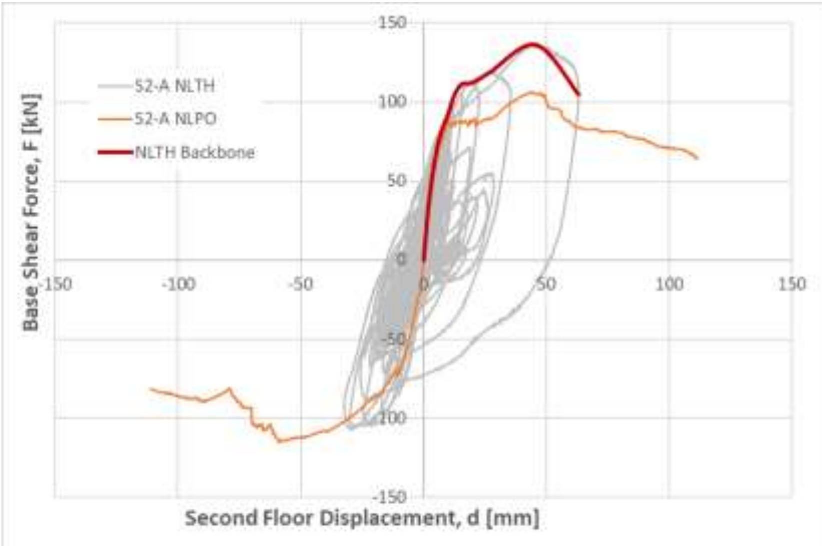

Figure 7.5 Hysteresis curve, Pushover capacity curve and Dynamic capacity curve of Model S2-A

The damage levels are then marked in two capacity curves and presented in Figure 7.6. Like observed above in Model S1-A, the damage levels occur above in the NLTH model compared to NLPO model. The crack pattern and the overall behaviour of the house stay similar in both the models.

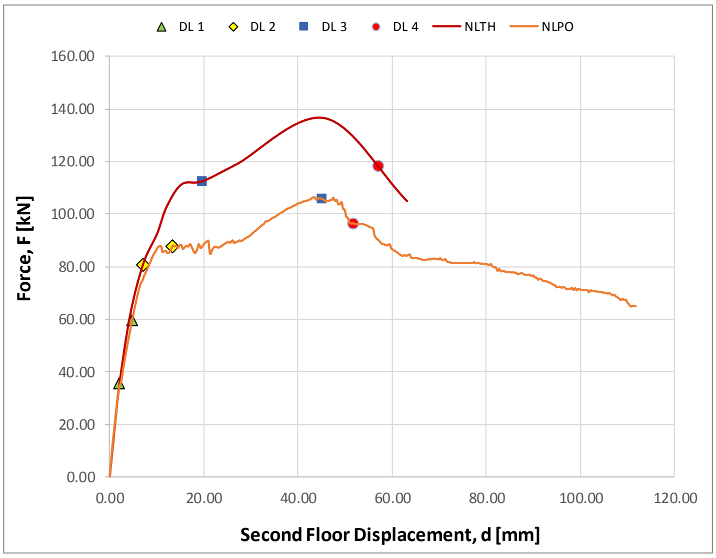

Figure 7.6 Damage levels of Model S2-A

7.3 Results of Model S3-A

The results of nonlinear time history analysis performed on model S3 strengthened using OSB panels (material A) are presented next.

7.3.1 Hysteresis Curve

The hysteresis curve showing the relation between base shear force and second floor net displacement is shown in Figure 7.7. The results are presented up to the end of the tenth run like in previous models. The maximum base shear force and second floor net displacement are found to be 134 kN and 84.2 mm, respectively, both in the tenth run. It can be seen in the figure that the energy dissipation and residual displacement is quite high in the final run.

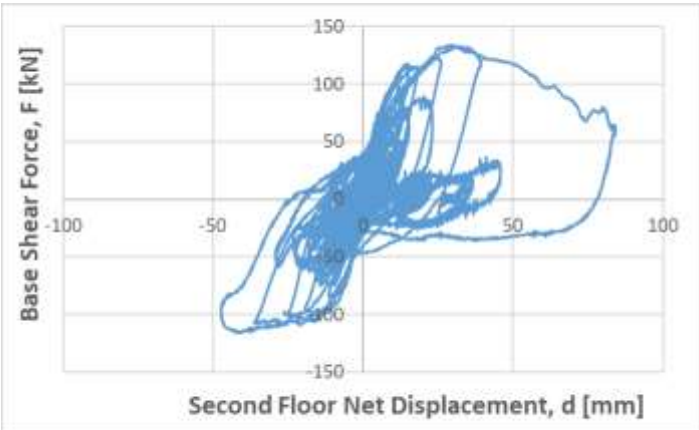

Figure 7.7 Hysteresis curve of Model S3-A

7.3.2 Damage Levels Identification

The summary of the damage levels identified in Model S3-A is presented below in Table 7.3. The finding is similar to the findings presented above for Model S1-A and Model S2-A.

Table 7.3 Summary of damage levels in Model S3-A

Damage Levels	Loading Direction	Observed Damage	Force	Second floor displacement	Normalised shear force	Interstorey drift	Global drift
			F	d2	k_G	d_{r1}	d_{r*}
			kN	mm		%	%
DL1	Positive	Initiation of rocking mechanism in piers	36.6	2.00	0.27	0.04	0.04

DL2	Positive	Crack appears in the middle of wide pier in ground floor	92.6	7.99	0.69	0.16	0.15
DL3	Positive	Severely damaged wide pier in ground floor	122.6	24.89	0.91	0.51	0.47
DL4	Positive	IDL is reached	93.6	59.50	0.70	1.50	1.12

7.3.3 Comparison with NLPO

Figure 7.8 shows the hysteresis curve, pushover capacity curve and the dynamic capacity curve of Model S3-A presented together. The initial stiffness of the building is beautifully captured by both NLTH and NLPO analyses. The maximum base shear force obtained from NLTH analysis is about 5.5% higher compared to the maximum base shear force obtained from NLPO analysis. The dynamic capacity curve is obtained by considering the points corresponding to maximum base shear force in the first 9 runs and the point corresponding to maximum second floor displacement for the tenth run.

Besides the close comparison in terms of initial stiffness and maximum base shear force between two analyses approach, the crack pattern, displacement profile and failure mechanism are also found to be similar. The damage levels are marked in both the capacity curves and presented in Figure 7.9. As observed in previous models, the damage levels in NLTH analysis occur above compared to the damage levels in NLPO.

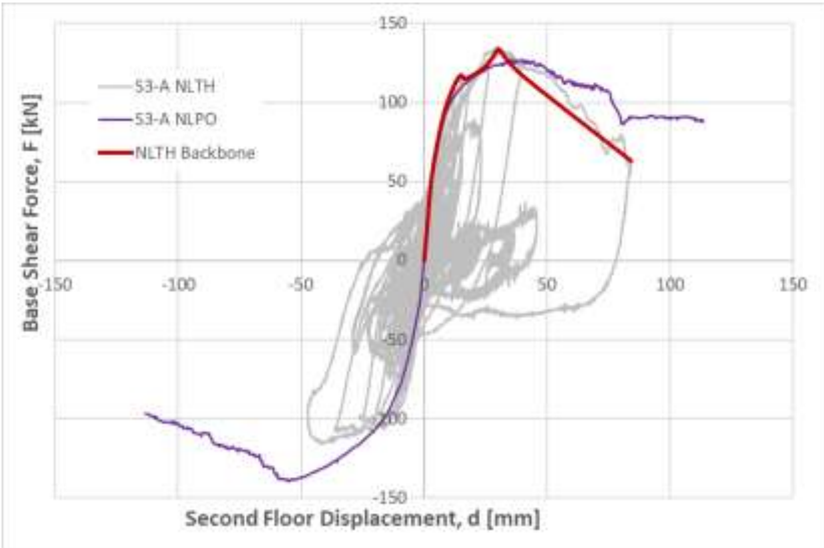

Figure 7.8 Hysteresis curve, Pushover capacity curve and Dynamic capacity curve of Model S3-A

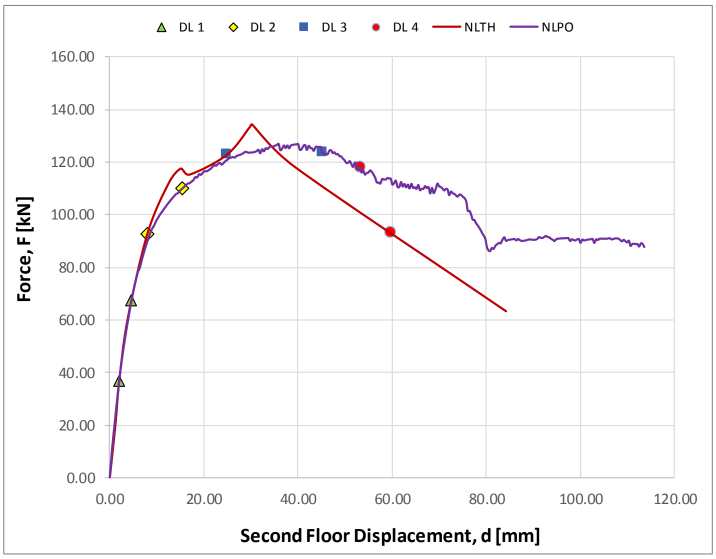

Figure 7.9 Damage levels of Model S3-A

7.4 Results of Model S1-B

The results of the models strengthened using material B (ECC) are presented in the remaining sections. As previous results have shown that the nonlinear pushover analysis and nonlinear time history analysis are fairly in good agreement with each other, to minimize the computation cost, the dynamic analyses in remaining models are performed only up to the end of the ninth run. This section shows the results of the dynamic analysis performed on model S1.

7.4.1 Hysteresis Curve

The hysteresis curve obtained from the dynamic analysis of model S1 strengthened using ECC (material B) is shown in Figure 7.10. The maximum base shear force and second floor displacement are found to be 150 kN and 32 mm, respectively, both at the ninth run. It can be seen in the hysteresis curve that the energy dissipation and the residual displacement is not high until the end of the nine runs.

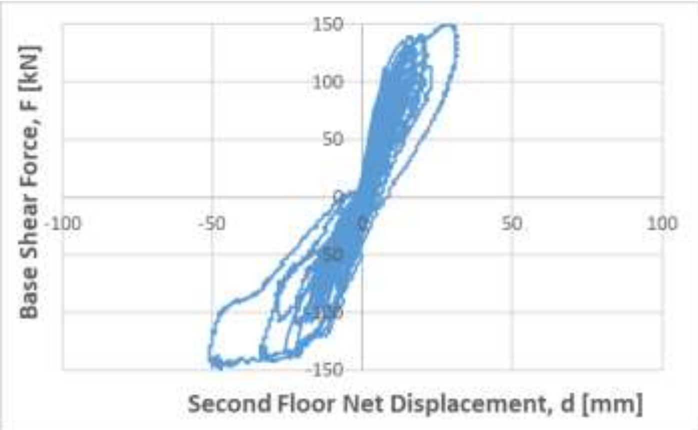

Figure 7.10 Hysteresis curve of Model S1-B

7.4.2 Damage Levels Identification

The damage levels are identified in model S1-B and presented in Table 7.4 with base shear force, second floor net displacement, normalised shear force, interstorey drift and global drift. As the interstorey drift limit (IDL = 1.5%) is not reached until the end of the ninth run, damage level DL4 is omitted in the result presented in the table.

Table 7.4 Summary of damage levels in Model S1-B

Damage Levels	Loading Direction	Observed Damage	Force	Second floor displacement	Normalised shear force	Interstorey drift	Global drift
			F	d2	k_G	d_{r1}	d_{r*}
			kN	mm		%	%
DL1	Positive	Initiation of rocking mechanism in piers	37.1	1.90	0.25	0.03	0.04
DL2	Positive	Crack appears in the middle of wide pier in ground floor	112.4	7.30	0.75	0.16	0.14
DL3	Positive	Severely damaged wide pier in ground floor	150.0	32.00	1.00	0.73	0.60

7.4.3 Comparison with NLPO

The pushover capacity curve, hysteresis curve and dynamic capacity curve of Model S1-B are presented together in Figure 7.11. As in previously presented results, it can be seen that the initial stiffness of the building obtained from NLPO and NLTH analyses are same. Also the maximum shear force obtained until the end of the ninth run in NLTH analysis and maximum base shear force obtained from NLPO analysis occur at the same second floor displacement. However, the maximum base shear force in NLTH is 14.5% higher compared to NLPO result. The dynamic capacity curve is obtained by considering the points corresponding to the maximum base shear force in all nine runs.

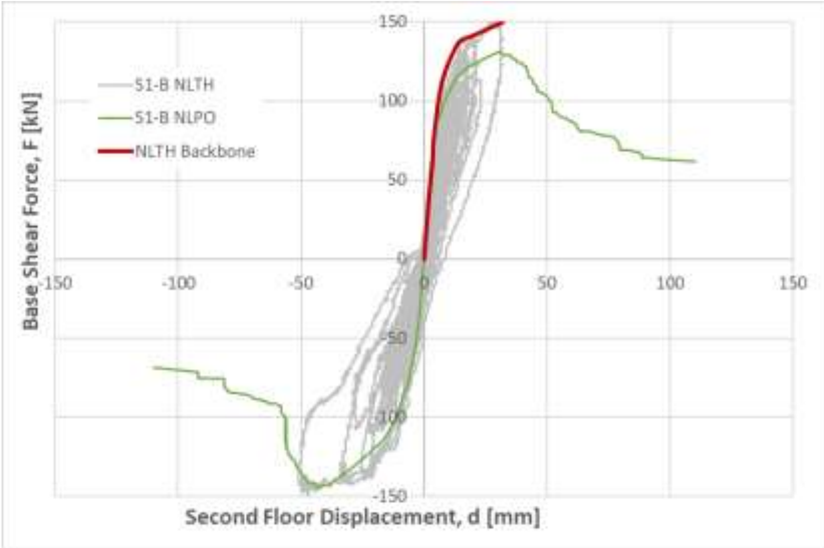

Figure 7.11 Hysteresis curve, Pushover capacity curve and Dynamic capacity curve of Model S1-B

Figure 7.12 shows the damage levels marked in the pushover capacity curve and dynamic capacity curve. The damage level DL3 is observed in the ninth run when the wide pier is fully cracked. As already indicated above, the damage level DL4 is not reached until the end of the analysis. As presented in previous results, it can be observed that the damage levels occur above in NLTH compared to NLPO. When compared with the results presented for Model U2 in section 4.4, it can be noted that the strengthening measure improves the performance of the building. The base shear force and second floor displacement corresponding to damage levels DL2 and DL3 are higher in Model S1-B compared to Model U2. Also, the delay in the damage level is seen in terms of the time. The damage level DL2 and DL3 occur at the fifth run and ninth run in Model S1-B compared to the fourth run and eighth run in Model U2. The other characteristics, such as: cracking behaviour, displacement profile etc. stays similar to other models.

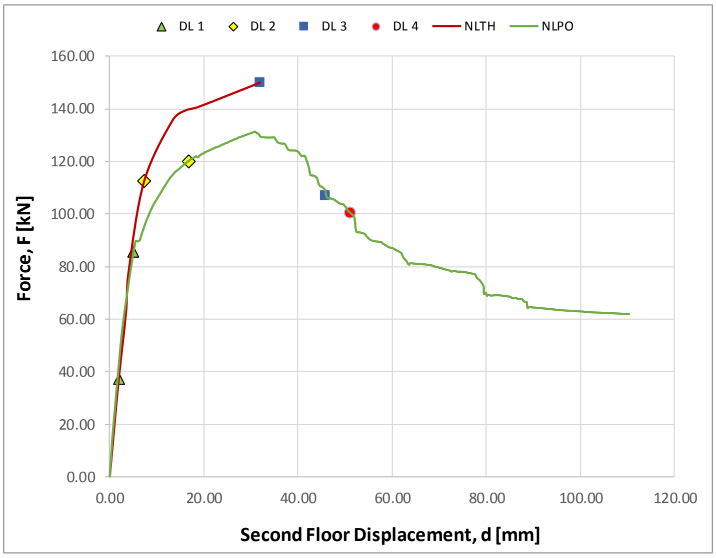

Figure 7.12 Damage levels of Model S1-B

7.5 Results of Model S2-B

The response of Model S2 strengthened using ECC when subjected to earthquake signal is presented in this section.

7.5.1 Hysteresis Curve

The hysteresis curve of Model S2-B is shown in Figure 7.13. It can be seen that also in Model S2-B, the energy dissipation and residual displacement is limited until the end of the ninth run. The maximum base shear force and second floor displacement are found to be 136 kN and 23 mm, respectively, both at the ninth run.

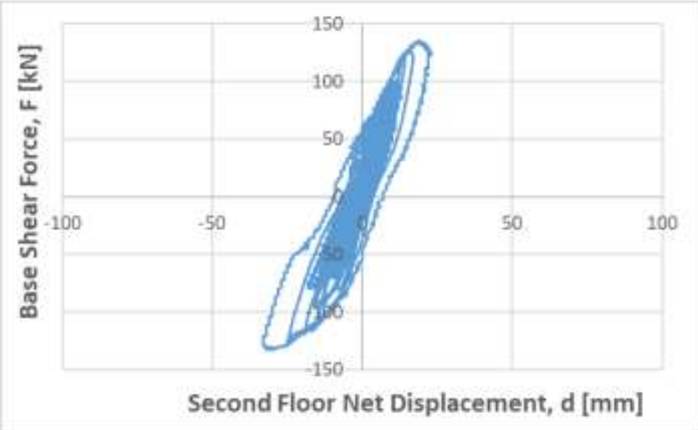

Figure 7.13 Hysteresis curve of Model S2-B

7.5.2 Damage Levels Identification

The damage levels identified in Model S2-B using the same criteria defined in previous models is shown in Table 7.5. Only the damage levels DL1, DL2 and DL3 are shown because the damage level DL4 did not occur until the end of the ninth run.

Table 7.5 Summary of damage levels in Model S2-B

Damage Levels	Loading Direction	Observed Damage	Force	Second floor displacement	Normalised shear force	Interstorey drift	Global drift
			F	d2	k_G	d_{r1}	d_{r*}
			kN	mm		%	%
DL1	Positive	Initiation of rocking mechanism in piers	36.3	1.94	0.27	0.03	0.04
DL2	Positive	Crack appears in the middle of wide pier in ground floor	87.9	6.58	0.65	0.12	0.12
DL3	Positive	Severely damaged wide pier in ground floor	127.4	15.20	0.90	0.32	0.27

7.5.3 Comparison with NLPO

The pushover capacity curve, hysteresis curve and dynamic capacity curve of Model S2-B are presented together in Figure 7.14. Both the analyses approach exhibit similar initial stiffness of the building. The maximum base shear force obtained until the end of the ninth run from NLTH analysis is 4 kN less compared to the maximum base shear force obtained from the NLPO analysis. Both the analyses produce similar cracking pattern and displacement profile.

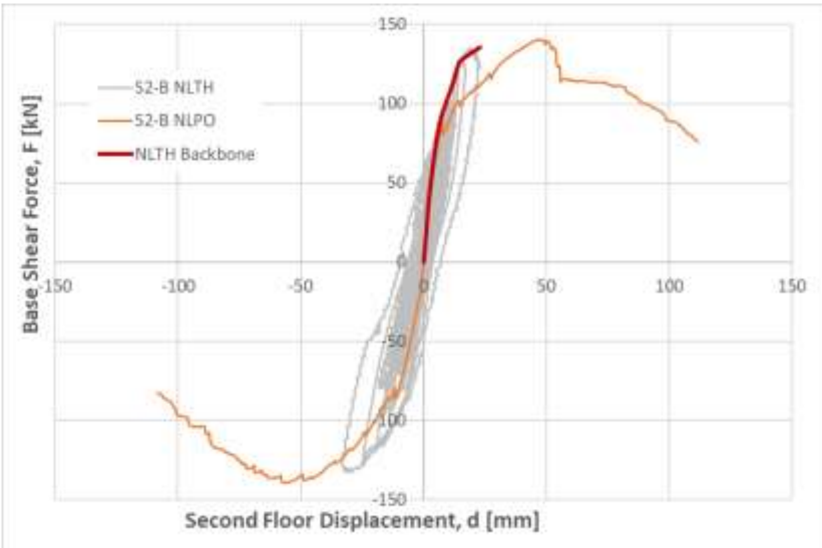

Figure 7.14 Hysteresis curve, Pushover capacity curve and Dynamic capacity curve of Model S2-B

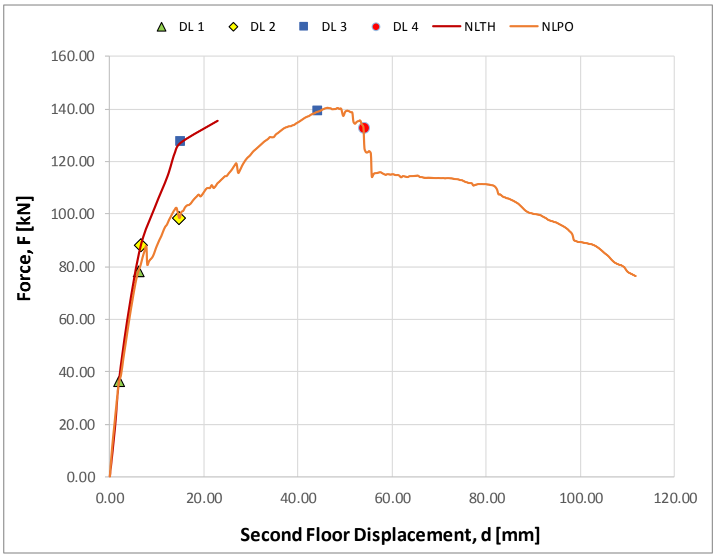

Figure 7.15 Damage levels of Model S2-B

The damage levels are marked in the capacity curve obtained from both the analyses and are presented in Figure 7.15. As in previous models, the damage levels occur above in NLTH analysis compared to NLPO analysis. The damage level DL4 is not marked in dynamic capacity curve because the interstorey drift limit is not reached until the end of the ninth run in NLTH analysis.

7.6 Results of Model S3-B

Finally, the results of Model S3 strengthened using ECC layer in piers and flanges and analysed dynamically are presented in this section.

7.6.1 Hysteresis Curve

The hysteresis curve showing the relation between the base shear force and the second floor net displacement is shown in Figure 7.16. The energy dissipation and residual displacement until the end of the ninth run is least for Model S3-B when compared with Model S1-B and Model S2-B. The maximum base shear force and second floor net displacement are found to be 184 kN and 30 mm, respectively, both occurring at the ninth run.

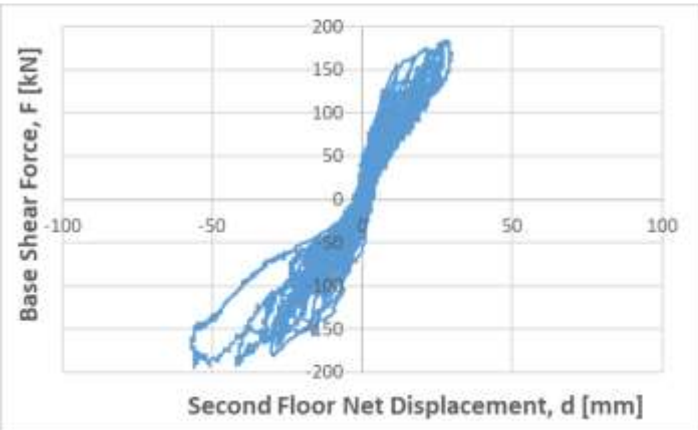

Figure 7.16 Hysteresis curve of Model S3-B

7.6.2 Damage Levels Identification

The damage levels are identified and presented along with the corresponding base shear force, second floor displacement, normalised shear force, interstorey drift and global drift in Table 7.6. The damage levels DL1 and DL3 occur at second and eighth run in both the strengthened and unstrengthened models. However the damage level DL2 occur at the fifth run in Model S3-B compared to the fourth run in Model U2.

Table 7.6 Summary of damage levels in Model S3-B

Damage Levels	Loading Direction	Observed Damage	Force	Second floor displacement	Normalised shear force	Interstorey drift	Global drift
			F	d2	k_G	d_{r1}	d_{r*}
			kN	mm		%	%
DL1	Positive	Initiation of rocking mechanism in piers	34.7	1.68	0.19	0.03	0.03
DL2	Positive	Crack appears in the middle of wide pier in ground floor	127.6	6.80	0.69	0.13	0.13
DL3	Positive	Severely damaged wide pier in ground floor	180.9	26.60	0.98	0.60	0.50

7.6.3 Comparison with NLPO

The pushover capacity curve, hysteresis curve and dynamic capacity curve are presented together in figure 7.17. As in previous results, it can be seen that both analysis approach exhibit same initial stiffness of the building. In fact it can be observed in Figure 7.17 that the pushover capacity curve is almost the backbone of the hysteresis curve until the end of the ninth run. The dynamic capacity curve is obtained by taking points corresponding to the maximum base shear force in each run.

The cracking pattern and displacement profile obtained from both the analysis approaches have good resemblance with each other as stated in previous analyses. The damage levels are marked in the capacity curves obtained from both the analyses and are presented in Figure 7.18. The damage level in NLTH occur above due to the accumulation of damage in the nonlinear time history analysis compared to the monotonic pushover analysis.

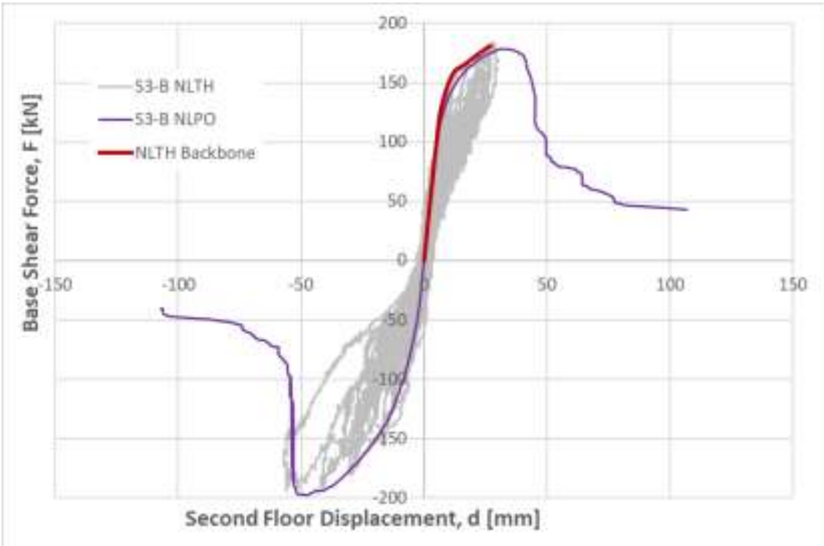

Figure 7.17 Hysteresis curve, Pushover capacity curve and Dynamic capacity curve of Model S3-B

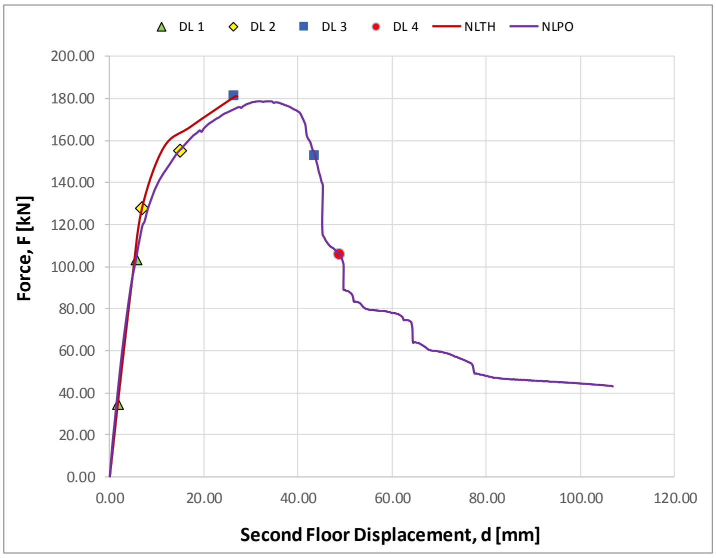

Figure 7.18 Damage levels of Model S3-B

7.7 Summary of NLTH Analyses

The results of the dynamic analyses performed on strengthened models are presented and compared with the results of the nonlinear push over analysis. It is observed that the same initial stiffness of the building is computed for both analyses approaches, and also the crack pattern and the displacement profile are similar. In general, the results obtained from NLTH analyses are higher in terms of the base shear force and lower in terms of the displacement ductility when compared with the results obtained from the NLPO analyses. As mentioned above, the reason for the lesser displacement capacity could be due to the accumulation of damage in NLTH which does not occur in the monotonic NLPO analyses. Fairly close agreement of results observed from the comparison of results from NLPO and NLTH analyses have shown that the monotonic NLPO analysis can indeed complement the computationally expensive NLTH analysis.

The damage levels in strengthened models are found to be delayed in terms of the base shear force and second floor displacement when compared with the NLTH analyses results of Model U2 (i.e. a specific damage level is achieved for larger values of forces and displacements). However, it should be noted that in most of the models the damage level occurred at the same time in both strengthened and unstrengthened cases: that means for the same accelerogram. Although the delay in the damage levels in terms of time could not be observed in these set of analyses, the delay observed in terms of base shear force and second floor displacement show the possibility of achieving also delay in time for different input earthquake signals, strengthening techniques and strengthening materials.

8 Conclusion

This study aims to assess the efficiency of different strengthening measures for URM buildings in terms of seismic capacity and prevention of the damage.

First, two buildings that resemble typical Dutch terraced houses in the Groningen province and were tested at TU Delft are considered as case study for the unreinforced building cases. The accuracy of the finite element modelling of the unstrengthened building, is validated by comparing the results of Model U1 and the house tested in TU Delft, TUD_BUILD_1. Although some discrepancies are observed between the tested specimen and outcomes of the finite element simulation, reasonably good agreement of two sets of results are found in terms of crack evolution, base shear capacity, and identification of the main failure mechanism. This provides a basis for the validation of the numerical approach and its use in the remaining studies. The damage levels are identified on the basis of the crack evolution in the model. The final damage level, DL4 is identified as the point when interstorey drift limit (1.5%) is reached.

The numerical results of the second unstrengthened building, Model U2, show that the capacity of the building increases when piers span over one floor only, compared to the building where piers span over two floors (i.e. the first storey floor is supported not only by the transversal walls, but also by the piers). The analyses of the displacement profiles at different damage levels indicates the development of a soft storey mechanism at ground floor of Model U2. The base shear capacity of Model U2 are 79.8 kN and 40.6 mm in positive and negative direction, respectively. Similarly, the ultimate displacement capacity, i.e. the displacement corresponding to DL4, is found to be 50.2 mm in the positive direction and 52.44 mm in the negative direction. These results show that the Model U2 is already sufficiently ductile for such building configuration and no much room for improvements is available. However, the building is relatively weak in terms of base shear force and its strength may be increased by the application of appropriate strengthening measures.

The results obtained from the NLTH analyses of Model U1 and Model U2 return higher base shear capacity and lower displacement capacity compared to the NLPO analyses. As a result, some difference is observed between base shear forces and second floor displacements at which the damage levels are identified. However, good agreement is observed between NLTH and NLPO in terms of initial stiffness exhibited by the building, prevailing failing mode and crack evolution.

Three different strengthening techniques are adopted to strengthen the second building, Model U2. The techniques considered in the study are: the strengthening of URM piers (S1), the strengthening of wall-to-pier connections (S2), and the strengthening of both piers and wall-to-pier connections (S3). Two different strengthening materials, Material A (OSB Panels) and Material B (ECC), are applied over the strengthened components. The strengthening materials are assumed to be perfectly bonded to the existing masonry.

The comparison between the results of the analyses performed on the reference unstrengthened model and the strengthened models show a significant increase of the base shear capacity of the building. Although the second floor displacement at which damage levels DL1-DL3 occur increased thanks to the applied strengthening measures, no significant increase in the ultimate displacement capacity (i.e. DL4) is observed. However, as already discussed above, it should be noted that the displacement capacity exhibited by the unstrengthened model is already satisfactory enough for the considered building typology. Also, it should be taken in account that the damage level DL4 is defined as the point when interstorey drift limit is reached i.e. 1.5%. This definition represents more of a lower bound value of DL4 for the strengthened cases which is supported by the small difference between DL3 and DL4. The findings of this study therefore highlights the need of a new definition of the ultimate displacement capacity for the strengthened cases. It is recommended to investigate new method of determining the ultimate displacement capacity based on both numerical and experimental studies of the strengthened buildings.

As the strengthening techniques S1 and S3 involved the strengthening of piers, the improvement in the stiffness of the building could be observed in those models. Although the techniques S1 and S2 are applied to different parts of the building, they still produce quite similar results in terms of base shear capacity. The results from both NLPO and NLTH analyses showed that the strengthening techniques did not influence the crack pattern, overall behaviour of the house and the displacement profile.

The effect of different strengthening materials could be observed mainly in terms of the base shear capacity and the post peak region. Although the models strengthened using material B, ECC exhibit higher base shear capacity, the responses are found to be less ductile compared to models strengthened using material A, OSB. Especially, the results of Model S1-B and S3-B are found to be the least ductile due to the toe crushing of ECC overlaid piers in those models. The results have indicated that the increase in the capacity of the building strengthened using ECC is higher compared to the models strengthened using OSB panels, but it should be noted that the material properties used for ECC are obtained directly from the literature and no calibration exercise is performed to take into account the perfect bond assumed between masonry and ECC layer.

References

1. Esposito, R. (2019). Desktop and numerical study on retrofitting measures for low-rise URM buildings: plan of approach. Report No. CM1B06-WP3-1, Version 02, 24 January 2019 2018. Delft University of Technology.
2. Esposito, R., Trewel, K.C., Ravenshorst, G.J.P., Schipper, H.R., Messali, F., Rots, J.G. (2017). Cyclic pushover test on an unreinforced masonry structure resembling a typical dutch terraced house. In Proceedings of 16th World Conference on Earthquake (16WCEE 2017), 9-13 January, Santiago, Chile.
3. Esposito, R., Messali, F., Ravenshorst, G.J.P., Schipper, H.R., Rots, J.G. (2019). Seismic assessment of a lab-tested two-storey unreinforced masonry Dutch terraced house. Bulletin of Earthquake Engineering, 1-23.
4. Xu, T. (2018). Modeling the seismic response of a two-storey calcium silicate brick masonry structure with nonlinear pushover and time-history analyses. Delft University of Technology, MSc Thesis.
5. Nederlandse Praktijkrichtlijn NPR 9998, Assessment of Structural Safety of Buildings in Case of Erection, Reconstruction and Disapproval - Induced Earthquakes - Basis of Design, Actions and Resistances. ICS 91.080.01; 93.020, November 2018.
6. Miglietta, M., Mazzella, L., Grottoli, L., Guerrini, G., Graziotti, F. (2018), Full-Scale Building Test - EUC BUILD 6. Test Results Report, EUCENTRE Research Report, v1.1, 31/07/2018.
7. Yi, T. (2014). Experimental Investigation and Numerical Simulation of an Unreinforced Masonry Structure with Flexible Diaphragams. Georgia Institute of Technology, Ph.D. Thesis.
8. Li, V. C. (2019). Engineered Cementitious Composites (ECC): Bendable Concrete for Sustainable and Resilient Infrastructure. Springer.
9. Pourfalah, S., Suryanto, B., Cotsovos, D.M. (2015). Modelling of Masonry Wall Retrofitted with Engineered Cementitious Composites. Infrastructure and Environment Scotlab 3rd Postgraduate Conference, 9 December 2015, Heriot-Watt University, Edinburgh.
10. Kyriakides, M.A., Billington, S.L., Hendriks, M.A.N. (2009). Simulation of Masonry Beams Retrofitted with Engineered Cementitious Composites. Computational Modeling Workshop on Concrete, Masonry and on Fiber-Reinfroced Composites, June 17-18, 2009, Delft, The Netherlands (pp. 31-34).
11. Messali, F., Bhattarai, S., Rots, J.G. (2018). EUC-BUILD-7: Blind Prediction Modelling and Analysis with DIANA 10.2. Delft University of Technology, Report version 1, 05/12/2018
12. Miglietta, M., Damiani, N., Mazzella, L., Grottoli, L., Guerrini, G., Graziotti, F. (2019), Full-Scale Shaking Table Test on a Dutch URM Cavity-Wall Terraced-House End Unit. A Retrofit Solution with Strong-Backs and OSB Boards, EUC-BUILD-7. Test Results Report, EUCENTRE Research Report, v 1.0, 07/03/2019.
13. Fontani, S. (2017). Literature Review of Retrofitting Methods for Unreinforced Masonry Structures. Delft University of Technology, Report version 3, 03/06/2017.

Appendix A. Crack Evolution in Model U1 and Model U2

<u>The shear crack strain of the cracks observed in Model U1 (NLPO) are presented below from Figure A 1 - Figure A 7.</u>

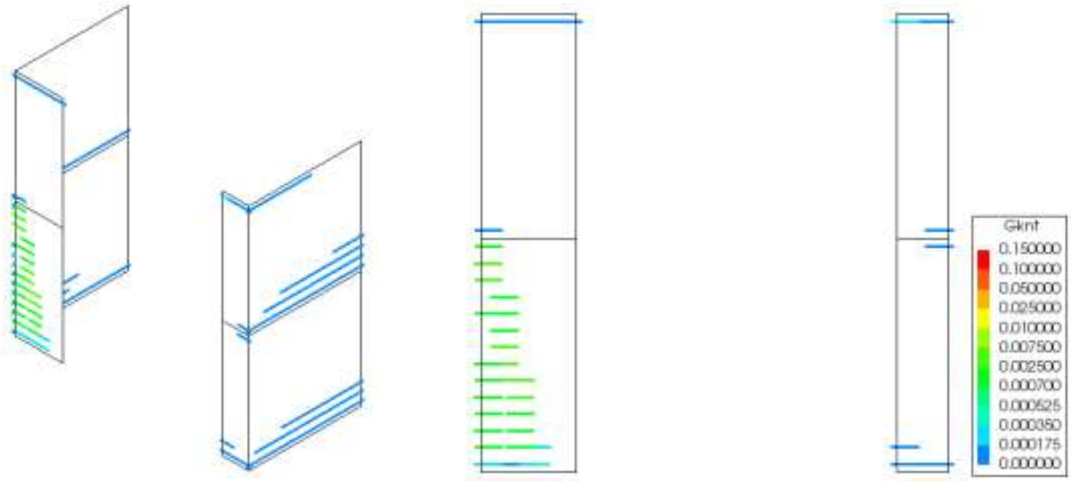

Figure A 1. Shear crack strain observed when cracks spread along the height of wide pier in ground floor in Model U1 (loaded in positive direction)

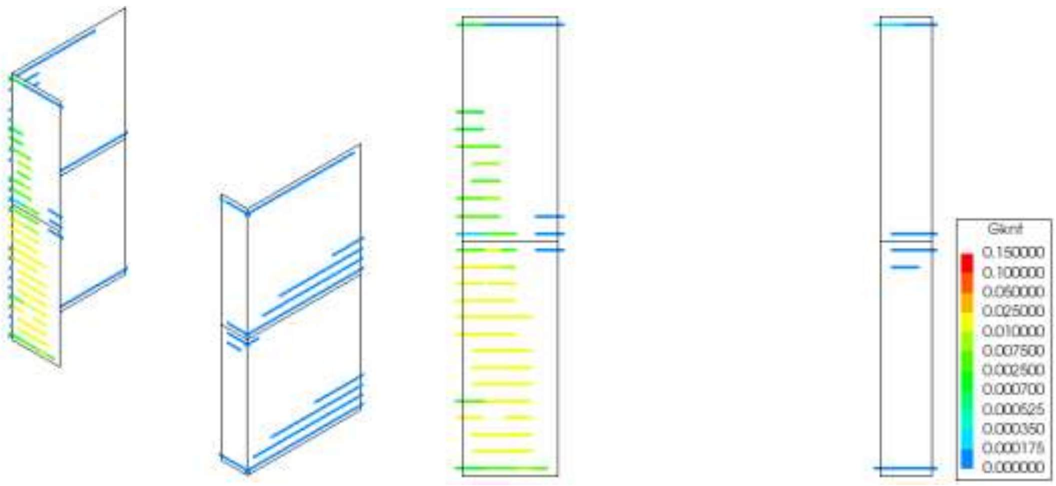

Figure A 2. Shear crack strain when the wide pier in ground floor is severely damaged in Model U1 (loaded in positive direction)

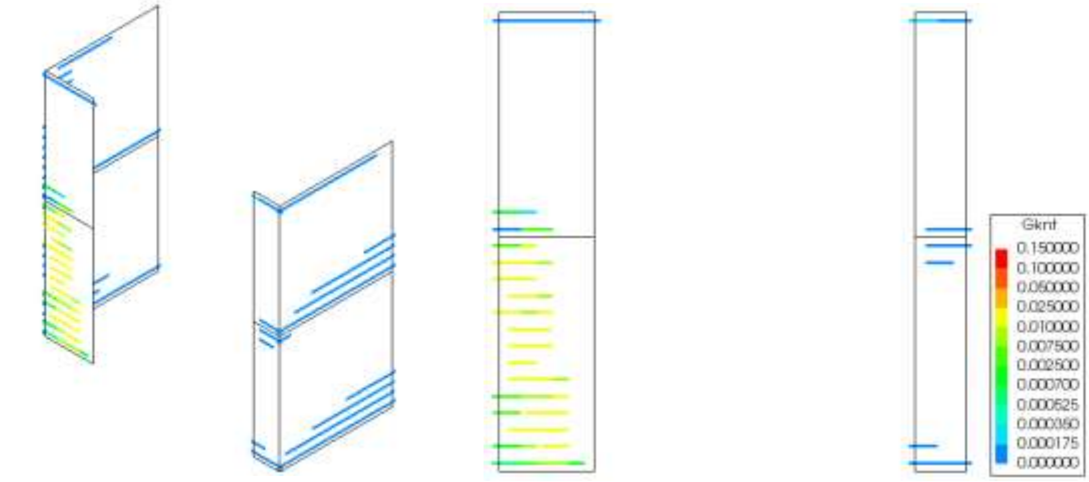

Figure A 3. Shear crack strain in Model U1 when global drift reaches 0.8% (loaded in positive direction)

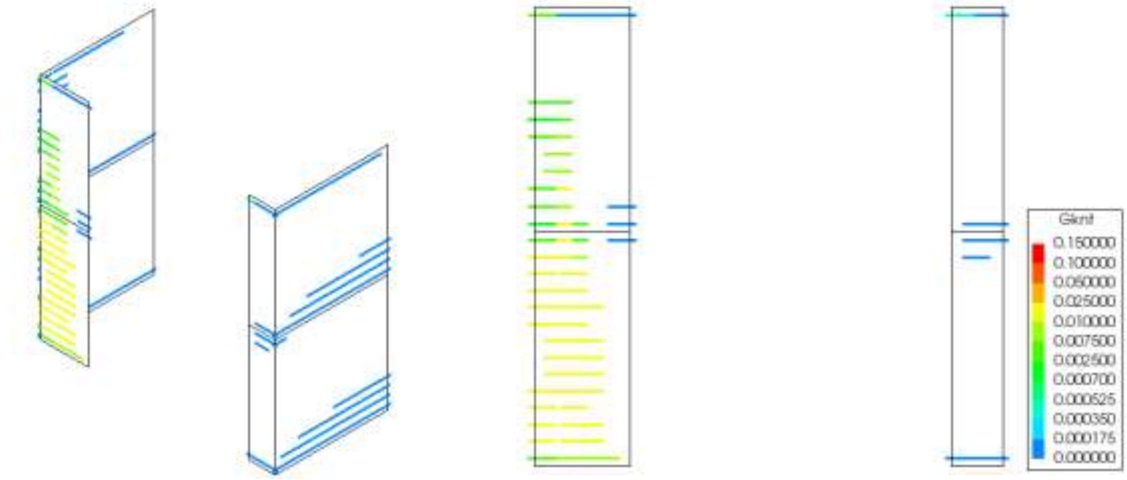

Figure A 4. Shear crack strain in Model U1 when interstorey drift of ground floor reaches 1.5% (loaded in positive direction)

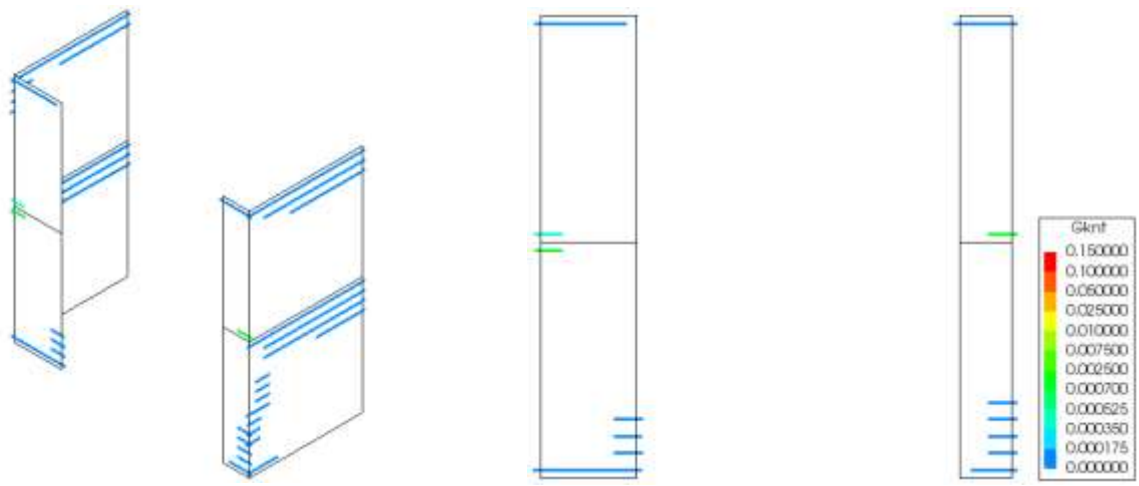

Figure A 5. Shear crack strain when cracks appear between connection of narrow pier and first floor in Model U1 (loaded in negative direction)

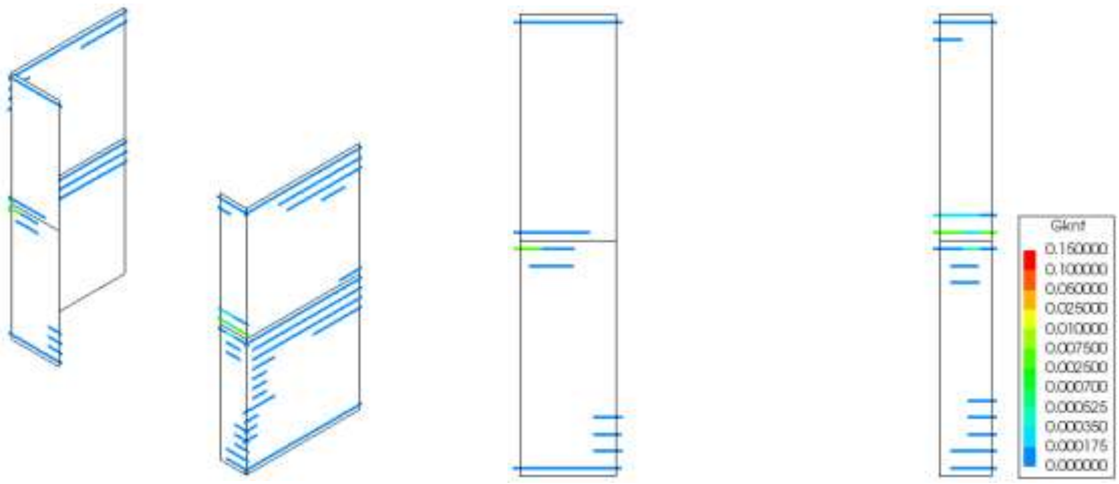

Figure A 6. Shear crack strain when the connection between narrow pier and first floor is fully cracked in Model U1 (loaded in negative direction)

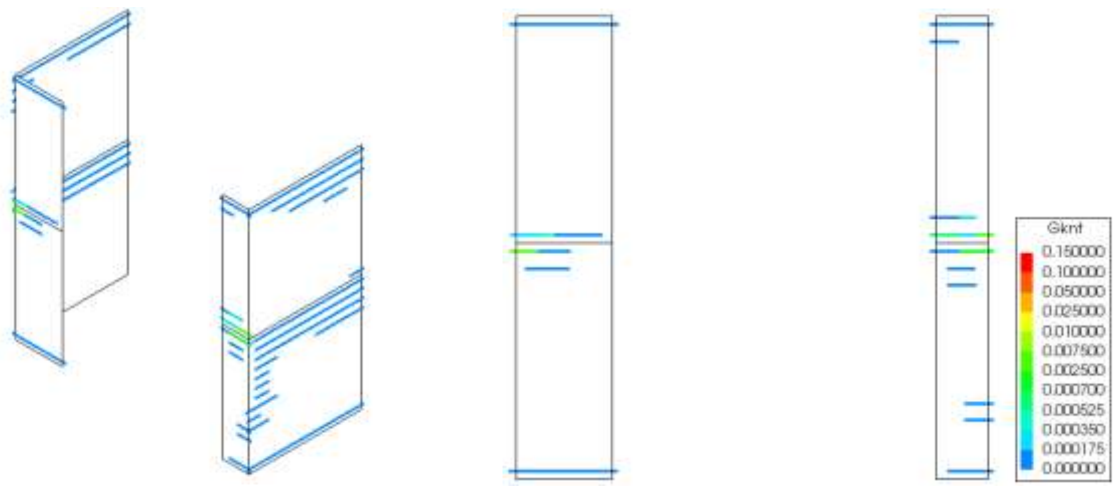

Figure A 7. Shear crack strain in Model U1 when IDL is reached (loaded in negative direction)

<u>The shear crack strain of the cracks observed in Model U2 at different damage levels after nonlinear pushover analysis are shown in Figure A 8 - Figure A 11.</u>

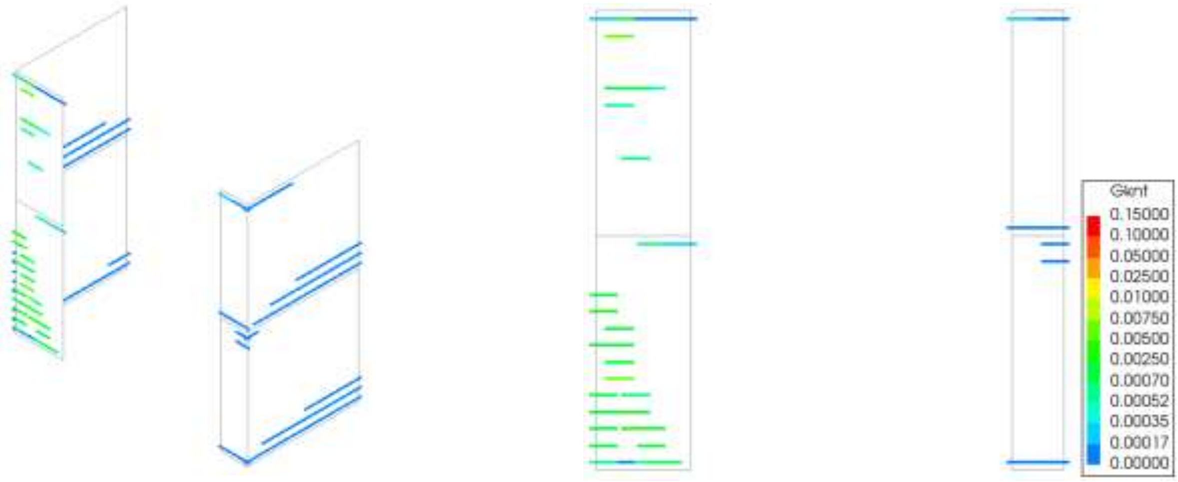

Figure A 8. Shear crack strain at DL2 in Model U2 when loaded in positive direction

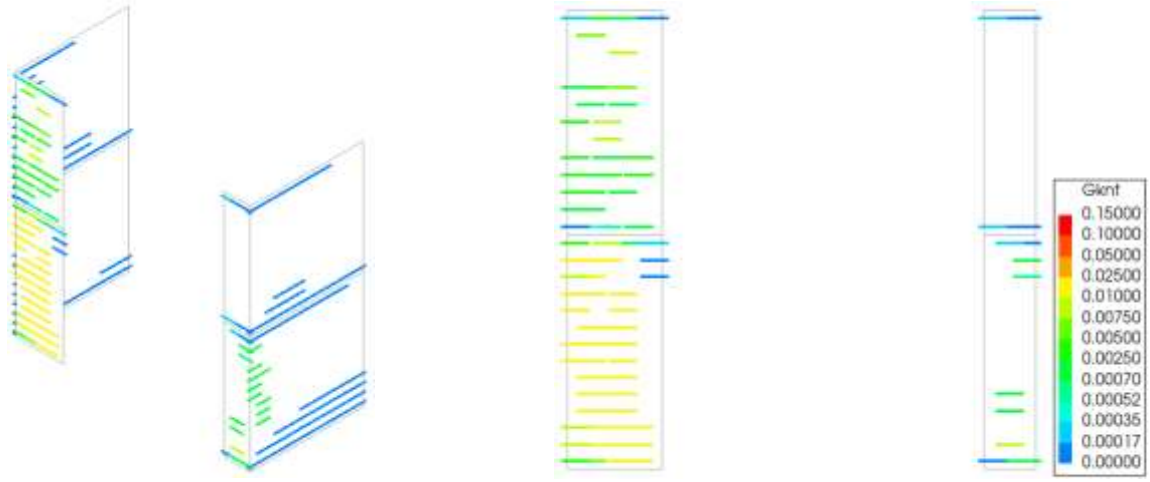

Figure A 9. Shear crack strain at DL3 in Model U2 when loaded in positive direction

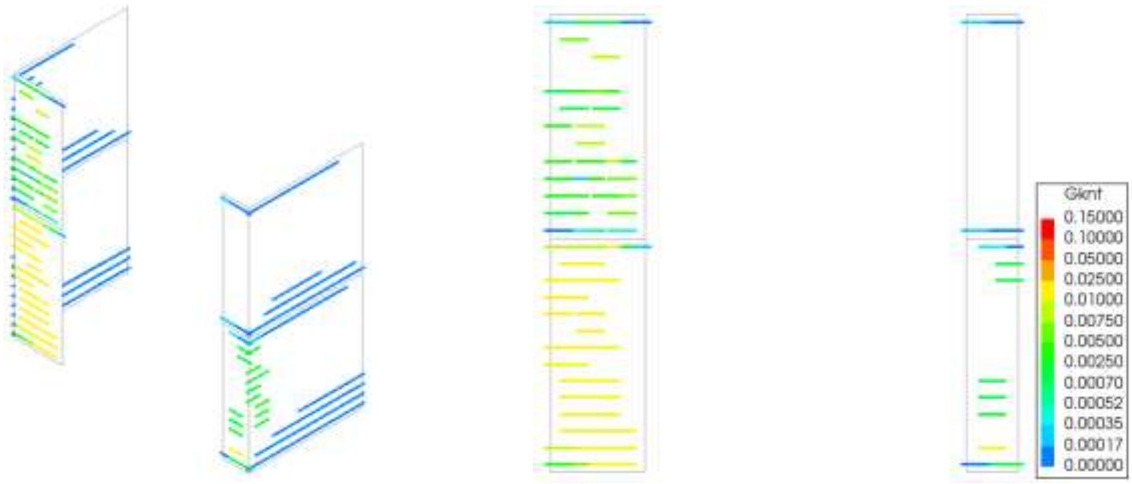

Figure A 10. Shear crack strain at DL4 in Model U2 when loaded in positive direction

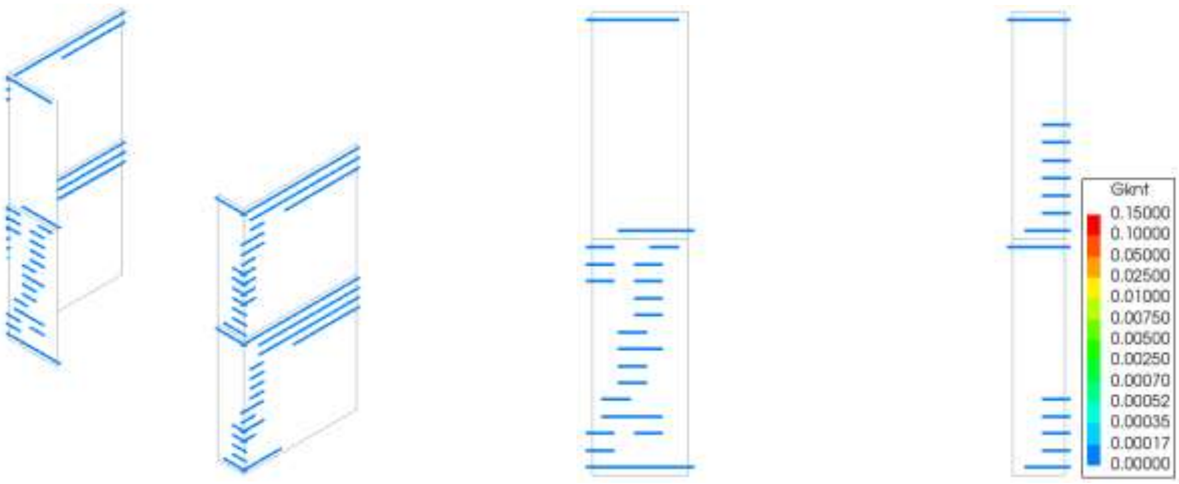

Figure A 11. Shear crack strain at DL2 in Model U2 when loaded in negative direction

The crack patterns observed in Model U1 at four different damage levels after dynamic analysis are shown in Figure A 12 - Figure A 15.

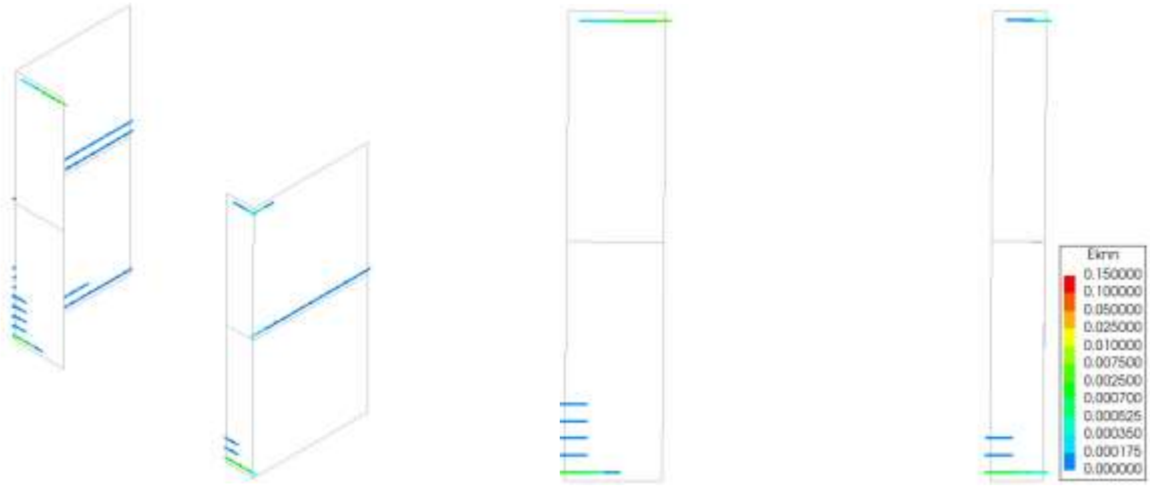

Figure A 12. Normal crack strain at DL1 in Model U1

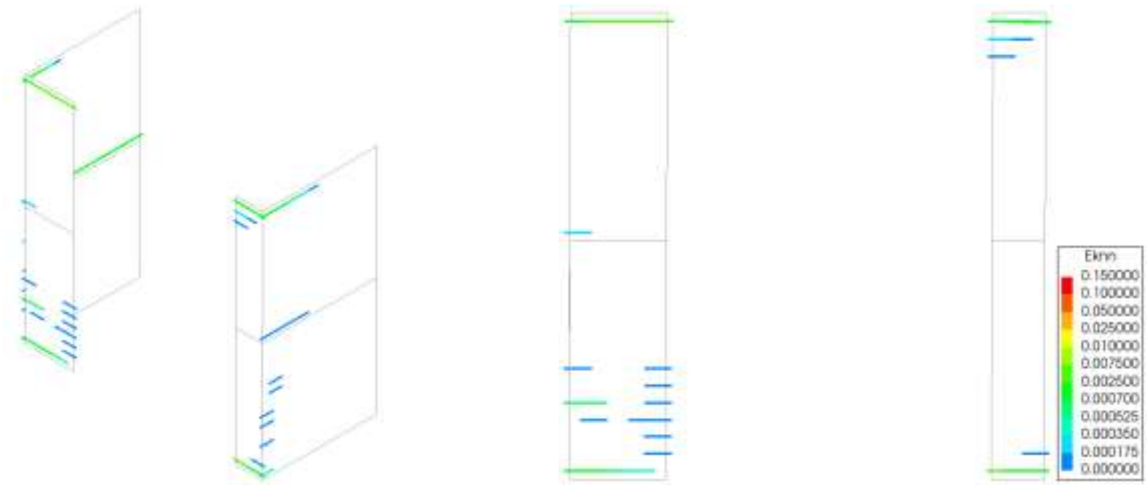

Figure A 13. Normal crack strain at DL2 in Model U1

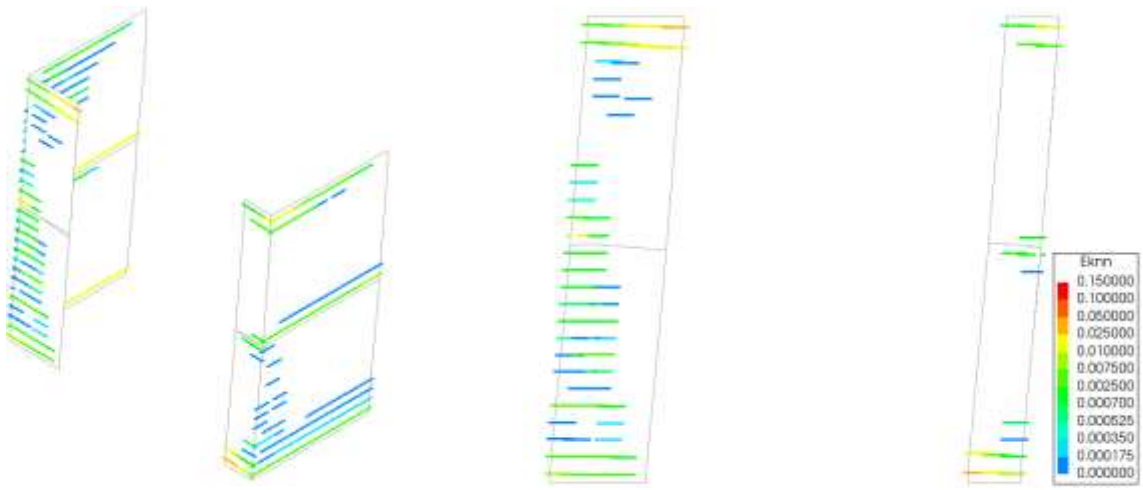

Figure A 14. Normal crack strain at DL3 in Model U1

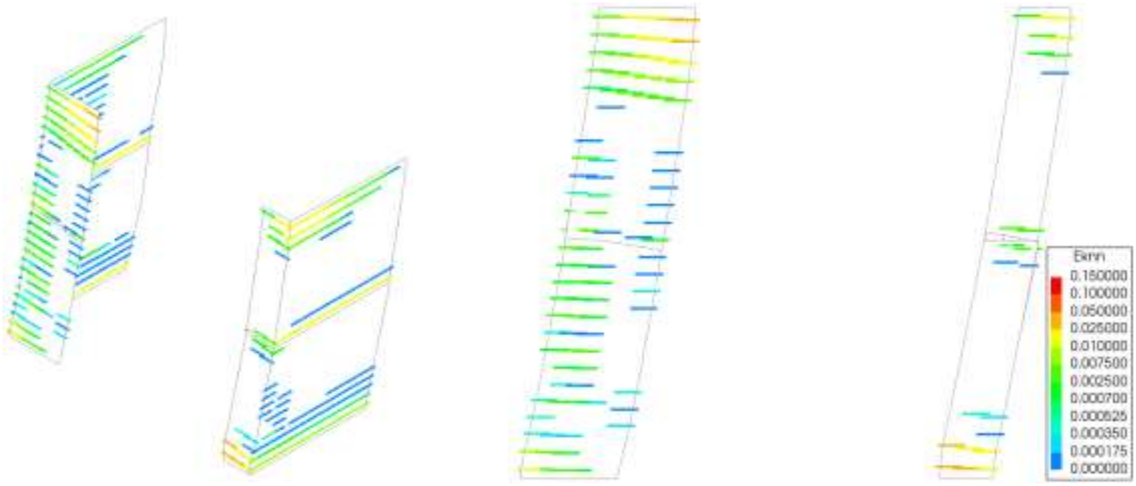

Figure A 15. Normal crack strain at DL4 in Model U1

Appendix B. Drift and Displacement Profile of Strengthened Models

The interstorey drift in ground floor and first floor level of Model S1-A are presented in Figure B 1. Also, the damage levels DL1, DL2 and DL3 are marked in the figure. It can be seen in the figure that the interstorey drift in two floor levels start to deviate rapidly after damage level DL2. The trend of the result is similar to that of Model U2. The displacement and thus the damage is accumulated at the first floor level. This finding is supported by the figure presented in Figure B 2 which shows the displacement profile of Model S1-A at different damage levels.

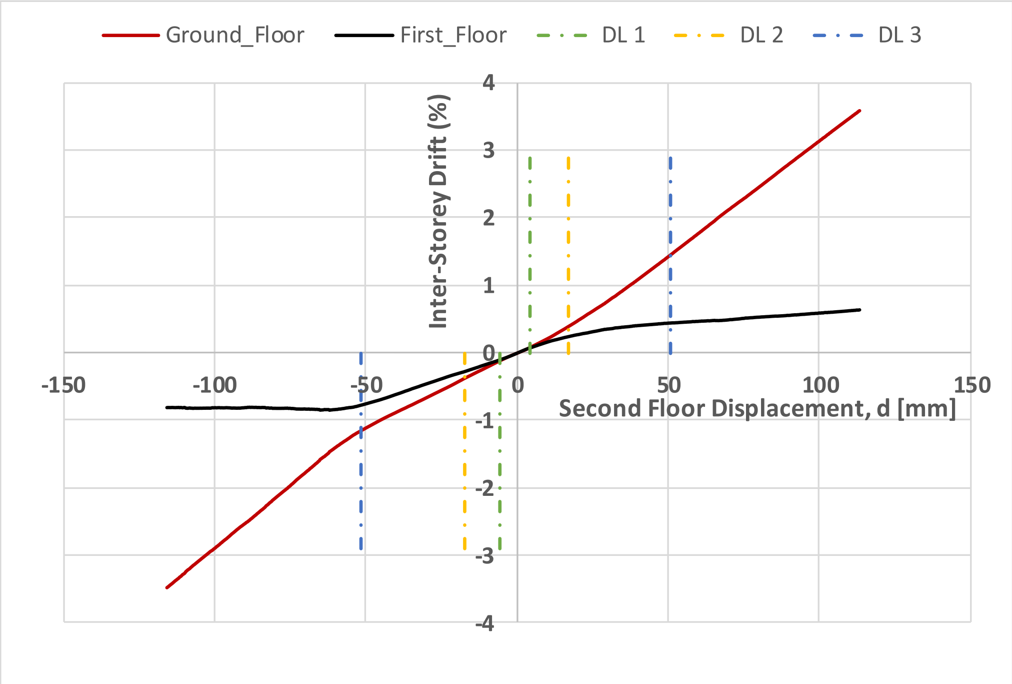

Figure B 1. Interstorey drift (%) in ground floor and first floor of Model S1-A

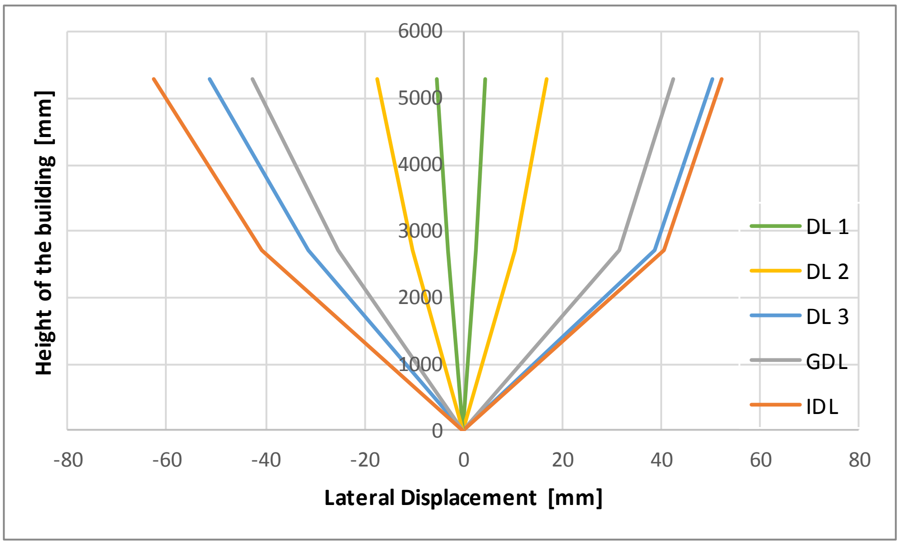

Figure B 2. Displacement profile of Model S1-A at different damage levels

Figure B 3 shows the interstorey drift in ground floor and first floor of Model S2-A. The damage levels DL1, DL2 and DL3 are also marked in the figure. It can be seen that the interstorey drift in ground floor i.e. at first floor level is higher which is in agreement with the displacement profile of Model S2-A presented in Figure B 4.

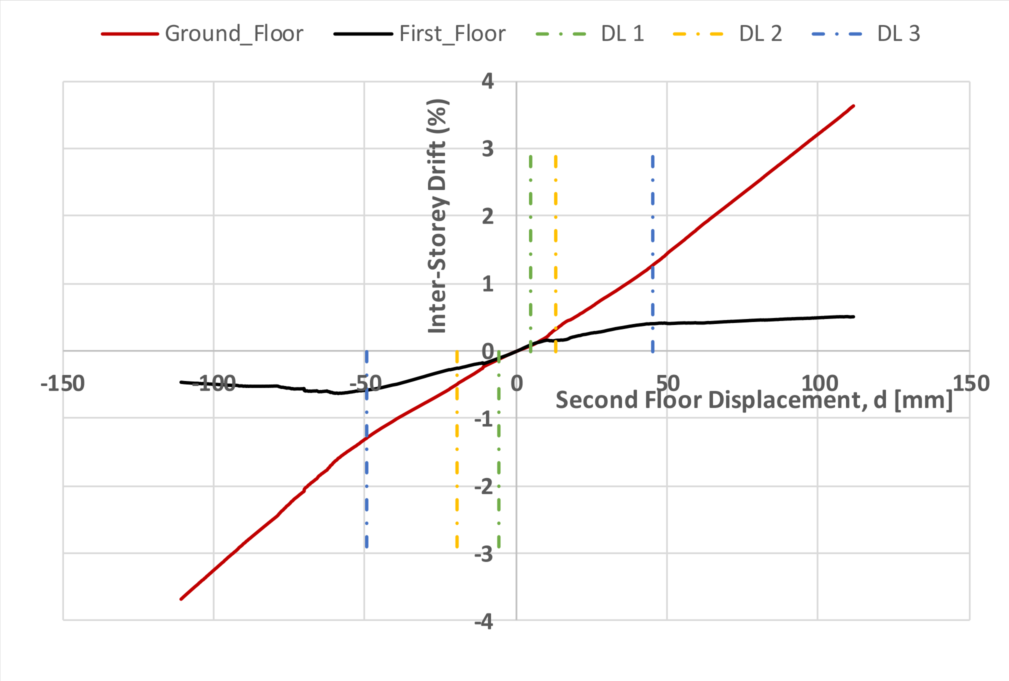

Figure B 3. Interstorey drift (%) in ground floor and first floor of Model S2-A

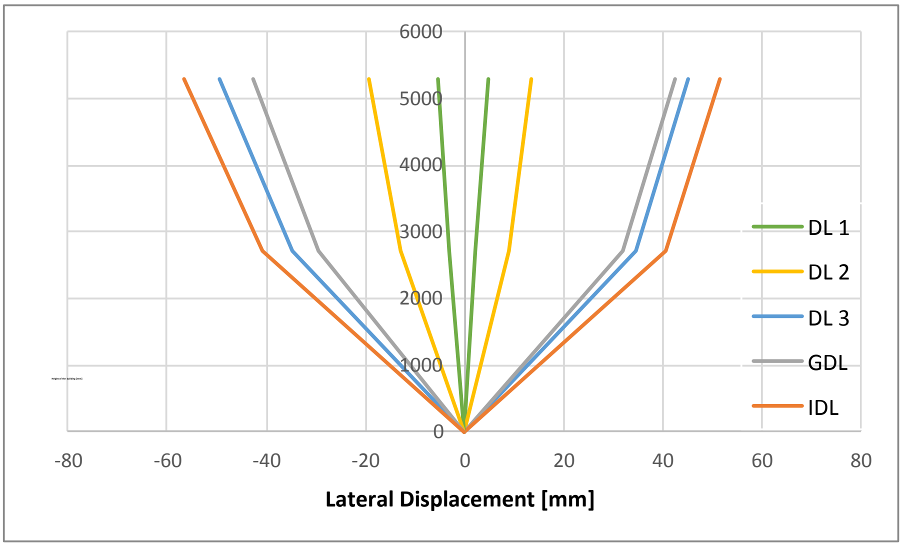

Figure B 4. Displacement profile of Model S2-A at different damage levels

The displacement profile of Model S2-A presented in Figure B 4 shows that the deformation is accumulated at the first floor level as observed above in Model U2 and Model S1-A.

The interstorey drift in the ground floor and first floor of Model S3-A is presented in Figure B 5. In addition, the damage levels DL1, DL2 and DL3 are also marked in the figure. The trend of the result is similar to Model U2, S1-A and S2-A. The interstorey drift in ground floor starts to increase more than the interstorey drift in first floor after damage level DL2. This strengthened model also exhibits the soft storey mechanism as deformation is accumulated more in the first floor level. The displacement profile of Model S3-A at four damage levels and the point when GDL is reached is shown in Figure B 6.

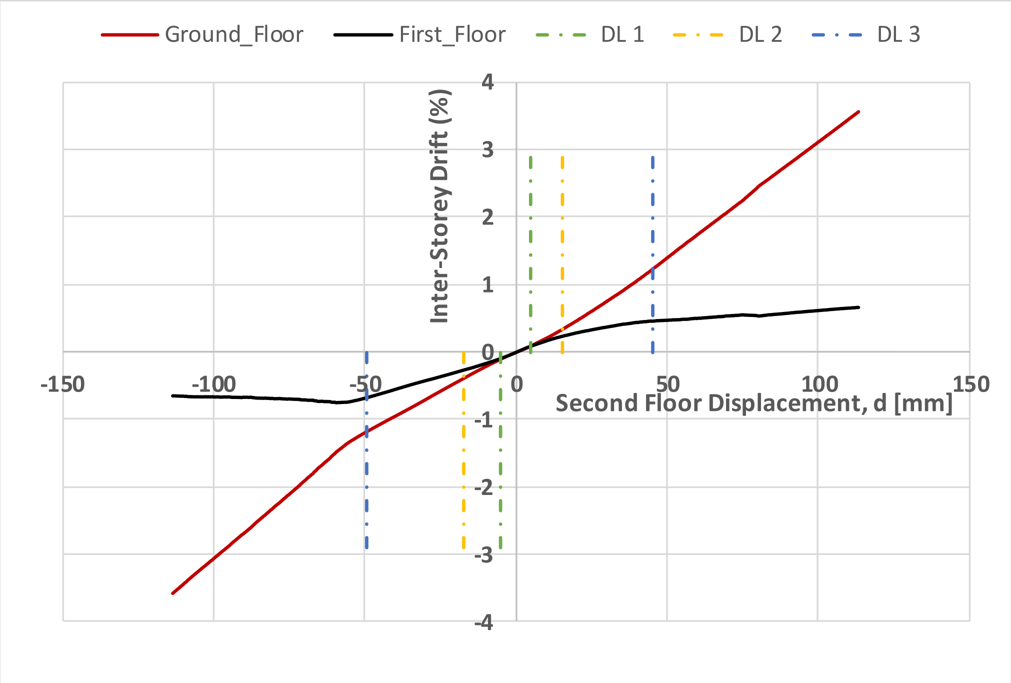

Figure B 5. Interstorey drift (%) in ground floor and first floor of Model S3-A

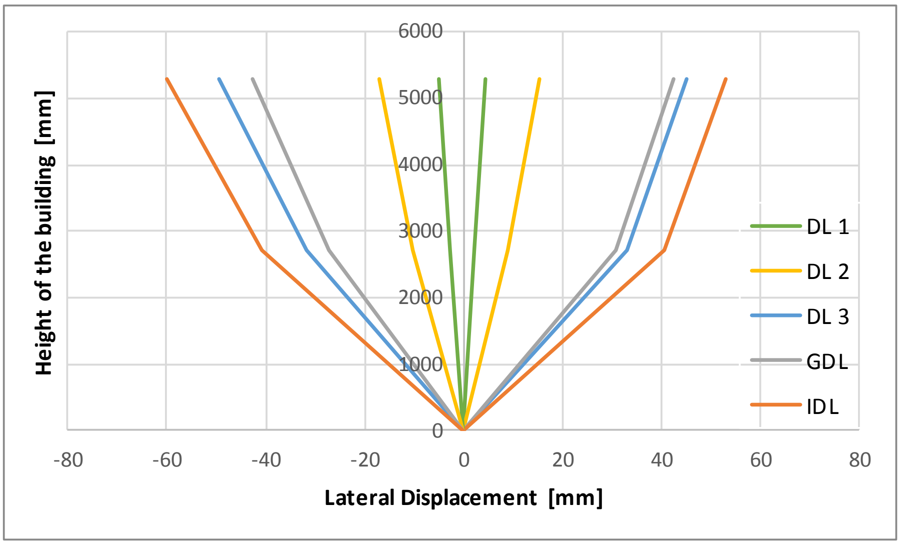

Figure B 6. Displacement profile of Model S3-A at different damage levels

The interstorey drift in the ground floor and first floor of Model S1-B is presented in Figure B 7. The damage levels DL1, DL2 and DL3 are marked in the figure. The results show that the Model S1-B also has the accumulation of deformation at the first floor level which can also be seen in the displacement profile of Model S1-B presented in Figure B 8. The Figure B 8 shows the displacement profile of Model S1-B at four damage levels and the point when (GDL) global drift limit is reached. The soft storey mechanism becomes more evident after the global drift limit is reached.

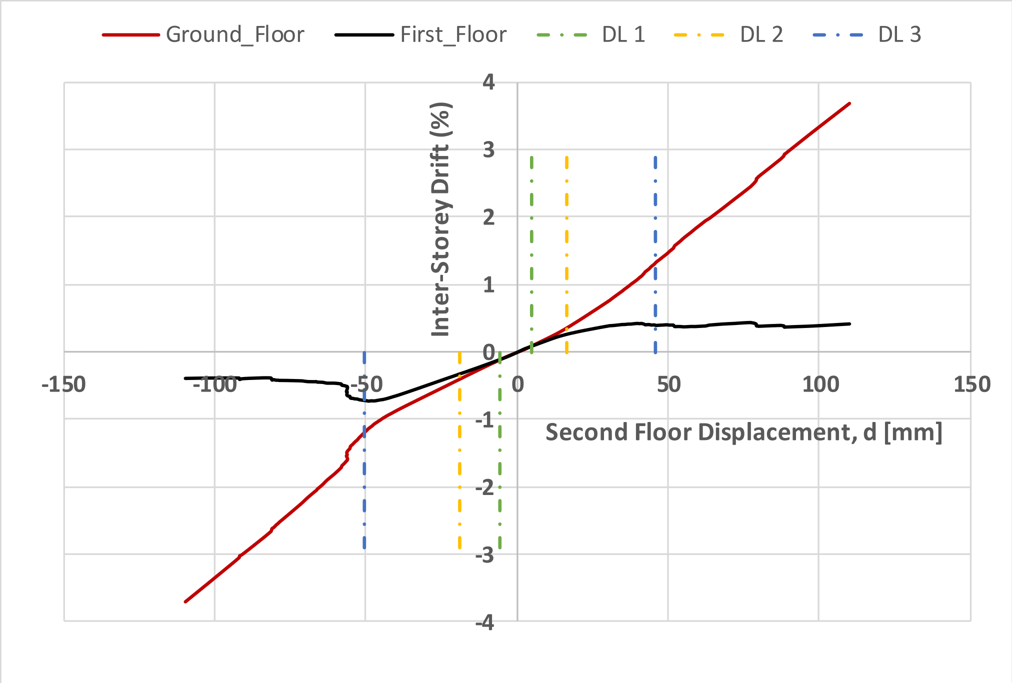

Figure B 7. Interstorey drift (%) in ground floor and first floor of Model S1-B

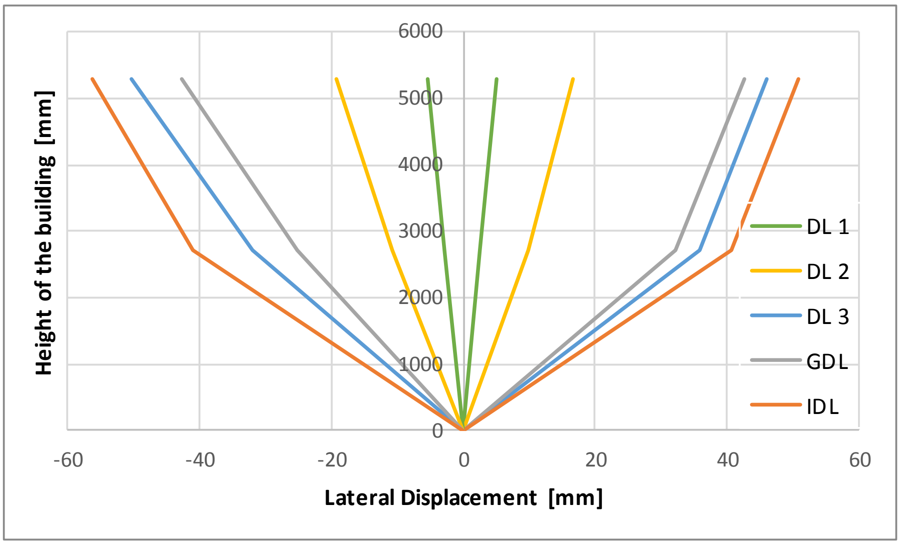

Figure B 8. Displacement profile of Model S1-B at different damage levels

The interstorey drift in ground floor and first floor of Model S2-B is presented next. The results are shown in Figure B 9 and the damage levels are marked as well. The trend of the results is similar to previous models which is further supported by the displacement profile of the building presented in Figure B 10. The damage (deformation) is accumulated in the first floor level thus exhibiting soft storey mechanism.

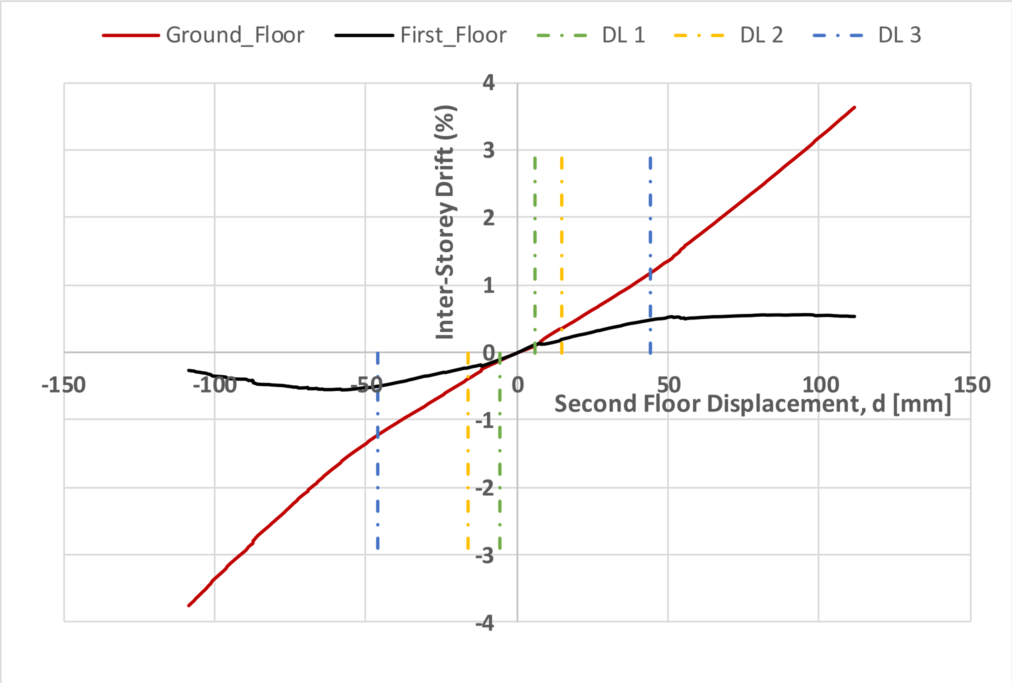

Figure B 9. Interstorey drift (%) in ground floor and first floor of Model S2-B

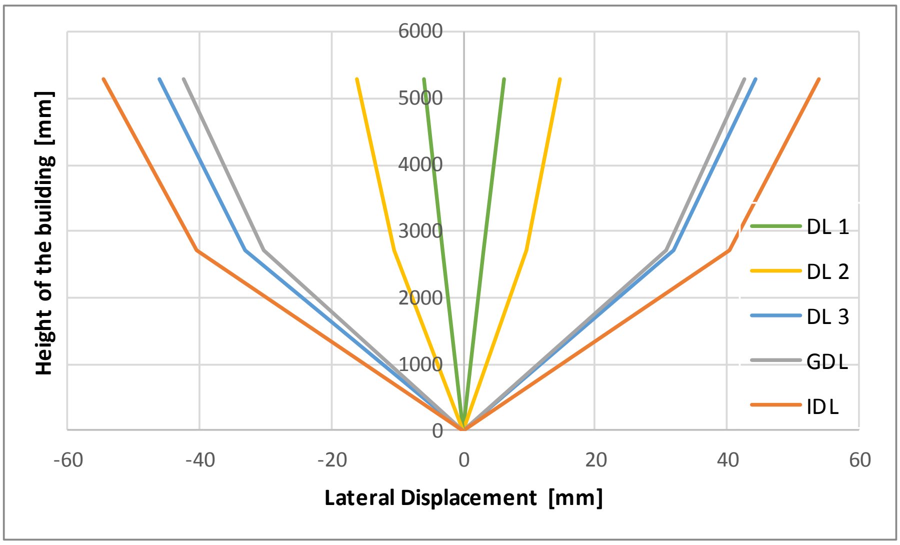

Figure B 10. Displacement profile of Model S2-B at different damage levels

The interstorey drift in ground floor and first floor of Model S3-B is presented in Figure B 11 which is similar to previous unstrengthened and strengthened models. The displacement profile of the building at different damage levels is presented in Figure B 12 and it is evident that the deformation is accumulated at the first floor level in Model S3-B as well.

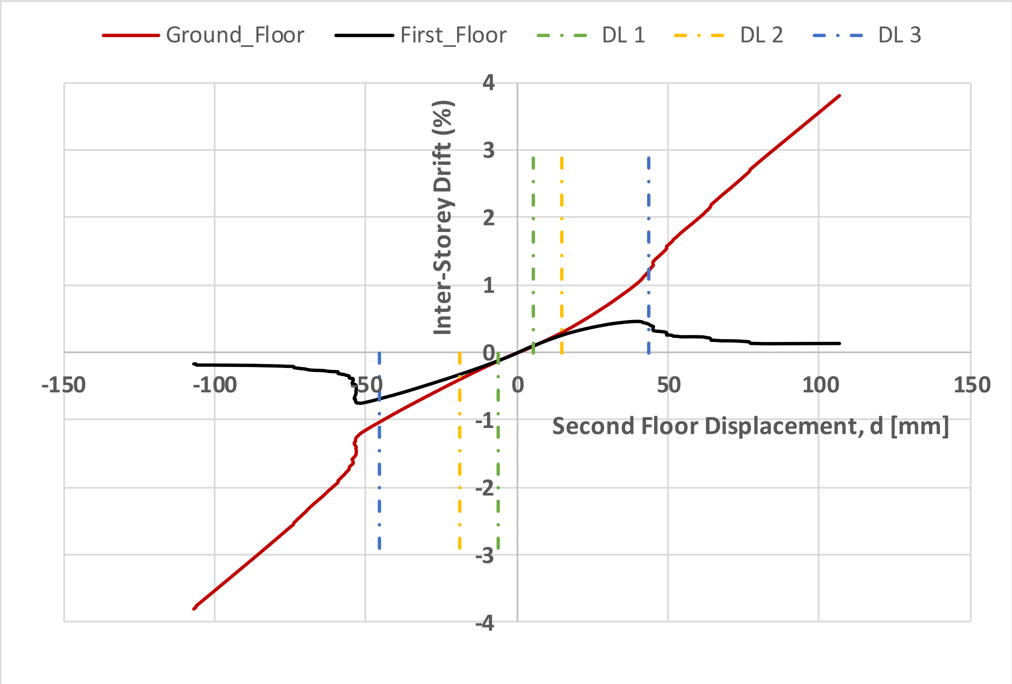

Figure B 11. Interstorey drift (%) in ground floor and first floor of Model S3-B

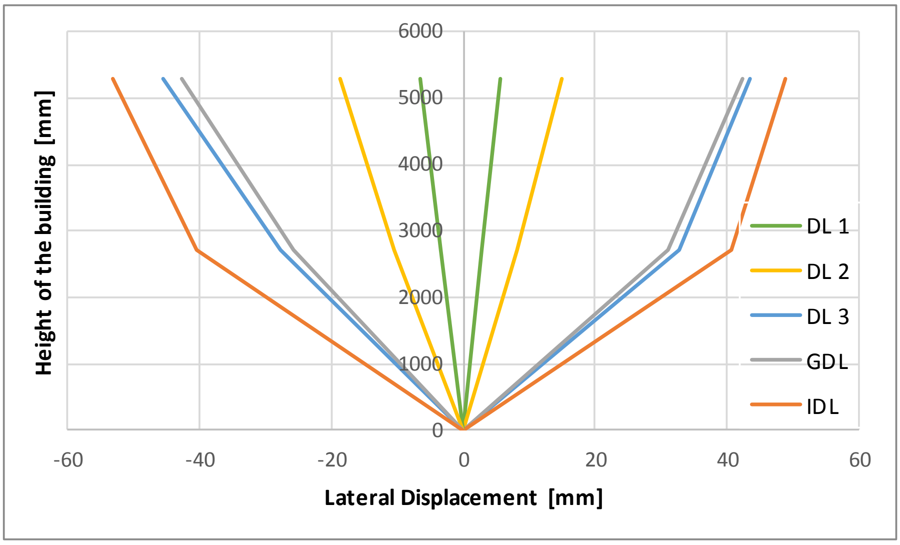

Figure B 12. Displacement profile of Model S3-B at different damage levels